UDK: 544.7+547.3+543.2 *DOI: 10.15407/Surface.2025.17.413*

MEDICAL NANOCOMPOSITES BASED ON HYDROPHILIC AND HYDROPHOBIC SILICAS AND THEIR PROPERTIES

T. V. Krupska, M. V. Borysenko, N. Yu. Klymenko, L. V. Zrol, O. A. Novikova, V. V.Turov

Chuiko Institute of Surface Chemistry of NAS of Ukraine, 17 Oleg Mudrak Str., Kyiv-03164, Ukraine, e-mail: krupska@ukr.net

Technologies have been developed for the production of nanocomposite systems based on hydrophilic and hydrophobic silicas or their mixtures with biologically active plant-based compounds, such as betulin, pectin and inulin. The physicochemical properties and structure of the adsorption layer have been studied, and the concentration ratios of the components at which the active substances are in their most active, nanoscale state have been determined. Information has been obtained on the possibilities of regulating the release rate of biologically active components from composite systems. Inulin and other bioactive substances (BAS) forms composite systems with hydrophilic or a mixture of hydrophilic and hydrophobic silica during mechanical processing, maintaining a high specific surface area of the composite system. At the same time BAS are uniformly distributed on the surface of mineral particles. Both in initial materials and in composite systems, adsorbed water is in the form of nanoscale or subnanoscale clusters formed by strongly-associated water, molecules of which simultaneously participate in the formation of 2–3 hydrogen bonds. A weakly polar organic medium has a disordering (chaotropic) effect on water. As the temperature decreases, the ordering of adsorbed water molecules increases, although in some systems, temperature intervals are fixed at which the cosmotropic effect of the surface on adsorbed water takes place. The addition of hydrophobic silica AM1 to the A-300/BAS composite system leads to an increase in the surface-water interaction. The magnitude of the interfacial energy correlates with a decrease in the radius of the adsorbed water clusters. Aqueous gels created from silica and BAS exhibit the properties of non-Newtonian fluids, which depending on the magnitude of shear strain can exhibit both pseudoplastic and dilatant properties.

Keywords: *hydrophilic and hydrophobic silicas, pectin, inulin, betulin, succinic acid, composite systems, strongly and weakly associated water.*

INTRODUCTION

Nanopharmacology encompasses the pharmacological use of nanoparticles, quantum dots, carbon nanotubes, gold and silver nanoparticles, and their combined use with traditional pharmaceuticals, as well as the study of the influence of nanoparticles on metabolic processes. Nanopharmacology is particularly active in the development of new types of anticancer drugs, drug delivery systems, and the construction of complex multi-layered drugs, for example, using liposomes, monoclonal antibodies, magnetic carriers, etc. [1–6].

In recent years, the creation of new types of functionalized materials for use in biotechnological processes and advanced biomedical materials has been achieved through the development of composite systems comprising hydrophilic and/or hydrophobic highly dispersed materials, organic substances of various chemical natures, water, and certain types of compounds that impart predetermined properties. In complex heterogeneous systems, their adsorption and technological characteristics depend largely on the self-consistent processes that occur during composite formation, i.e., the formation of supramolecular systems with minimal thermodynamic potentials. These effects can be used in the development of methods for controlling the properties of a composite system by varying its hydrophobic-hydrophilic interactions, the processes of cluster

formation of aqueous and aqueous-organic systems included in the composites, and the influence on the phase state of the components [7, 8]. Sufficiently technologically advanced methods have been developed for converting hydrophobic, highly dispersed adsorbents into a highly hydrated state [9, 10], which can serve as a technological basis for the preparation of complex heterogeneous systems and their use in aqueous media, which are the basis of most biological fluids.

Unlike liquids, solid particles with different hydrophobic-hydrophilic properties (in the dry state) can form a virtually homogeneous mixture after mechanical mixing, in which both types of particles are part of common aggregates and interact within them via van der Waals forces. The difference in the interaction energies of hydrophobic, hydrophilic, and mixed particles is not great. However, the possibility of the coexistence of dissimilar particles in the volume can be disrupted by the addition of a liquid phase (surfactant, water, or hydrophobic liquid) [11, 12]. Spontaneous separation of components in mixtures of powders or viscous liquids (microcoagulation) caused by Brownian motion cannot occur or occurs very slowly; however, this process can be significantly accelerated under the influence of mechanical stress applied to the composite system during its mixing, especially in the presence of surfactants. Since coagulation reduces the free energy of a multicomponent system, it should lead to an increase in the binding energy of liquid components to the surface of dispersed particles. This effect can be used to structurally modify the mineral component of a composite system.

In recent studies carried out at the Chuiko Institute of Surface Chemistry [13], it has been shown that water adsorption in oxide nanostructured materials occurs via a cluster formation mechanism, in which clusters, the size of which is determined by the morphology of interparticle gaps and the hydrophobic-hydrophilic properties of the surface, are adsorbed on the primary surface centers rather than individual molecules. Clustered water has a number of unusual properties that distinguish it from bulk water: For example, polar organic substances, including mineral acids, dissolve poorly in nanosized water clusters [14]. A weakly polar medium can displace water, replacing it at the surface, which leads to an increase in the average radius of adsorbed water clusters [15].

A large body of scientific information has been obtained in the study of hydration problems in hydrophobic materials. It has been established that, using dosed mechanical loads, powders of hydrophobic substances can be transferred to an aqueous medium, with the energy of interaction of water with a hydrophobic surface being even greater than with a hydrophilic one [16,17]. It has been shown that the introduction of a small amount of a solid hydrophobic agent, such as methylaerosil, into the mineral base of composite systems can lead to a tenfold increase in water binding [18, 19]. Thus, a significant base for fundamental research has been created for the development of a new generation of composite systems for medical purposes.

SILICA MATERIALS AND RESEARCH METHODS

Materials. Highly dispersed silica A-300, produced by the Kalush Experimental Plant of the Chuiko Institute of Surface Chemistry, National Academy of Sciences of Ukraine, was used. Its specific surface area (by nitrogen at 76 *K*) was 295 m^2/g, and the total pore volume was about 1 cm^3/g. It should be noted that the structure of nanosilica particles (unlike silica gels) is not rigid and strongly depends on preliminary preparation. In particular, if its initial bulk density after production is 50 mg/ml, various methods of mechanical or hydraulic compaction can increase it to 200 mg/cm^3 [17]. This occurs mainly due to changes in the structure of aggregates and does not affect the structure of primary silica particles [18, 19].

Hydrophobic silica of the AM1 brand was used as methylsilica, with a specific surface area S_{BET} = 175 m^2/g and a total pore volume V_p = 0.8 cm^3/g (Kalush, Ukraine), obtained by chemical modification of the surface of the initial A-200 nanosilica with dimethyldichlorosilane. As a result of the reactions, pairs of dimethylsilyl groups are formed, crosslinked by siloxane bridges $=Si(CH_3)_2$-O-$Si(CH_3)_2$-.

X-ray diffraction (XRD). X–ray diffraction patterns were recorded over $2\theta = 5 – 70°$ range using a DRON–3M (Burevestnik, St. Petersburg) diffractometer with Cu K_α ($\lambda = 0.15418$ nm) radiation and a Ni filter. The XRD data could be used for simple estimation of average sizes of crystallites using Scherrer or Debye–Scherrer equations [20, 21].

Infrared spectroscopy. Infrared spectra of the studied samples were recorded using a Fourier transform infrared (FTIR) IRTracer–100 (Shimadzu) spectrophotometer with a diffuse reflectance (DR) attachment DRS–8000A. To record the IR spectra, samples with A-300 or AM1 alone or with KBr (1:300) were pressed into thin pellets (~20 mg).

Thermogravimetry. Thermograms (thermogravimetry, TG at the average weight errors ±0.1 mg, differential TG, DTG, and differential thermal analysis, DTA data) were recorded using a Derivatograph Q–1500 D apparatus (Paulik, Paulik & Erdey, MOM, Budapest, Hungary) upon heating of samples (~0.2 g) in air at a heating rate of 10°C/min from 20°C to 1000°C. The TG curves show that the amounts of water in samples under measurements are smaller than the initial ones due to water evaporation upon sample preparation.

NMR spectroscopy and cryoporometry. Low-temperature ^{1}H NMR spectra of static samples were recorded using a high-resolution NMR spectrometer (Varian 400 "Mercury") with an operating frequency of 400 MHz. Eight 60° probe pulses were used with a duration of 1 μs and a bandwidth of 20 kHz. The temperature was using a Bruker VT-1000 thermal attachment with an accuracy of ±1 degree. Signal intensities were determined by measuring peak areas using a signal decomposition procedure assuming a Gaussian waveform and optimizing the zero line and phase with an accuracy of at least 5 % for well-resolved signals and ±10 % for overlapping signals. To prevent overcooling of water in the objects under study, measurements of the concentration of unfrozen water were carried out by heating of samples pre-cooled to 210–215 K. Temperature dependences of the intensity of ^{1}H NMR signals were carried out in an automated cycle, when the sample was kept at a constant temperature for 5 min, and the measurement time was 1 min.

The process of freezing (thawing) of water bound to solids occurs with changes in the Gibbs free energy caused by the influence of a solid surface, confined space effects, solutes, colligative properties of solutions (cryoscopic effects), and co-solvents. Frozen water does not contribute the recorded ^{1}H NMR signals due to a narrow bandwidth of 20 kHz and a large difference in the transverse relaxation time of mobile (liquid water and solutions) and immobile (frozen water, solids) phases [22]. Water (or other liquids) can be frozen in narrower pores (or voids between nanoparticles) at lower temperatures as described by the Gibbs–Thomson relation for the freezing point depression for liquids confined in cylindrical pores at radius R [22–25]. This relation is the base of cryoporometry giving information of the size distributions of pores (voids) infilled by unfrozen water.

The area under $\Delta G(C_{\text{uw}})$ curve determines the modulus of the total changes in the Gibbs free energy ΔG *vs*. the amount of unfrozen water (C_{uw}) that are caused by interactions of water with silica and NaCl crystallite surfaces [22]

$$\gamma_S = -A \int_0^{C_{uw}^{\max}} \Delta G(C_{uw}) dC_{uw} , \qquad (1)$$

where $C_{uw}^{\max}$ is the total amount of water unfrozen at $T = 273$ K, and A (> 0) is a constant dependent on the type of units used in this equation.

Water can be frozen in narrower pores (or voids between nanoparticles) at lower temperatures as described by the Gibbs–Thomson relation for the freezing point depression for liquids confined in cylindrical pores at radius R [22–25]

$$\Delta T_m = T_{m,\infty} - T_m(R) = -\frac{2\sigma_{sl} T_{m,\infty}}{\Delta H_f \rho R} = \frac{k_{GT}}{R}, \quad (2)$$

where $T_m(R)$ is the melting temperature of ice in cylindrical pores of radius R, $T_{m,\infty}$ the bulk melting temperature, ΔH_f the bulk enthalpy of fusion, ρ the density of the solid, σ_{sl} the energy of solid–liquid-air interaction, and k_{GT} is the Gibbs–Thomson constant (here k_{GT} = 50 K nm for water).

Adsorption from solutions. Adsorption of methylene blue (MB) dye (M = 319.85 g/mol, manufactured by Khimlaborreaktiv LLC) on silica-containing media was studied under static conditions at T = 23÷25°C. For this purpose, aqueous solutions of different concentrations (from 15.63 to 156.32 μmol/l) in a volume of 10 ml were added to the weighing of the corresponding sample (m = 100 mg) and mixed for ~1 hour. The solutions were adjusted to the desired pH using standard HCI or NaOH titers. The solid phase was separated by centrifugation for 20 min at a speed of 3000 rpm. The concentration of MB in the solution was determined spectrophotometrically by measuring its absorption spectra on a spectrometer (Specord M-40, Carl Zeiss Jena, Germany) at a wavelength of 660 nm (l = 1 cm). The amount of dye adsorption (A_∞) was determined by the difference between its initial and equilibrium concentration in the solution before and after contact with the sorbents.

DESIGN OF COMPOSITE SYSTEMS BASED ON HYDROPHILIC SILICA AND ORGANIC ACIDS: GALLIC, GLYCERYSINIC AND ITS SALTS

Gallic acid (3,4,5-trihydroxybenzoic, $C_7H_6O_5$) is a polyphenol of plant origin. It is found in red wine, grape leaves, oak bark and many other plants [26, 27]. It has high biological activity – antioxidant [28–30], anti-inflammatory [31-33], anti-cancer [34–38], and tonic [39–41]. There is extensive information on the activity of GA in the treatment and restoration of cartilage tissue [42, 43]. However, since GA is poorly soluble in cold water, its bioavailability is low and special methods are required to increase it. Promising methods in this direction include changing the phase state of GA by immobilizing it on the surface of a mineral carrier (highly dispersed silica) in the form of nanosized clusters and using mediator substances capable of simultaneously forming complexes with GA and specific to phospholipids, which form the basis of cell membrane receptors.

Glycyrrhizic acid (20β-Carboxy-11-oxo-30-norolean-12-en-3β-yl-2-O-β-D-glucopyranuronosyl-α-D-glucopyranosideuronic acid) (gross formula $C_{42}H_{62}O_{16}$), which is a tribasic saponin consisting of a triterpenoid aglycone, glycyrrhizic acid (GLA), combined with a disaccharide of glucuronic acid, can become such a mediator. GLA is contained in licorice roots (Glycyrrhiza glabra L). It is used as a food sweetener and in licorice preparations, as a drug with antiviral and anti-inflammatory activity [44]. Recently, GLA has been actively considered as a substance that increases the biological activity of other drugs [45–47]. This effect may be based on the ability of GLA to integrate into cell membranes and change their physical and functional properties. One of the possible mechanisms of the antiviral action of GA is considered to be the prevention of the fusion of the virus envelope with the plasma membrane of the host cell.

The aim of this work was to create composite systems based on highly dispersed silica with GA, GLA and GLA salts in which the organic phase is in a clustered state, to study the structure of the bound water layer in composites and their differences from bound water in silica.

GA (I), GLA (II) and its salts, monoammonium (MonAm) and monopotassium (MonK), chemical grade (ch), produced in China.

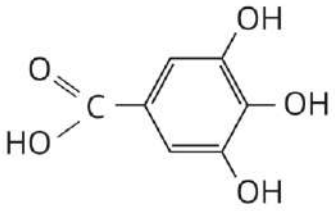

(I)

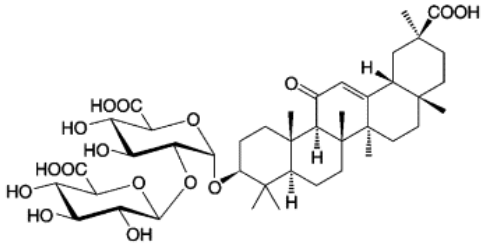

(II)

To prepare the samples, 10 g of silica A-300 with a bulk density of C_d = 50 mg/ml, containing 50 mg/g of residual water (absorbed from the air) were ground in a porcelain mortar and compacted to C_d = 200 mg/ml. This material was used as the starting material for the preparation of composite systems with GA, GLA and its salts. For this, the weighed portions of acids (or salts) were mixed with A-300 in a proportion of 1/10 and additionally ground for 10 min until a homogeneous composite system was formed. These samples contained 50 mg/g of water. To increase the amount of water, 100 mg/g of distilled water was added to the samples and they were additionally ground for 1–2 min, after which they were kept in a closed ampoule for 1–2 hours.

Fig. 1 shows thermograms of the studied composite systems prepared on the basis of gallic acid (*a*), glycyrrhizic acid (*b*), its monoammonium (*c*) and monopotassium (*d*) salts. Several inflections on the weight loss curves are observed on the thermograms, which manifest themselves as maxima on the DTG curves. Peaks in the region of T = 50–150°C are related to physically adsorbed water. This water can be associated with both the surface of silica and the organic phase of the composite systems. Peaks with maxima in the region of T = 200°C can be attributed to the destruction of acid crystal hydrates. At a higher temperature, the destruction of organic acids occurs, which occurs in several stages – resinification and carbonization. Accordingly, additional peaks appear on the DTG curves.

Electron micrographs of the initial GC, GLC powders and composite systems prepared by mechanical treatment of acid mixtures (or salts) with A-300 nanosilica powder are shown in Fig. 2. The initial acids have a pronounced microcrystalline structure, with crystals of 5–30 μm in size. After mechanical treatment, a composite structure is formed in which only silica aggregates are visually observed. It can be concluded that for all samples, mechanical treatment results in crushing of acid crystals (or salts) and uniform distribution of the organic phase in the interparticle gaps of silica.

The phase state of acids (salts) immobilized on the surface of nanosilica can be determined using X-ray phase analysis data (Fig. 3*a*). All samples, except for A-300/GA, were completely X-ray amorphous. In the case of GA, against the background of an intense signal of the amorphous phase (which applies to both silica and GA), weakly intense peaks of GA nanocrystals are observed. The width of the signal (Fig. 3*b*) can be used to estimate the size of the crystallites, which, according to the Debye-Scherrer formula, are about 40 nm.

The state of water adsorbed on the surface at the same (h = 100 mg/g) hydration of the samples can be determined using IR spectroscopy data (Fig. 4). Water is observed as several merged signals v^{-1}=2750–3800 cm^{-1}. In all composite systems, there is also a low-intensity signal of silanol groups that do not participate in the formation of hydrogen bonds at v^{-1}=3750 cm^{-1}.The ^1H NMR spectra of water in the studied samples of hydrated silica A-300 and composite systems created on its basis, taken at different temperatures, are shown in Fig. 5. The measurements were carried out in air and in a weakly polar organic solvent – chloroform. In order to prevent the appearance of an intense signal of liquid-phase chloroform protons in the spectra, its deuterated form ($CDCl_3$) was used, in which the content of non-deuterated chloroform was less than 0.5%. The signal of residual amounts of $CHCl_3$ is observed in some samples containing chloroform as a weakly intense signal with a chemical shift of δ_H = 7.2–7.5 ppm (Fig. 5).

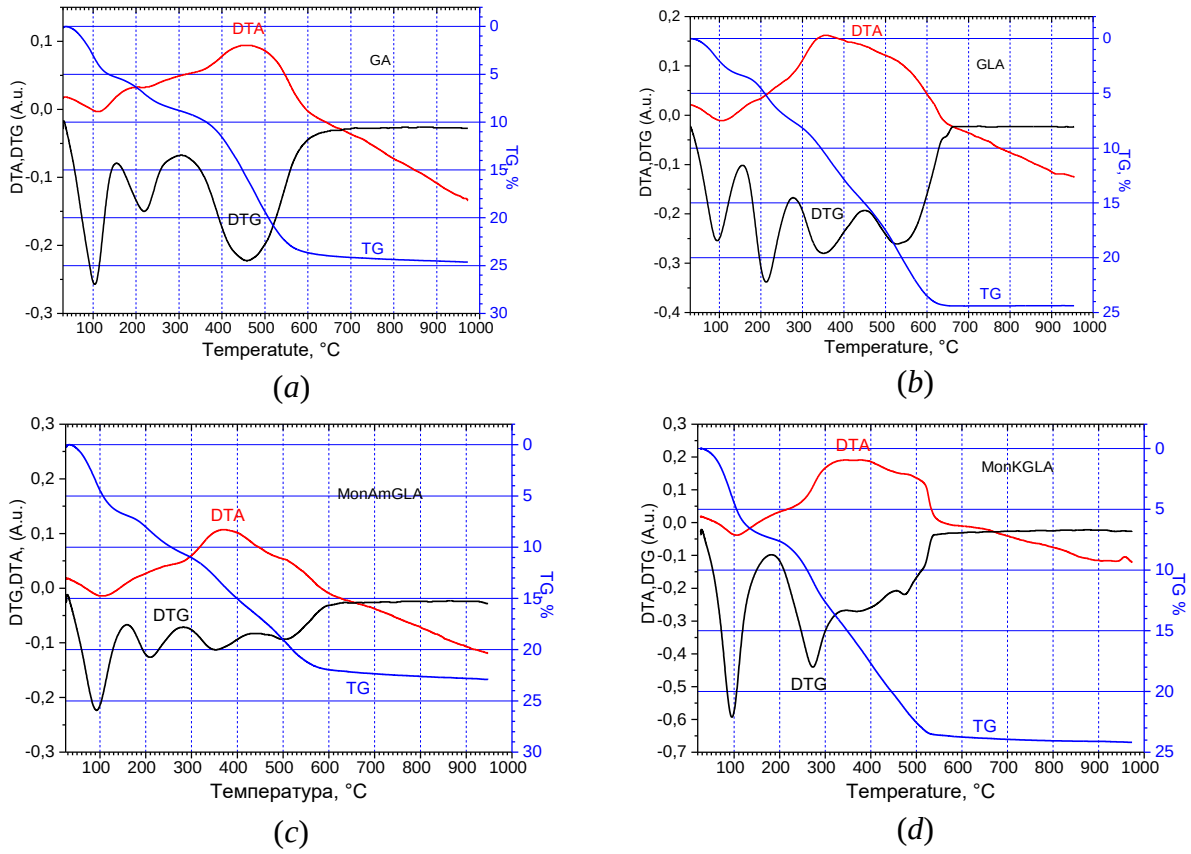

Fig. 1. Thermograms of composite systems prepared on the basis of nanosilica, gallic acid (*a*), glycyrrhizic acid (*b*), its monoammonium (*c*) and monopotassium (*d*) salts

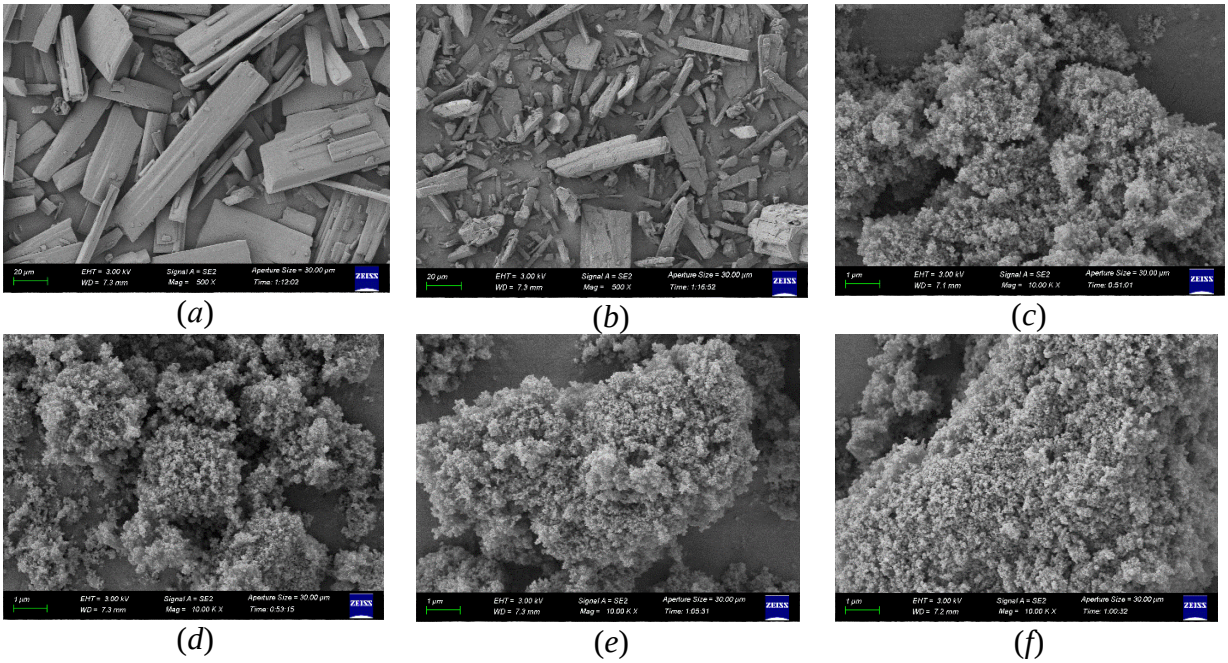

Fig. 2. Electron micrographs of the initial powders of GA, GLA and composite systems prepared by mechanical treatment of mixtures of acids (or salts) with A-300 nanosilica powder: GA (*a*); GLA (*b*); composite system GA/SiO_2 (*c*); composite system GLA/SiO_2 (*d*); composite system MonKGLA/SiO_2 (*e*); composite system MonAmGLA/SiO_2 (*f*)

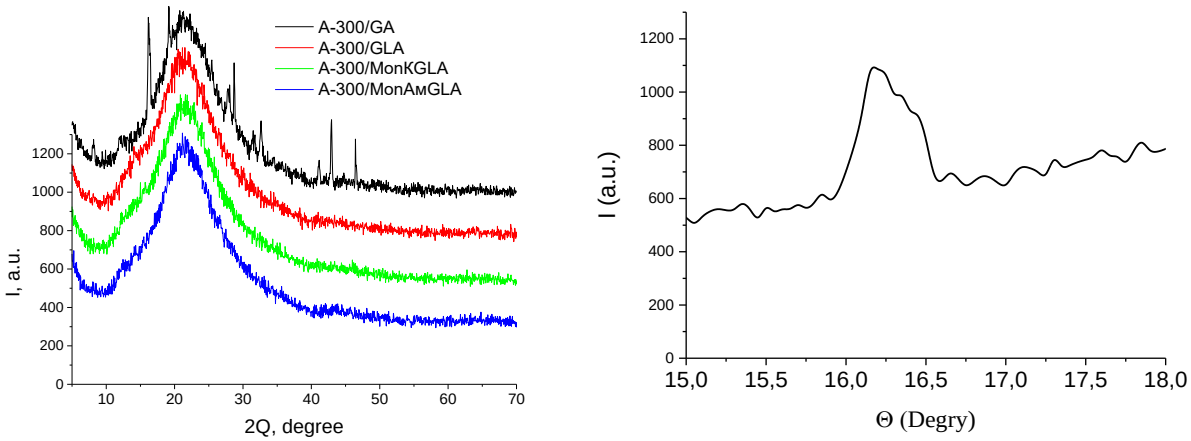

(*a*) (*b*)

Fig. 3. X-ray diffraction patterns of composite systems obtained by immobilizing GA, GLA and its salts on the surface of A-300 nanosilica (*a*); the width of the residual peak of the crystalline form of GA immobilized on the surface of A-300 (*b*)

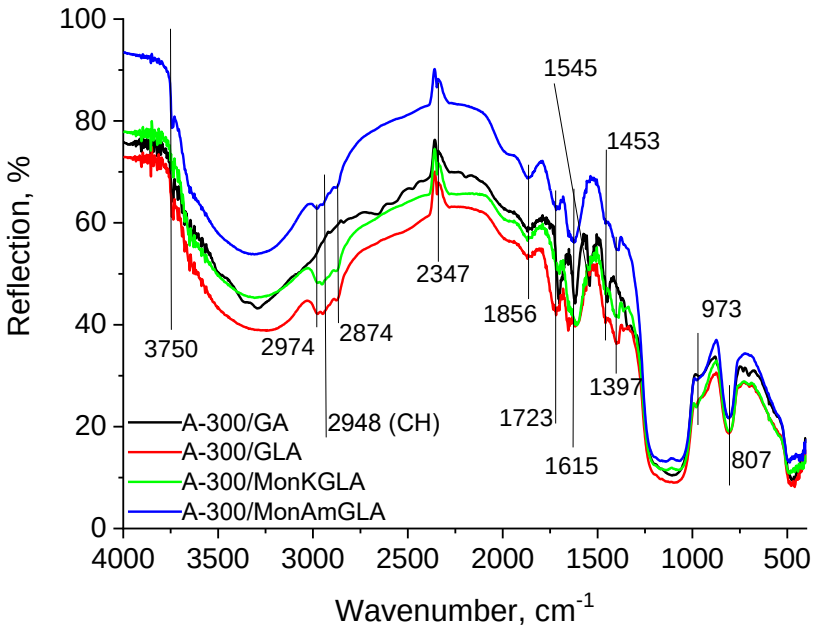

Fig. 4. IR spectra (reflection) of composite systems prepared on the basis of GA, GLA and its salts at h = 100 mg/g

The main signal of water (Fig. 5) is observed in the spectra in the temperature range of 215–287 K at δ_H = 4–6 ppm. The chemical shift of water corresponds to strongly associated water (SAW), each molecule of which takes part in the formation of 2.5–3 hydrogen bonds with neighboring molecules [22]. In addition to it, in a chloroform medium (and in some samples in air), the spectra contain a relatively weak signal of weakly associated water (WAW, δ_H = 1–1.5 ppm), corresponding to water molecules either not participating in the formation of hydrogen bonds or included in clusters in which there are few such bonds (on average, less than one hydrogen bond per water molecule). The fact that the SAW and WAW signals are observed separately indicates that these clusters exchange water molecules (or protons) slowly (on the NMR time scale) [48]. They are probably spaced apart or separated from each other by a layer of chloroform.

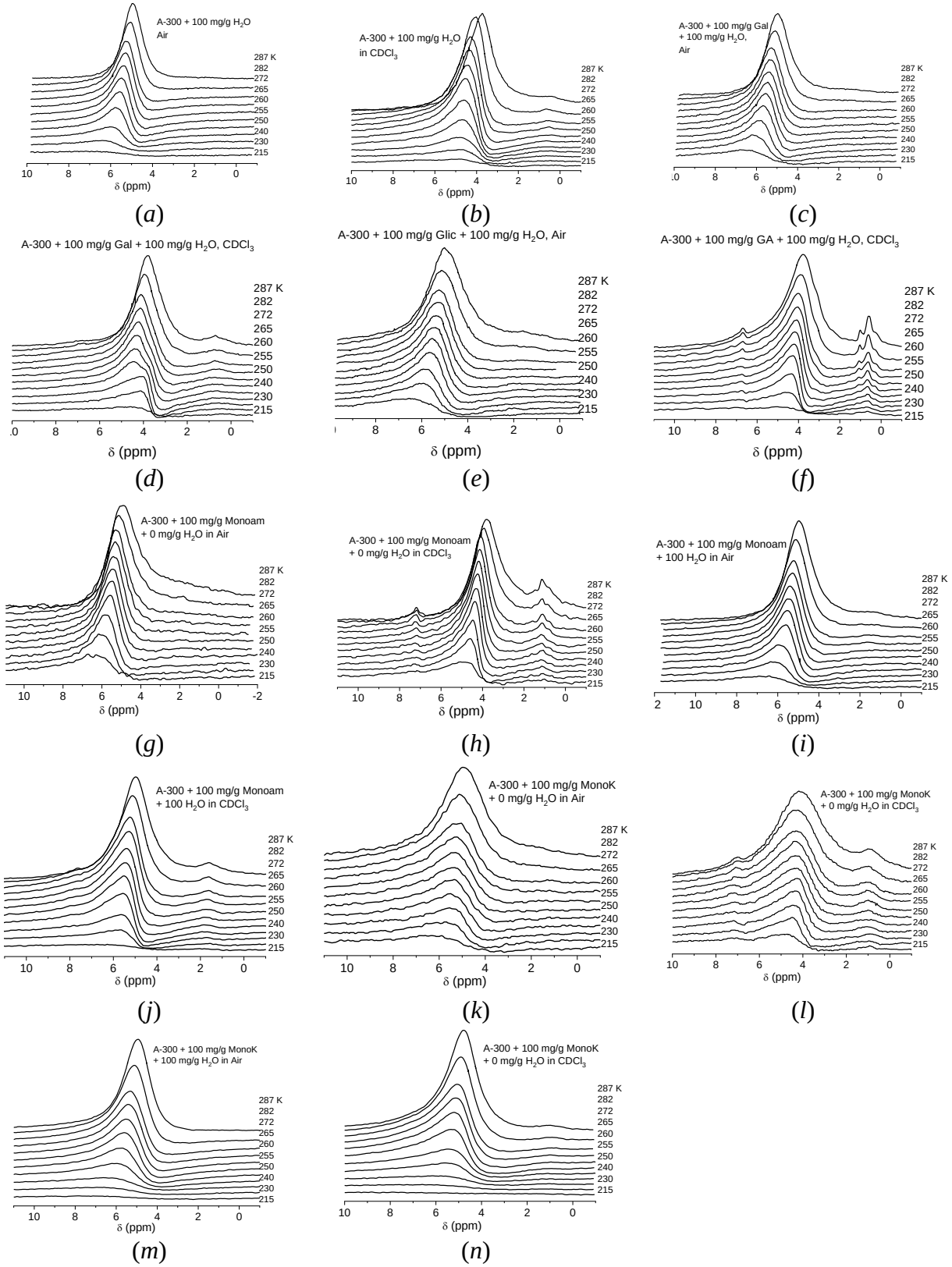

Fig. 5. ^{1}H NMR spectra of water in hydrated silica A-300 (*a*, *b*) taken at different temperatures; composite systems created on the basis of pyrogenic silica A-300 and galic acid (*c*, *d*); A-300 and GA (*d*, *f*); A-300 and monoammonium salt of GLA (*g*, *h*, *i*, *j*); A-300 and monopotassium salt of GLA (*k*, *l*, *m*, *n*) in air and in a medium of a weakly polar organic substance – deuterochloroform

A significant decrease in the freezing temperature of interfacial water is due to adsorption interactions, which in nanostructured systems are caused by the effects of water clustering and changes in the structure of the hydrogen bond network [22, 49]. With decreasing temperature, the intensity of the water signal decreases as smaller and smaller water clusters freezes. It should be noted that Fig. 5 records the reverse process - an increase in temperature from the minimum value (T = 215 K) up to T = 287 K, i.e. the process of melting of water clusters from the smallest (at low temperature) to large (at high temperature) is observed. The large width of the SAW signal can be associated with the presence of several types of water clusters with slightly different chemical shift values, which overlap. With decreasing temperature, the chemical shift of the SAW signal increases due to the increase in the ordering of the hydrogen bond network in the SAW clusters.

If we assume that at T = 287 K all the water is in a liquid state and is equal to the total hydration of the sample (h = 50 or 150 mg/g), then the amount of non-freezing water ($C_{uw} = h \cdot I/I_{287}$) can be easily calculated from the intensity of the water signal at an arbitrary temperature (I). For the studied systems, the corresponding dependencies are shown in Fig. 6*a*, *b*. Since there is a directly proportional dependence [50] between the free energy of ice and temperature in a wide temperature range (T < 273 K), and under equilibrium conditions the free energy of ice is equal to the free energy of non-freezing water, the dependences $C_{uw}(T)$ can be transformed into dependences of the change in the Gibbs free energy on the concentration of non-freezing water (Fig. 6*c*, *d*). From the data in Fig. 6 it follows that during the heating of the samples, not all interfacial water passes from the solid to the liquid state. Some of it remains solid up to T = 287 K. That is, the surface of composite systems is capable of stabilizing the metastable state of ice (MsIce) in nanosized pores in a wide temperature range. The amount of such metastable ice is quite large and can reach 10–15% of the total water content in the samples.

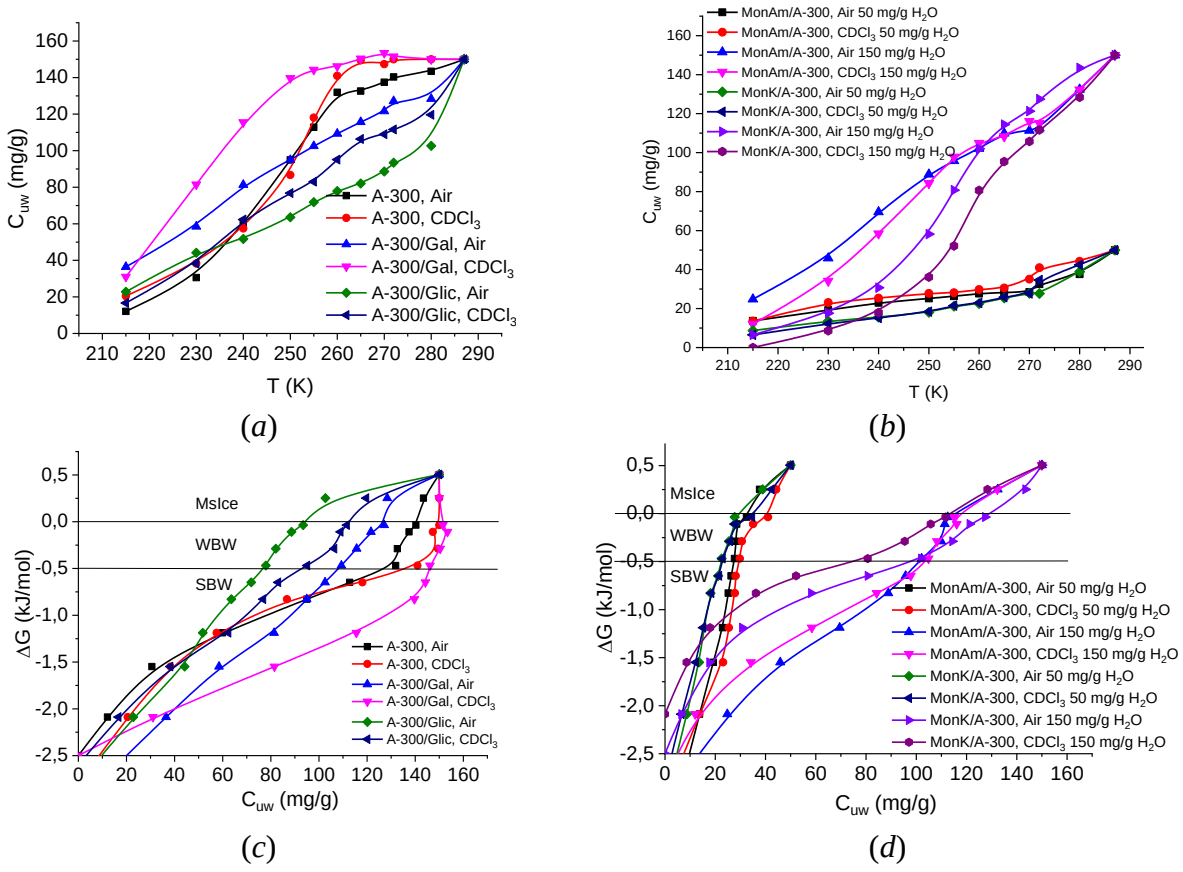

Fig. 6. Temperature dependences of the concentration of non-freezing water (*a*, *b*) and the dependences of the change in Gibbs free energy on the concentration of non-freezing water constructed on their basis (*c*, *d*)

The part of water that freezes at $T > 265$ K ($\Delta G < 0.5$ kJ/mol) is weakly bound (WBW), and the rest is strongly bound (SBW) [22]. The amounts of strongly bound (C_{uw}^{S}), weakly bound (C_{uw}^{W}) water and metastable ice (C_{ms}^{Ice}) for all the studied systems are given in Table 1. In addition, Table 1 presents the values of the maximum decrease in the Gibbs free energy in the layer of strongly bound water (ΔG^{S}) and the interfacial energy (γ_S), which is determined in accordance with formula (1) and is equal to the total decrease in the free energy of interfacial water caused by adsorption interactions. For clarity, the γ_S values of the studied systems are presented in the form of diagrams in Fig. 7.

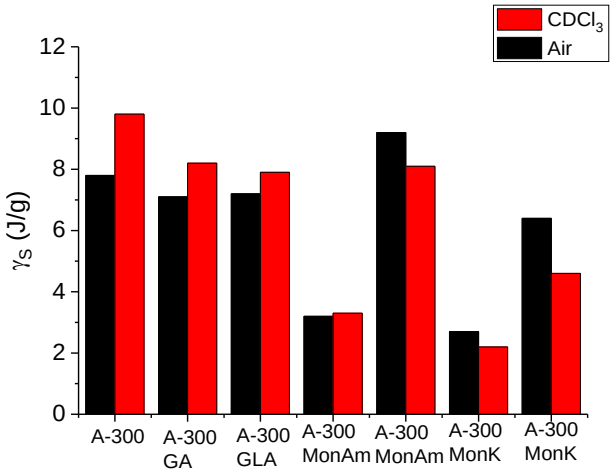

Fig. 7. Diagrams of the change in interfacial energy depending on the composition of the composite, the environment and the amount of adsorbed water

Table 1. Thermodynamic characteristics of interfacial water in hydrated silica A-300 and composite systems based on it in air and $CDCl_3$

System	h (mg/g)	C_{uw}^{S} (mg/g)	C_{uw}^{W} (mg/g)	C_{ms}^{Ice} (mg/g)	ΔG^{S} (kJ/mol)	$-\gamma_S$ (J/g)	$+\gamma_S^{Ice}$ (J/g)
A-300, Air	150	125	15	10	-2.5	7.8	0.15
A-300, $CDCl_3$	150	140	10	0	-2.8	9.8	-
A-300/GA, Air	150	110	15	25	-3.0	7.1	2.10
A-300/GA, $CDCl_3$	150	145	5	0	-2.5	8.2	-
A-300/GLA, Air	150	75	20	55	-2.8	7.2	1.10
A-300/GLA, $CDCl_3$	150	95	15	40	-2.6	7.9	0.68
A-300/MamGLA, Air	50	28	5	17	-3.5	3.2	0.29
A-300/MamGLA, $CDCl_3$	50	30	11	9	-3.0	3.3	0.14
A-300/MamGLA, Air	150	100	15	35	-3.0	9.2	0.49
A-300/MamGLA, $CDCl_3$	150	105	15	30	-2.8	8.1	0.44
A-300/MKGLA, Air	50	22.5	10	17.5	-3.0	2.7	0.27
A-300/MonKGLA, $CDCl_3$	50	22.5	7.5	10	-2.8	2.2	0.21
A-300/MonKGLA, Air	150	100	30	20	-2.5	6.4	0.23
A-300/MonKGLA, $CDCl_3$	150	75	35	40	-2.1	4.6	0.60

Among the general regularities in the dependence of the interfacial energy on the solid component and the observation environment, it should be noted that in an air environment, immobilization of GA or GLA on the silica surface has little effect on the γ_S value, although the amount of strongly bound water decreases noticeably. Probably, the effect of decreasing C_{uw}^{S} is compensated by some increase in the amount of WBW and MsIce (Table 1). Unlike many systems described earlier [22], a weakly polar organic environment leads to an increase in the interfacial energy (Fig. 7). This tendency is not observed for GLA salts immobilized on the surface of A-300 silica. For the monopotassium salt of GLA, a significant decrease in the γ_S value is recorded compared to the original silica both in an air environment and in a $CDCl_3$ environment.

The formation patterns of metastable ice should be particularly discussed. In the initial silica, superheated ice is practically not formed (Fig. 6*a*, *c*, Table 1). Immobilization of organic acids, regardless of their chemical nature, promotes the stabilization of metastable ice. The chloroform environment in all systems reduces its amount.

The described regularities can be largely determined by the influence of the heterogeneous system surface on the structure of adsorbed water clusters, calculated in accordance with Eq. (2) (Fig. 8). In the initial silica (h = 150 mg/g), two maxima are observed in the distributions at R = 1.5 and 2.5 nm. In a chloroform medium, the average radius of water clusters increases slightly due to the fact that the maximum at R = 2.5 disappears, and one maximum is formed instead at R = 2 nm. Immobilization of GA or GLA on the silica surface leads to the formation of a large number of small water clusters on the surface, but at the same time the shape of the distribution curves changes, and some of the interfacial water is in the form of metastable ice. A chloroform medium stabilizes the formation of relatively large water clusters, but this does not lead to a decrease in the interfacial energy. In composite systems based on GLA salts, the type of distributions becomes more complicated. A significant number of both small and large clusters of adsorbed water are present.

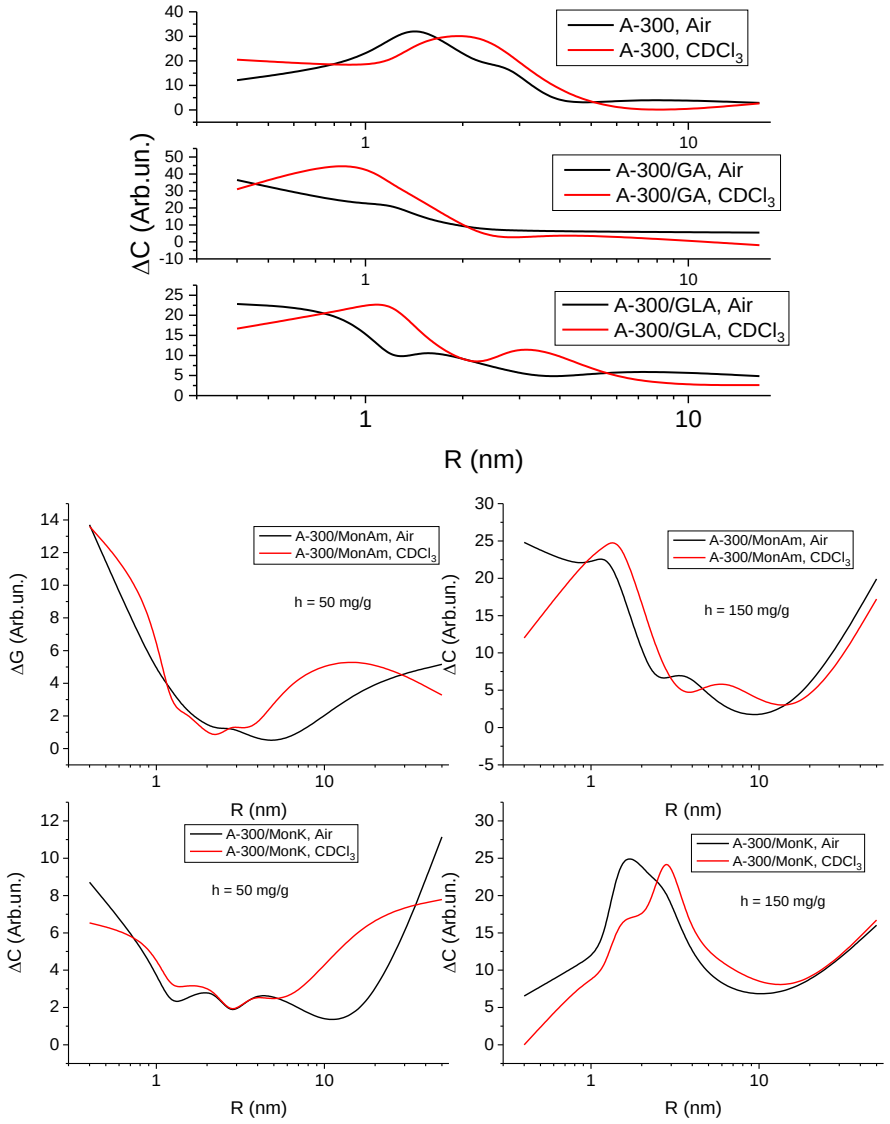

Fig. 8. Distributions of adsorbed water cluster radii in the original silicas and composite systems created on its basis

Rheological measurements are usually used for viscous continuous media consisting of concentrated solutions of low-molecular substances, polymer solutions, suspensions of solid particles in aqueous or organic liquids, and emulsions formed by liquids that are insoluble in each other [51–54]. In this case, the viscoelastic properties are primarily influenced by the interphase interactions of the substances that make up the heterogeneous system. Based on the dependences of viscosity on shear load, the ratio of the concentrations of the solid and liquid phases, temperature, and other parameters, it is possible to draw reasonable conclusions regarding the phase state of the system. The general principles used in the mechanics of liquid fluids can also be transferred to studies of the properties of hydrated powders or solid suspensions. In this case, the rheometer should be classified as a destructive method, which can lead to a partial or complete irreversible change in the sample during the measurement process.

For hydrated powders of the original silica and silica with GA, GLA and its salts immobilized on its surface, measurements were made of the complex viscosity as a function of the magnitude of shear deformation (Fig. 9*a*, *b*) and the viscosity as a function of the shear rate (Fig. 9*c*, *d*).

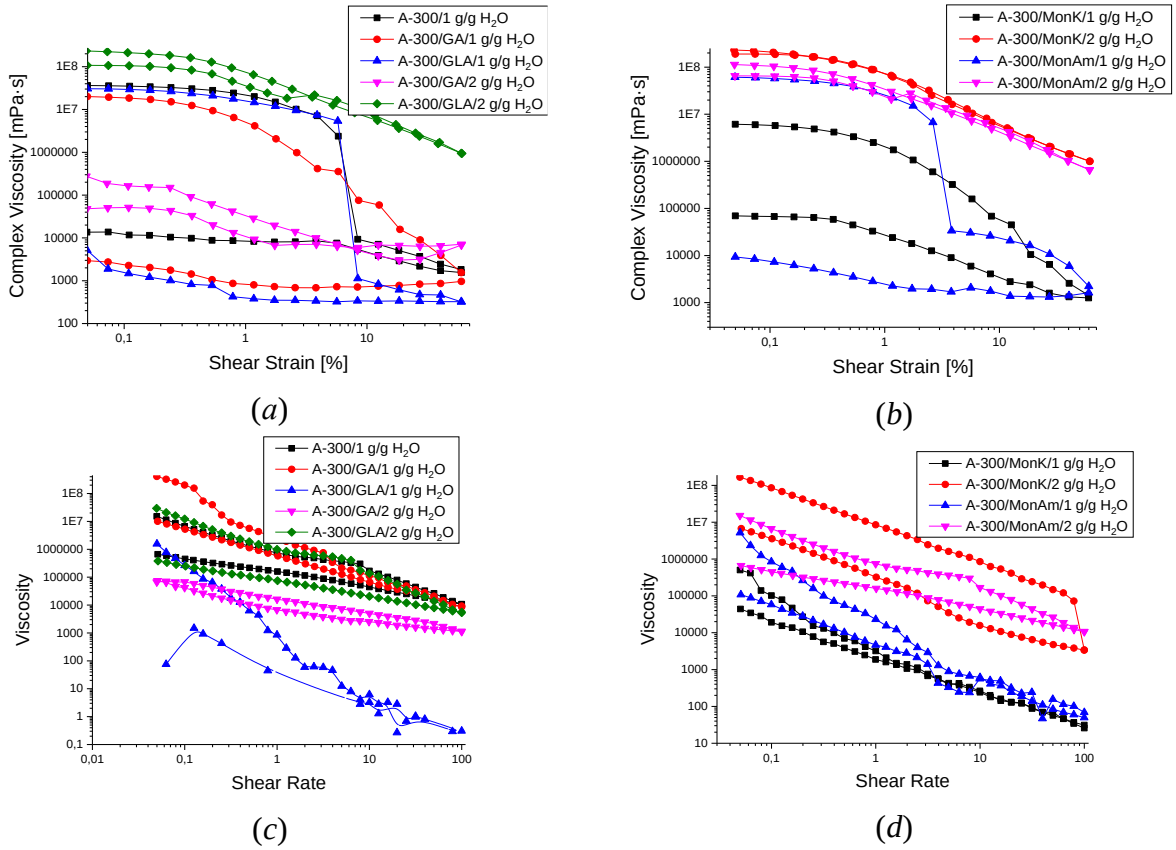

Fig. 9. Dependences of complex viscosity on the magnitude of shear deformation (*a*, *b*) and viscosity on the shear rate (c, d) for hydrated powder of compacted silica A-300 and silica with GA, GLA and its salts immobilized on its surface

For different types of dispersed systems, the type of dependences $\eta(\gamma)$ differs greatly. This is due to the complex nature of the dependence of the complex viscosity on the composition of the colloidal system and the molecular interactions occurring in it during the mechanical action of the rheometer rotor on the hydrated silica powder with substances immobilized on its surface. Unlike aqueous suspensions, in hydrated powders in the interparticle gaps there can be not only organic substances and water adsorbed to the surface, but also air, the volume of which can be comparable to the volume of water. Under the influence of the mechanical load created by the rheometer, there can be a reorganization of silica aggregates, the movement of organic substances along its surface

and partial removal of air from the interparticle gaps (which is accompanied by an increase in the bulk density of the material). Accordingly, significant changes in the dynamic viscosity of the samples under study will occur.

The initial silica after its preliminary compaction has a bulk density of C_d = 200 mg/cm^3. After it absorbs 1 g/g of water, the bulk density increases approximately twofold. However, a significant part of the interparticle gaps continues to be filled with air. At the initial section of the $\eta(\gamma)$ curve for the initial silica (Fig. 9*a*), some decrease in the complex viscosity with increasing shear strain is observed. Then, at γ = 7%, a sharp jump in the η value occurs, indicating a fundamental change in the state of the sample. The probable cause is the partial (or complete) removal of air from the interparticle gaps of the silica, which is accompanied by the formation of a continuous (or almost continuous) water film in them, which ensures easy displacement of the silica particles relative to each other under load. In fact, a phase transition of the solid-water-air system into the solid-water system takes place. This system remains stable even in the case of a decrease in the dynamic load.

The dependence $\eta(\gamma)$ for silica with glycerol acid immobilized on its surface has a similar appearance (Fig. 9*a*). In the case of gallic acid, the process of air removal from the interparticle gaps and the formation of a continuous water film in them does not have a stepwise nature, but is extended over a wide range of shear load changes. As expected, an increase in the amount of adsorbed water reduces the amount of air in the interparticle gaps and the dependences $\eta(\gamma)$ become smoother (Fig. 9*a*). It should be noted that an increase in the amount of water in the sample can lead to both a decrease in the dynamic viscosity in the case of GA (relative to the initial one) and to its significant increase in the case of GLA (Fig. 9*a*). A probable cause of the increase may be the formation of a viscous GLA hydrate in the interparticle gaps of silica, which sharply increases the magnitude of interparticle interactions.

For the GLA salts immobilized on the silica surface, the presence of a large amount of air in the interparticle gaps, which is removed during the growth of the mechanical load, is observed for the A-300/MonAmGLA sample containing 1 g/g of adsorbed water (Fig. 9*b*), and for A-300/MonKGLA the process of air removal is extended over a wide range of shear load. For the samples containing 2 g/g of adsorbed water, a strong increase in viscosity is observed, caused by the "gluing" of silica particles by hydrated acid salts.

For comparison, Fig. 9*c*, *d* shows the viscosity measurements from the shear rate for all the studied systems. In contrast to the data on the complex viscosity measurements, these measurements turned out to be significantly less informative, since they do not explicitly contain information regarding the ratio of the shares of mechanical energy spent on plastic deformation and the reorganization of the internal structure of the particles of the sample.

So, when immobilized by the method of joint grinding in a porcelain mortar on the surface of pyrogenic silica A-300 organic acids, which differ greatly in chemical nature (GA, GLA and its salts), they pass into a nanosized X-ray amorphous state.

Water adsorbed on the surface of such composite systems is also in a clustered state, and the radius of the adsorbed water clusters is in the range of 0.4–50 nm. The chloroform environment has a complex effect on the size of the water clusters. In general, there is a tendency for the radius of water clusters to increase when air is replaced by a chloroform environment. However, this does not always lead to a decrease in the interfacial energy.

The possibility of the existence of metastable ice in the temperature range up to 287 K, stabilized by the surface of composite systems, was discovered. The amount of such ice can reach 20% of the total water content in the sample.

The possibility of using the measurement of the complex viscosity of hydrated silica powders and silica containing immobilized GA, GLA or its salts to study the processes of interparticle and interphase interactions in complex systems containing solid, liquid and gaseous phases, as well as their change under the influence of periodic mechanical loading is shown.

STABILIZATION OF WEAKLY ASSOCIATED WATER FORMS BY THE SURFACE OF COMPACTED METHYLSILICA AND ITS COMPOSITES WITH BETULIN

Betulin is a white powder with a bitter taste, soluble in alcohol, ether, chloroform and benzene, slightly soluble in cold water, petroleum ether and other organic solvents. It exhibits various types of biological activity and is used in the synthesis of compounds of interest as pharmaceuticals, in particular for the production of betulinic acid. The main source of betulin is birch bark, from which it was isolated almost a century ago [55–64]. It is obtained by boiling birch bark in water, followed by extraction with organic solvents, in particular alcohols. Most of the betulin is found in the outer part of the bark, which provides the birch's white color. The content of belulin in the outer part of the birch bark ranges from 10 to 35%. In addition to birch, betulin is also found in other plants. In particular, alder bark, thistle heart, some types of orchids, etc.

Betulin is an effective means of complex treatment of cancer patients. It stimulates the ability of white blood cells to produce interferons, thus strengthening the immune defense, which helps prevent metastasis [65–74]. Tumor cells can grow in conditions of oxygen deficiency, they transform energy metabolism in such a way that, compared to normal cells, they consume 20 times more nutrients. There are many more lipid channels in the membrane of tumor cells through which nutrients enter; these channels are essentially “holes”. Since the betulin molecule is a triterpenoid alcohol, it binds to lipids in the tumor cell membrane, which makes cell membranes denser, partially blocking the supply of nutrients to tumor cells. Betulin does not have this kind of effect on healthy cells, since the membrane of a healthy cell is more stable.

The low bioavailability of betulin is largely due to poor solubility in aqueous media. The weak hydrophilic properties of betulin make it difficult for it to penetrate into liquid water structured by a network of hydrogen bonds [75–80]. As well-known water's form with broken hydrogen bonds is water in the supercritical state, that is located at a temperature above 374 K and a pressure greater than 221 atm. The physico-chemical properties of such water are completely different from liquid water. Its dielectric constant decreases by almost an order of magnitude, it is able to easily dissolve non-polar substances, while maintaining the ability to dissolve inorganic salts. Under normal conditions, non-associated (not involved in the formation of hydrogen bonds) water is encountered when studying water dissolved in weakly polar organic substances or located in a gaseous state, but its concentration or density is not high [81, 82].

Water at the interfacial boundary of some types of adsorbents, among which chemically and structurally modified silicas are of particular interest, can serve as an analogue of rather dense aggregates of weakly associated water (WAW). Precisely in them, in a hydrophobic medium, the presence of a significant amount of weakly associated forms of water was recorded [83–87]. Like supercritical water, WAW is miscible with weakly polar substances and, therefore, can provide transport substances that are poorly soluble in water, such as betulin, from the surface to the absorption site of the gastrointestinal mucosa.

The aim of the work was to create a composite system in which betulin is immobilized on the surface, stabilizing a significant amount of water in a weakly associated state, and its removal to the external environment is limited by the formation of a mixture of WAW and a weakly polar organic substance added to the composite, as well as a certain amount of air in the interparticle gaps.

The TEM micrograph of the used methylsilica AM1 is shown in Fig. 10. AM1 is based on primary particles with a radius of 5–20 nm. They form aggregates up to 100 nm in size, which, in turn, are part of agglomerates (1–20 μm). There are cavities in the gaps between methylsilica aggregates, which provide the porous structure of the material.

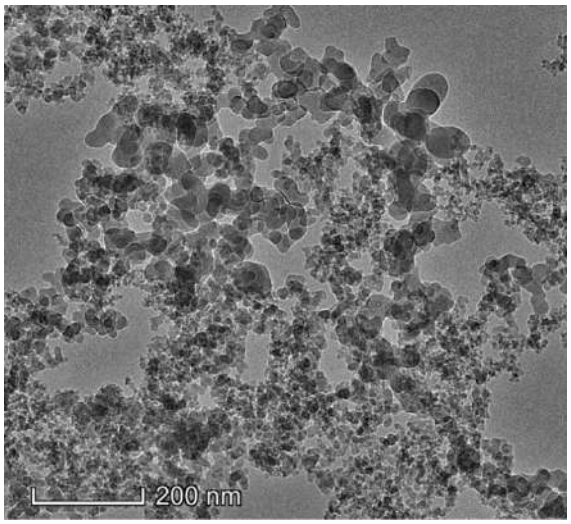

Fig. 10. TEM micrograph of methylsilica AM1 (TECNAI G2 F30, FEI-Philips)

In the IR spectra of methylsilica hydrated by compacted (Fig. 11), containing 20 mg/g of water in the range of 3400–3900 cm^{-1}, there are bands corresponding to monomeric molecules and small (2–3 molecules) associates of water [88]. The fragmentation of the bands in the absorption region of water hydroxyl groups can be associated with the presence of clusters of unassociated water of different sizes. However, the spectra do not contain bands characteristic of water structured by a network of hydrogen bonds or they are weakly intense.

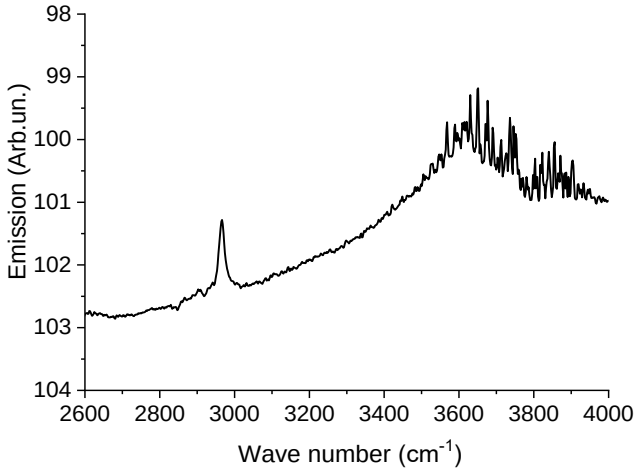

Fig. 11. IR spectrum of "wetting-drying" methylsilica AM1 after 20 min treatment containing 20 mg/g of residual water (reflection spectrum obtained on a Shimadzu spectrometer, Japan)

Betulin produced by Aldrich with a purity of 99.9% was used. Powders of methylsilica AM1 and betulin were mixed in a ratio of 4/1 to prepare the composite system. The mixture was thoroughly ground in a porcelain mortar until a compacted material with bulk density C_d = 150–200 mg/cm^3 was formed, which corresponded to compaction of the initial methylsilica in 3–4 times. Hydrated powders were obtained in two ways. In the first method, 100 mg/g water was added to the composite, shaken for 2-3 minutes in a glass vessel and left to equilibrate for 2–3 hours. In the second method, mechanochemical activation was carried out in a porcelain mortar with the required amount of water for 5–10 minutes. Wherein, the composite system was additionally compacted to C_d = 250 mg/cm^3; however, in this case, some part of the water could evaporate from the composite system. The hydration of individually taken methylsilica was also carried out in a similar way [89–91]. In the following, mechanically activated samples of composites are designated as “MA” in the figures.

Conclusions about the structure of water as a system of molecules involved in the formation of a network of hydrogen bonds can draw by determining the chemical shifts of adsorbed water. Herewith into account the fact that the maximum number of hydrogen bonds in which each water molecule can participate equals four. This case is realized for hexagonal ice, in which protons have a chemical shift δ_H = 7 ppm [91]. Non-associated water in the gas phase has a chemical shift δ_H = 0–1 ppm [92]. That is, the average number of hydrogen bonds that each water molecule formscan estimate by the value of the chemical shif [22, 92]. Liquid water is characterized by the value of the chemical shift of protons δ_H = 5 ppm, which indicates the formation of 2–3 hydrogen bonds by each molecule. Usually, as the temperature decreases, the chemical shift of adsorbed or liquid water increases, which is due to an increase in the orderliness of the hydrogen bond network. We can think that in the case when δ_H < 2 ppm weakly associated water (WAW), and in the case of δ_H > 4 ppm is strongly associated water (SAW) [22, 92]. In this case, however, it should be taken into account that the addition of acidic products prone to dissociation of protons (for example, strong acids or hydrogen peroxide) to the system, the chemical shift of water protons is determined not only by the association of its molecules, but also by hydrated protons, the chemical shift of which can be δ_H = 9–12 ppm [22].

Recorded at different temperatures ^{1}H NMR spectra of water, adsorbed on betulin powder are shown in Fig. 12*a*. One signal is observed in the spectra with a chemical shift δ_H = 5 ppm, the intensity of which decreases with decreasing temperature in accordance with the freezing of adsorbed water. On the basis of measuring the intensity of the signal of non-freezing water, its concentrations (C_{uw}) were calculated at different temperatures (Fig. 12*b*), and using formulas 1–3, the dependences of the change in the Gibbs free energy on the concentration of non-freezing water and the distribution of adsorbed water clusters over the radii (Fig. 12*c*, *d*, respectively).

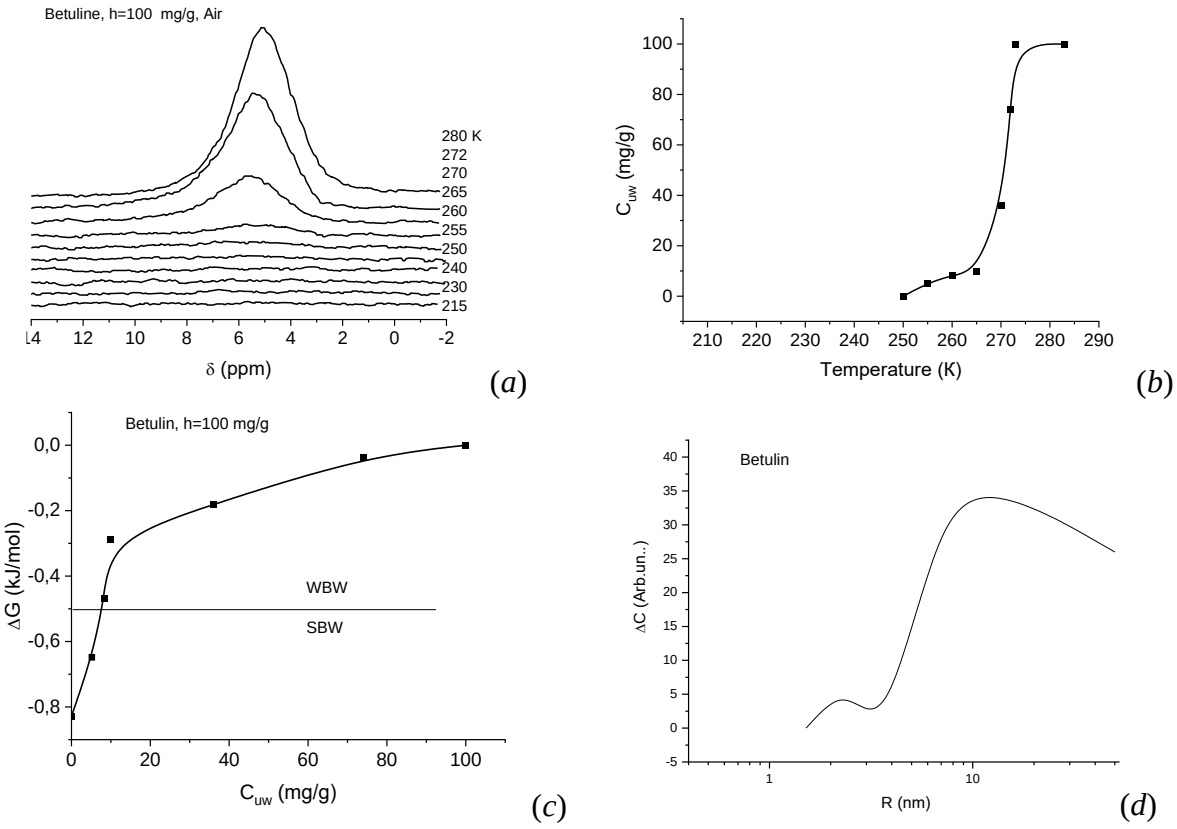

Fig. 12. Recorded at different temperatures ^{1}H NMR spectra of water (*a*), temperature dependence of the concentration of non-freezing water (*b*), dependence of the change in the Gibbs free energy on the concentration of non-freezing water (*c*) and size distribution of adsorbed water clusters for hydrated betulin powder at *h* = 100 mg/g

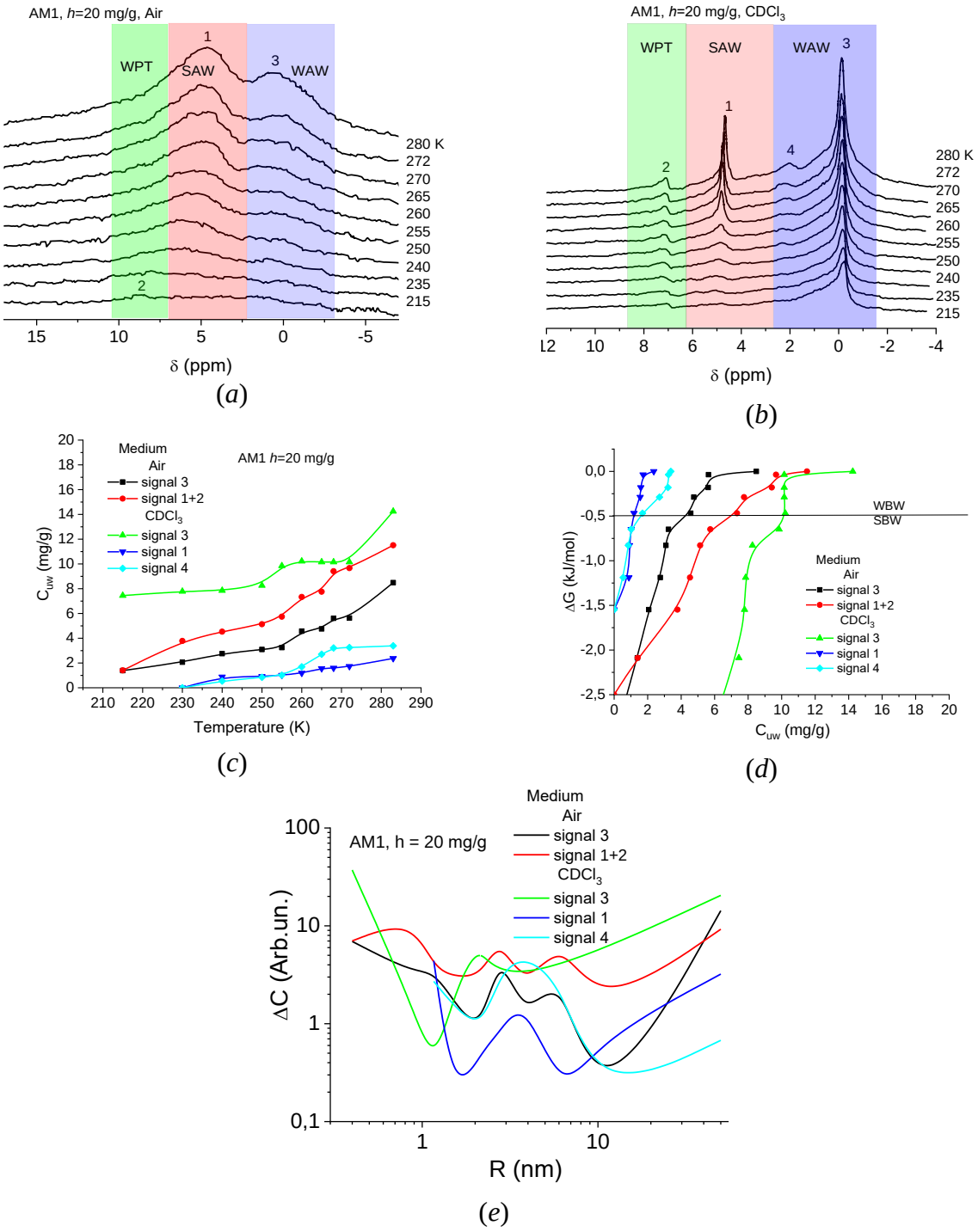

Fig. 13. Recorded at different temperatures ^{1}H NMR spectra of water, adsorbed by AM1 metylsilica in air (*a*) and in $CDCl_3$ medium (*b*), the temperature dependences of the concentration of different forms of non-freezing water (*c*), dependences of the change in the Gibbs free energy on the concentration of non-freezing water (*d*) and radial distribution of adsorbed water clusters at h = 20 mg/g (*e*)

Thermodynamic properties of interfacial water are shown in Table 2. In this case, the amount of strongly and weakly bound water (C_{uw}^S и C_{uw}^W, respectively) was determined, which were calculated on the basis of the dependences $\Delta G(C_{uw})$, assuming that water in which ΔG < -0.5 kJ/mol refers to strongly bound; the value of the water-surface interfacial energy, which determines the total decrease in the free energy of water, due to the presence of a phase boundary,

and the maximum decrease in the Gibbs free energy in a layer of strongly bound water – ΔG^S, which characterizing the maximum influence of the surface on the water that is on the border with it. Since, depending on the type, clusters differ in the amount of the substance included in their composition, to compare their energy contribution to the interfacial energy, one can use the specific value $\gamma_S^* = \gamma_S/(C_{uw}^W + C_{uw}^S)$. In fact, the specific interfacial energy characterizes the decrease in the free energy of water in clusters of a certain type, assigned per unit mass of this water. For each group of signals related to one system in Table 2 also shows the total values of interfacial energy $\Sigma\gamma_S$, related to all water, regardless of its type.

Since the signal of water adsorbed by betulin has a chemical shift δ_H = 5 ppm, all adsorbed water can be considered strongly associated, the structure of which is close to that of liquid water. It exists predominantly in the form of clusters with R = 20–50 nm. The content of water clusters with R = 2–5 nm does not exceed 5% (Fig. 12*d*). Since the free energy of water in large clusters differs weakly from the free energy of bulk water, the main part of water is weakly bound (Fig. 12*c*, Table 2) and the interfacial energy of the water–surface system is only 0.93 J/g. Accordingly, betulin is a weakly hydrophilic agent, which is probably the reason for its poor solubility in water.

The ^{1}H NMR spectra recorded at different temperatures of water, adsorbed in AM1 interparticle gaps in air and in $CDCl_3$ medium, the temperature dependences of the concentration of different forms of non-freezing water, and size distribution of adsorbed water clusters when 100 mg/g of water is used for "wetting-drying" compacted are shown on Fig. 13. In the process of mechanochemical activation, 80 mg/g H_2O evaporated, i.e. h = 20 mg/g.

Table 2. Characteristics of interfacial water in hydrated betulin, methylsilica AM1 and composites 4/1 AM1/Betulin

Sample/*h* (mg/g)	Medium	Signal	C_{uw}^S (mg/g)	C_{uw}^W (mg/g)	ΔG^S (kJ/mol)	γ_S/γ_S^* (kJ/g)
Betulin/100	air	3	17	83	-0.8	0.93/9.3
AM1 Activated with water/20	air	3	4.4	3.6	-3	0.4/50
		1+2	7.2	3.8	-2.5	0.62/56 $\Sigma\gamma_S$ 1.02
	$CDCl_3$	3	10.2	3.6	-6	1.8/130
		1	1.2	1.2	-1.5	0.09/41
		4	1.6	1.6	-1.5	0.11/30.5 $\Sigma\gamma_S$ 2.0
AM1/Betulin/100	air	1-3	9	91	-2.2	1.18/11.8
AM1/Betulin Activated with water/100	air	1	27	68	-2.2	2.39/25.2
	$CDCl_3$	3	27	8	-5	4.05/115
		1	15	49	-2.2	1.56/24.4 $\Sigma\gamma_S$ 5.61

Several signals are present in the spectra which related to different forms of adsorbed water. In an air medium (in addition to water, the interparticle gaps contain air, Fig. 5*a*) at low temperatures, water signals with chemical shifts δ_H = 0 and 8 ppm are observed are signals 3 and 2, respectively. As the temperature rises, signal 2 transforms into signal 1 with a chemical shift δ_H = 5–6 ppm. Signal 3 refers to water that does not form hydrogen bonds (weakly associated water), signals 1 is to strongly associated water. The chemical shift of the water responsible for signal 2 exceeds the maximum chemical shift value for tetracoordinated water (δ_H = 7 ppm). Therefore, a certain part of the water molecules responsible for this signal is probably in the protonated state (the state with the transferred H_3O^+ proton, WPT). Thus, it can be stated that a essential part of the water in compacted methylsilica AM1 can be in a weakly associated state and forms aqueous systems with a broken network of hydrogen bonds. Weakly associated water should be considered as an analogue of supercritical water, which exists at low temperatures and pressures only in the form of nanosized clusters.

Replacing the air medium with a medium of a weakly polar organic solvent, deuterochloroform (Fig. 13*b*), stabilizes the weakly associated forms of water to an even greater extent. About 75 % of the water present in the interparticle gaps can be considered weakly associated. In addition, signal 4 appears in the spectra with a chemical shift δ_H = 2 ppm, which corresponds to water with a partially broken network of hydrogen bonds. It is likely that a concentrated mixture of weakly associated water and chloroform, stabilized by a hydrophobic surface, is formed in the nanosized interparticle gaps AM1.

As the temperature decreases, all types of interfacial water freeze, forming ice (Fig. 13*c*). For SAW, this is a natural process − as a result of freezing, a tetragonal structure of hexagonal ice is formed. However, the formation of ice from WAW and its structure are unknown. It can be assumed that WAW freezes in the form of amorphous ice, since upon thawing (fluctuation), it again passes into a weakly associated state with a broken network of hydrogen bonds. Both SAW and WAW are characterized by the presence of not only strongly but also weakly bound water (Fig. 13*d*, Table 2), i.e. water, in which the change in free energy due to adsorption interactions does not exceed 0.5 kJ/mol. Therefore, the WAW freezing process can be carried out with little energy consumption. The total interfacial energy ($\Sigma\gamma_S$) in the weakly polar medium of chloroform turned out to be twice as high as in the air medium (Table 2). That is, chloroform stabilizes the nanosized state of water clusters in the gaps between hydrophobic AM1 particles.

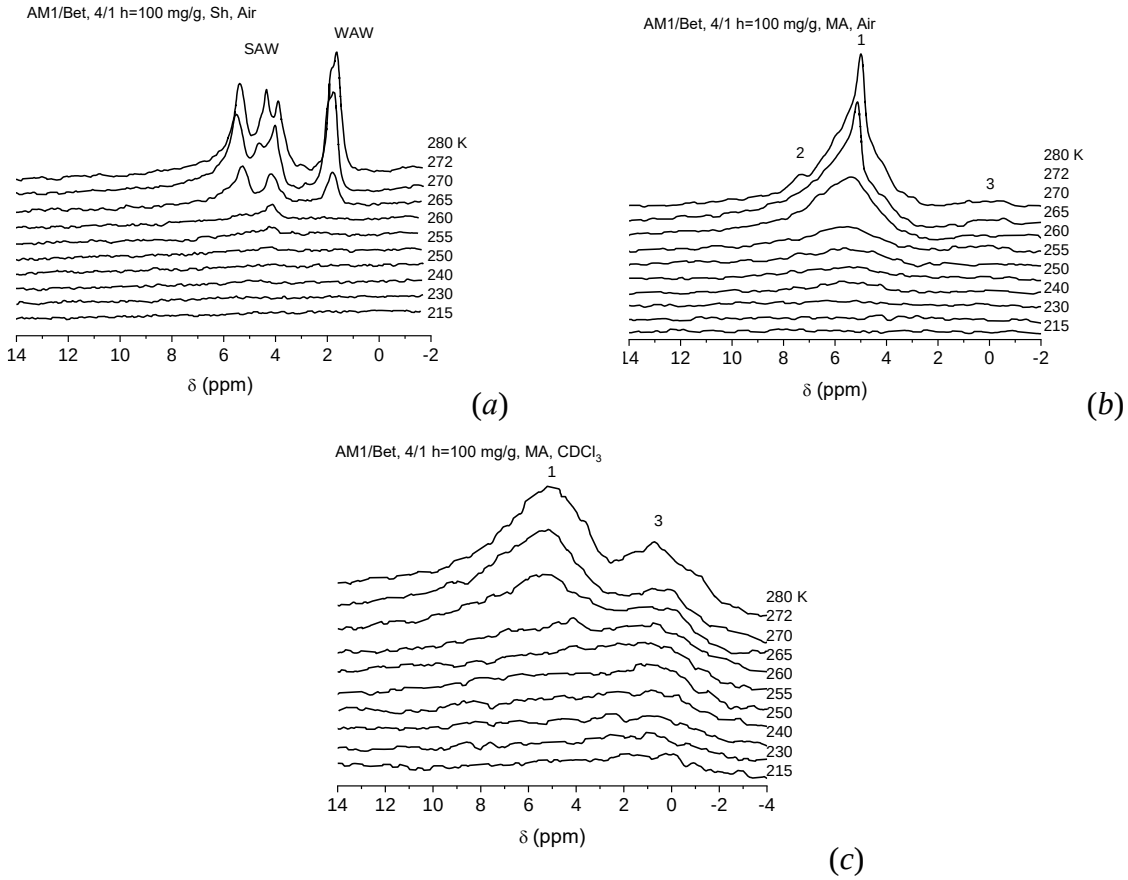

Fig. 14. Spectra of water taken at different temperatures, adsorbed by the AM1/Betulin composite system, containing 100 mg/g of adsorbed water, prepared by equilibrating the system by shaking (*a*) or mechanochemical activation with water (*b*, *c*) in air (*a*, *b*) and with the addition of $CDCl_3$

It should be noted that, in contrast to the supercritical state of water, surface stabilized weakly associated water exists only in the form of nanosized clusters (Fig. 13*e*), the radius of which is in the range of 0.5–50 nm. Several maxima are observed in the size distributions of SAW

and WAW clusters; however, weakly associated water is characterized by the presence of a larger number of small clusters. This is also evidenced by the lower values of ΔG^S (signal 3, Table 2), which characterizes the maximum decrease in the free energy of water in the adsorption layer.

The spectra of water taken at different temperatures, adsorbed by the AM1/Betulin composite system with a concentration ratio of 4/1, containing 100 mg/g of adsorbed water, prepared by equilibrating the system by shaking (Sh) (*a*) or mechanochemical activation with water (MA) (*b*, *c*) in air (*a*, *b*) and with the addition of $CDCl_3$ in an amount not exceeding 200 mg/g (*c*) shows on Fig. 14. When balancing by shaking (Fig. 14*a*), four signals are observed in the spectra in the range of chemical displacements δ_H = 1–6 ppm. The left group, which consists of three signals, refers to strongly associated, and the right signal, to weakly associated water. As the temperature decreases, the intensity of all signals decreases rapidly. Dependences of the amount of non-freezing water on temperature are shown in Fig. 15*a*.

The mechanochemical activation of composites with water is accompanied by a significant broadening of the WAW and SAW signals (Fig. 15*b*), which may be associated with a decrease in the mobility of adsorbed water molecules [93–95]. The addition of chloroform to composite systems leads to the stabilization of weakly associated forms of water (Fig. 14*c*), the amount of which becomes commensurate with the amount of strongly associated water. In the air environment (Fig. 15*c*), on the dependence on $C_{uw}(T)$, there are sections where the amount of WAW decreases with increasing temperature. It is likely that, with increasing temperature, part of the weakly associated water transforms into strongly associated water (perhaps, with the moving of water from narrow nanopores to larger pores in which SAW clusters are formed).

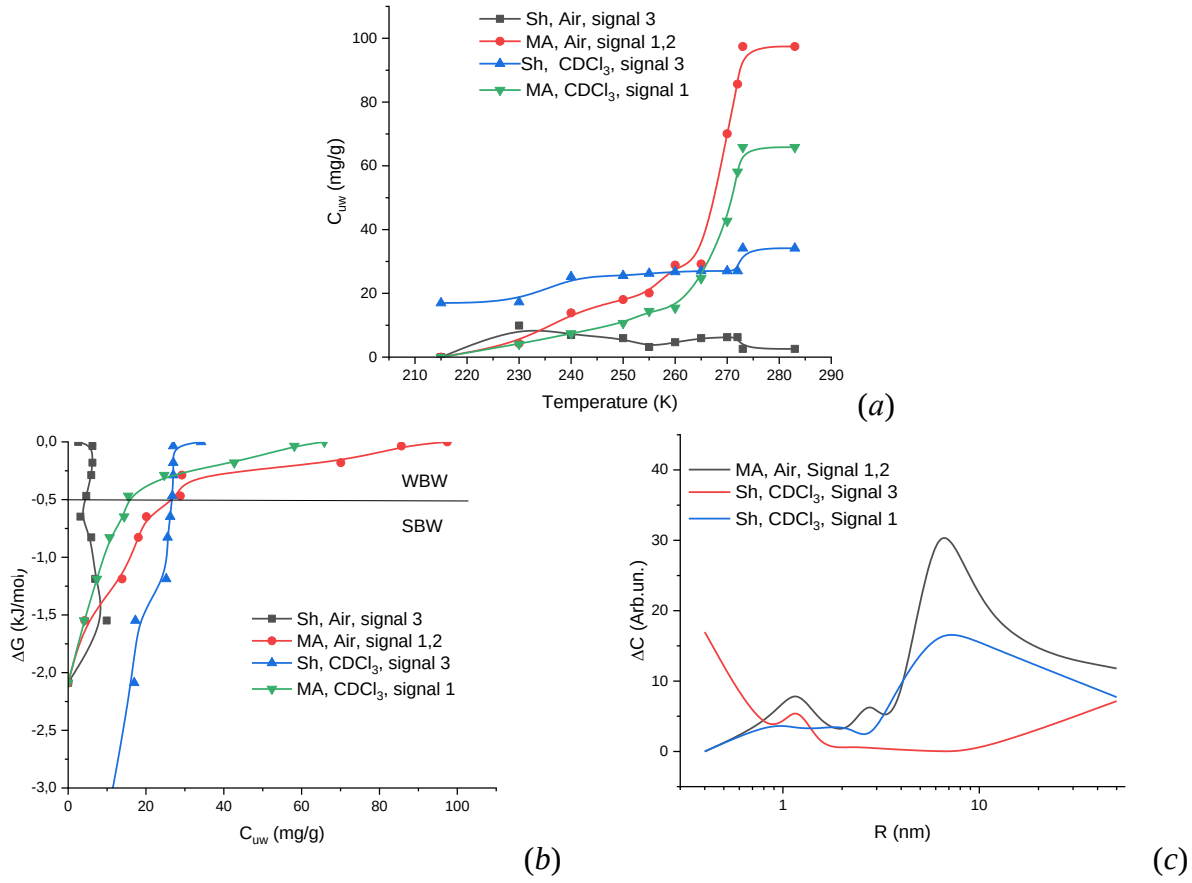

Fig. 15. Dependences of the concentration of non-freezing water on temperature (*a*), the change in the Gibbs free energy on the concentration of non-freezing water (*b*) and the distribution of adsorbed water clusters over the radii in AM1/Betulin hydrated composite systems balanced by shaking or mechanochemical activation in air and with the addition of $CDCl_3$

When using the data in Fig. 15*a*, according to formulas (1–3) for the AM1/Betulin composite systems, the dependences of the change in the Gibbs free energy on the concentration of non-freezing water (Fig. 15*b*) and the distribution of adsorbed water clusters over the radii were calculated (Fig. 15*c*). The thermodynamic parameters of the layers of adsorbed water are presented in Table 2. In the case of balancing by shaking the AM1/Betulin composite at h = 100 mg/g, the interfacial energy γ_S = 1.18 J/g is close to the interfacial energy of water adsorbed by pure betulin (Table 2). Mechanical activation increases the interaction energy of the surface with water due to a significant increase in the amount of strongly bound water. The addition of chloroform leads to an even greater increase (up to 5.61 J/g) in the γ_S value. For the non-activated composite, both strongly and weakly associated water is predominantly in the form of clusters with R = 8–25 nm (Fig. 15*c*). After mechanoactivation, small water clusters are formed from R = 0.4–5 nm, the number of which increases with increasing hydration. Additives of chloroform also increase the number of small water clusters (Fig. 15*c*). In this case, the values of interfacial energy and the amount of strongly bound water increase.

Weakly associated water in the AM1/Betulin composite systems is characterized by significantly lower values of ΔG^S than strongly associated water (up to -6 kJ/mol), which characterizes the maximum decrease in the free energy of strongly bound water, i.e. the lowest temperatures. Such water corresponds to clusters of minimum radius measured in tenths of nanometers. Similar results are also observed for hydrated methyl silica (Table 1). It follows from the radius distributions of adsorbed water clusters (Fig. 15*c*) that there are present small clusters of weakly associated water on the surface. The amount of adsorbed water in different types of the studied systems differs significantly, therefore, the value of the specific interfacial energy (γ_S*) should also be analyzed. As follows from the data in Table 2, compared to water adsorbed by betulin, for hydrated methylsilica, the value of γ_S* is several times higher. This applies to both strongly and weakly associated water. The chloroform medium almost doubles the interfacial energy. An increase in the amount of adsorbed water leads to some decrease in the value of γ_S*. These trends are also preserved for the composite system containing AM1 and Betulin. In this case, the maximum values of the specific interfacial energy (130 J/g) are observed for strongly associated water in the $CDCl_3$ medium.

Since water molecules in such clusters do not form hydrogen bonds, and their size can be quite large, the question arises about their structure. It is likely that such water polyassociates are formed in a limited space between hydrophobic methylsilica particles, when the formation of hydrogen bonds is hindered by spatial effects, and the shape of the interparticle gaps is close to slit-like. The stabilization of such unusual surface water clusters can be facilitated by the presence in them of a significant number of centers with opposite signs of charge, which induce charges of opposite signs in a hydrophobic medium by the mechanisms of dispersion interaction.

It is shown that silica chemically modified by grafting dimethylsilyl groups can be subjected to structural modification by mechanical activation with water, resulting in the formation of a compact material with a bulk density of 200–250 mg/cm^3, in which part of the interfacial water passes into a weakly associated state. The addition of chloroform entails the formation of a common water-chloroform system, in which almost all water becomes weakly associated.

A method has been developed for the formation of a hydrated silica/betulin composite system, which makes it possible for a significant amount of weakly associated forms of water to exist in the surface layer, some of whose properties are close to those of supercritical water. The contact of composite particles with a liquid hydrophobic medium, simulating hydrophobic areas of the gastrointestinal mucosa, further increases the amount of weakly associated water. These data are confirmed by FTIR spectra, in which unassociated and strongly associated clusters of adsorbed water are observed simultaneously.

The binding energy of water and the size of adsorbed water clusters depend on the mode of hydration. In the case of soft hydration by shaking with water, large clusters of strongly

associated water are formed on the surface, localized on the molecules of adsorption-fixed betulin. During hard hydration (grinding with water in a porcelain mortar), water penetrates into the gaps between hydrophobic particles of methylsilica or methylsilica with immobilized betulin and forms clusters of weakly associated water, the radius of which can be 0.4-8 nm. This type of interfacial water exists in a wide temperature range, its amount increases with increasing temperature.

NANOCOMPOSITE SYSTEMS PECTIN/SILICA AND THEIR PROPERTIES

Silica adsorbents are widely used as medical means to cleanse the body of toxic substances, which are metabolic products or those that entered the body as a result of food poisoning [96–98]. Fumed silica belongs to hydrophilic substances and has a high affinity for protein molecules, and also limitedly sorbs organic molecules with an average molecular weight. However, in modern pharmacology there is a demand for the creation of adsorbents in which the surface is formed by natural biopolymeric compounds, such as polysaccharides.

Pectins are a promising natural adsorbent. The largest amount of pectin substances is found in plant tissues: juicy fruits and root crops. The raw materials for the industrial production of pectin are mostly apple and citrus pomace, sugar beet pulp, fodder watermelon, sunflower baskets, pumpkin, i.e. food production waste [99]. Pectin biopolymers have unique biological and functional characteristics. They are widely used in the food, medical and cosmetology industries [100].

A significant disadvantage of poorly water-soluble biopolymers is their low specific surface area. Therefore, the therapeutic dose of pectins used as adsorbents is several tens of grams. Pectins are polysaccharides of higher plants, responsible for many of their physiological functions [101]. According to their chemical structure, they are compounds of a heterocyclic nature. D-galactopyranosyluronic (D-galacturonic) acid, connected by α-1,4-glycosidic bonds into a filamentous molecule of polygalacturonic acid, is considered the main part of the molecule of pectin substances [102].

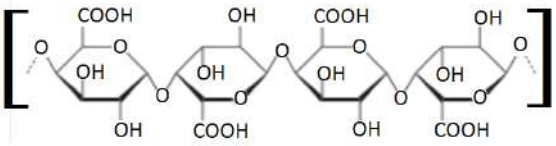

The technology for obtaining pectin is based on the classical method of its production: the pulp separated from the stone is homogenized and hydrolyzed at a pH of 2.0–2.5 and a temperature of 75–80°C for 1.5–2 hours. The mixture is filtered, the hydrolyzate is precipitated with alcohol or acetone. The coagulate is separated in a centrifuge (6000 rpm) with subsequent washing, filtration and drying in a vacuum drying unit. The molecular weight of pectin substances depends, first of all, on the nature and quality of the raw material source, the method of isolation and the method of its preparation for production. The average molecular weight of pectins ranges from 10 to 400 kDa, which corresponds to a degree of polymerization from 50 to 2000. Commercial pectin preparations have an average molecular weight of 30 to 120 kDa depending on the type of preparation [100, 103].

Pectins can be classified as physiologically active substances, since they affect cellular metabolism. In particular, there is evidence of the anticancer activity of pectins [104–107]. Thus, samples of citrus pectins showed a pronounced antitumor effect on adenocarcinoma C_{127}, reducing the metabolic and proliferative activity of its cells, and also demonstrating a pronounced cytotoxic effect. The greatest effect was demonstrated by low-esterified low-molecular pectin. In addition, pectins serve as natural adsorbents capable of removing toxic substances from the body. This makes them a promising component of nanocomposite systems for medical purposes.

Polymeric substances, such as pectins or other biopolymers in their natural form, are materials with a small specific surface area. Therefore, to increase it, it is possible to create composite systems with synthetic adsorbents, in particular with silicas, which have not only a high

specific surface area, but also a high affinity for polymer molecules [96, 97, 108, 109]. Particularly noteworthy is the prospect of using organosilicon adsorbents, which, in addition to high adsorption characteristics, have increased biocompatibility [9, 110–112]. Their disadvantage, however, is their hydrophobic properties, which complicate the process of their use in aqueous environments. In recent years, simple methods have been developed for wetting hydrophobic powders under mechanical load [19, 113]. It should be noted that in the case of using combined materials consisting of a hydrophobic carrier adsorbently modified by a hydrophilic agent, such as pectin, the possibility of wetting the composite with water is significantly facilitated.

The purpose of this work was the construction of composite systems based on pectin and silica (hydrophobic and hydrophilic and their mixtures), the study of their adsorption parameters in relation to the cationic dye methylene blue, and the effect of pectin on the hydration characteristics of silica sorbents.

Apple pectin (China), hydrophilic compacted silica brand. The composite system A-300/Pectin, AM1/Pectin and A-300/AM1/Pectin was prepared by thoroughly grinding compacted A-300 and/or hydrophobic AM1 with pectin to a homogeneous state [114, 115]. The amount of pectin in the composite was 5 or 10%. Wetting of systems containing AM1 was carried out by grinding with water according to the method described in [19, 113].

Hydrated pectin and two types of Pectin/H_2O/AM1 composite systems with component ratios of 1/1.25/5 and 1/2/0.5 were used for NMR studies. Hydrated pectin was prepared by adding the required amount of water to dry pectin and equilibrated for 24 h. Composites were prepared by grinding pectin and AM1, followed by adding the required amount of water with which the composite was ground for another 5–10 min. Deuterated chloroform and trifluoroacetic acid (TFAA) were used as organic components for NMR studies.

Fumed silicas belong to nonporous adsorbents, however, due to significant interparticle interactions, primary particles with a diameter of 10^{-3} nm form a mesoporous structure in which the pore volume can reach 1–1.2 cm^3/g [108, 111]. TEM micrographs of particles of a mixture of hydrophilic (A-300) and hydrophobic (AM1) silicas are shown in Fig. 16. In general, the particles of the agglomerates are 1–20 μm, in which the mesoporous structure of the interparticle spaces is very well observed. Unlike "hard" porous silicas of the silica gel type, in pyrogenic silicas the porous structure is unstable, and the surface and total volume of pores can change under the influence of mechanical loads, which are used as a factor for their structural modification [113, 115]. The “soft” nature of pyrogenic silicas also allows replacing air in the interparticle gaps with water by using mechanical processing in the presence of an aqueous phase [19, 113].

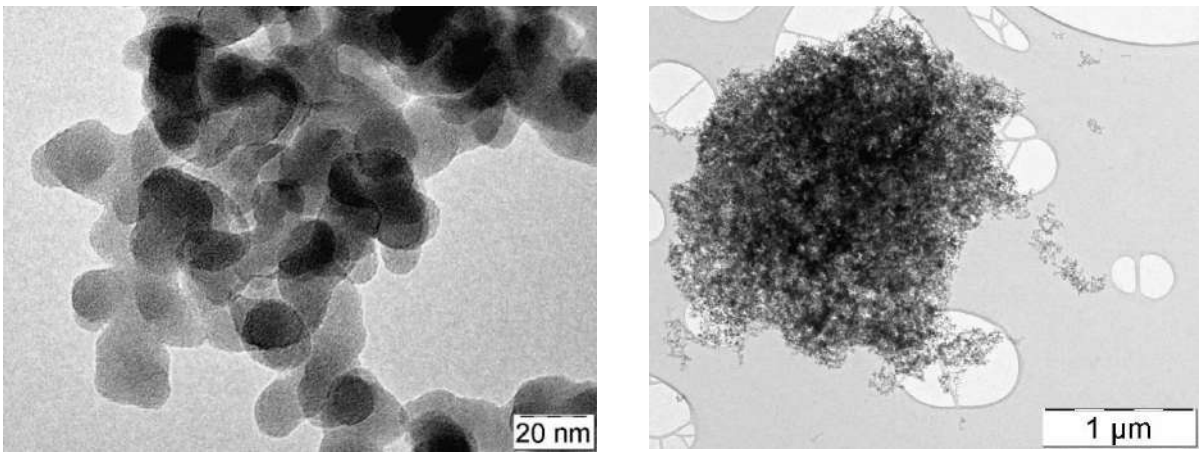

(*a*) (*b*)

Fig. 16. TEM microphotographs of the mechanically activated mixture of hydrophobic and hydrophilic silicas

For testing most medical sorbents, pharmacopoeial standards recommend marker substances [116]. They include differently charged dyes with different molecular weights. The sorption properties of the created composite systems were studied for their ability to bind the cationic dye MB, which has a hydrophobic aromatic fragment and is used to study the adsorption of positively charged substances with a low molecular weight on surfaces that, like silica A-300, have a negative charge [117].

The adsorption isotherms of MB from a model solution at pH = 5.5 and a solution with pH = 1.5, which simulates the physiological environment of the stomach are shown in Fig. 17. The contact time (1 h) of the studied samples with MB corresponded to the time of silica stay in the gastrointestinal tract and represents the duration of its maximum effective action [118, 119]. At the same time, measurements of MB adsorption on the surface of individually taken AM1 did not reveal a change in the optical density of the solution, which can be interpreted as the absence of adsorption.

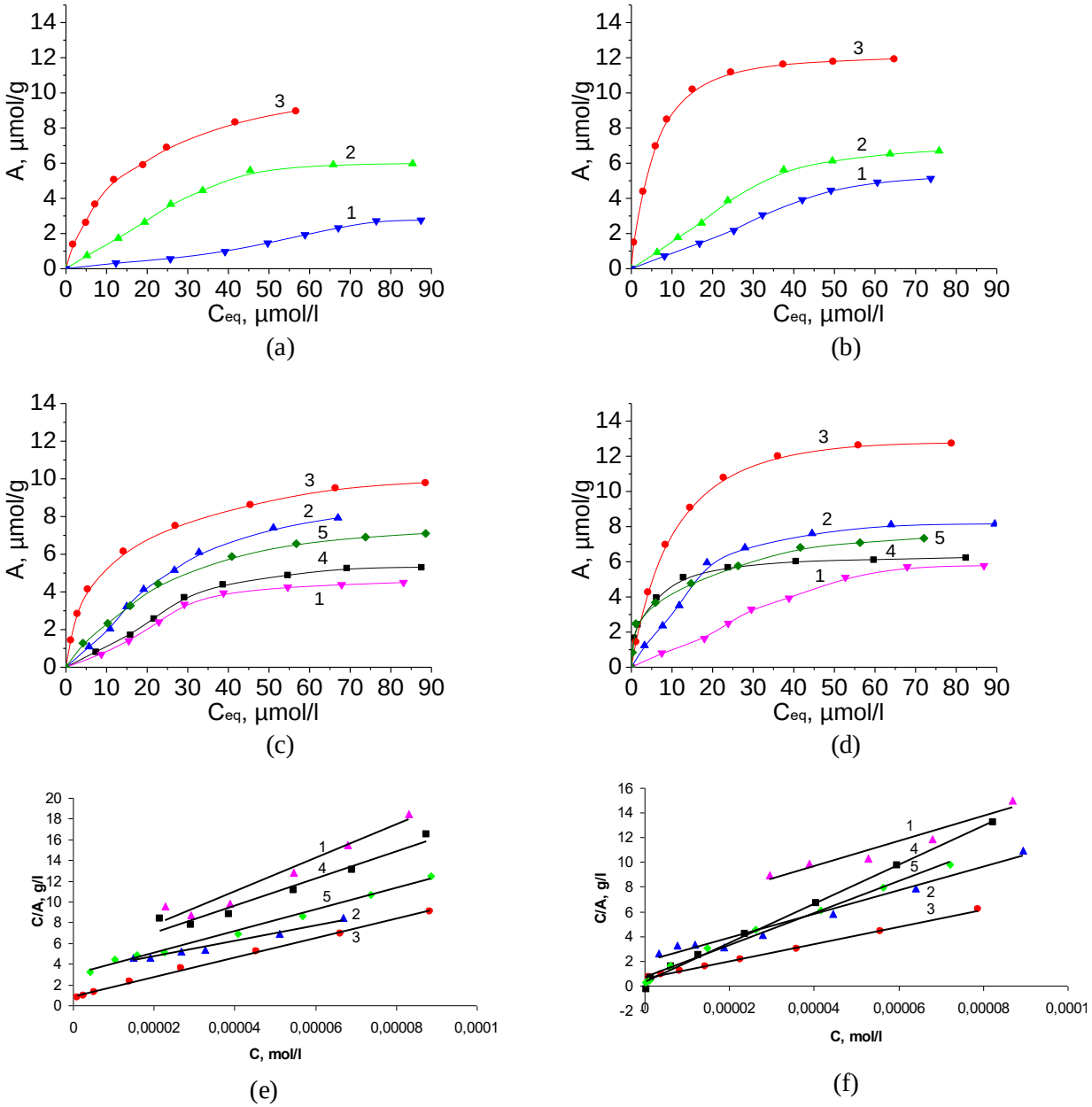

Fig. 17. Adsorption isotherms of MB and MC isotherms in Lengmuir coordinates on the surface of AM1/pectin (1), A-300/pectin (2), A-300/AM1/Pectin (3), A-300 (4) and A-300/AM1 (5) at pH 1.5 (*a*, *c*, *e*) and 5.5 (*b*, *d*, *f*) are shown. Pectin content in the composite: 5% (*a*, *b*) and 10% (*c*, *d*, *e*, *f*)

According to the adsorption data, it was determined that the adsorption isotherms of the dye on the surface of all the studied samples have the form of Langmuir isotherms (Fig. 17). They have a fairly steep initial section and quickly reach saturation. This form of the isotherm could be indicated a strong interaction of the dye with the surface [120].

Linearization of the obtained adsorption isotherms made it possible to determine the value of the limiting adsorption (A_∞) of MB for the studied samples (Table 3).

It is possible to reveal some regularities in the influence of the composition of the composite on the amount of cationic dye adsorption. There is a tendency for MB adsorption to increase with a decrease in pH from 5.5 to 1.5 (Fig. 17, Table 3). This is usually associated with a change in the surface charge of silica in an acidic environment from negative to positive [121]. However, as follows from the data in the Table 3, for most of the studied systems the difference in the value of A_∞ with a change in pH is quite small. That is, electrostatic interactions of dye molecules with the surface are not decisive. Since the MB molecule has hydrophobic fragments, and the surface of hydrophobic silica AM1, which is used for the preparation of composites, is hydrophobic, it could be assumed that hydrophobic (dispersion) interactions can be dominant in adsorbenet-adsorbate interactions. However, cationic dye adsorption was not observed on the surface of hydrophobic AM1. Adding pectin to AM1 promotes dye adsorption on such a composite due to the appearance of new types of adsorption centers. Thus, for AM1/Pectin with a pectin content of 5%, the lowest MB adsorption is observed, compared to other studied samples. When increasing the amount of pectin to 10% in the AM1/Pectin composite at an acidic pH value, MB adsorption increases by 1.6 times, in contrast to pH 5.5. Adsorption of MB on the surface of A-300/pectin composite with 10% pectin content is 7.4 and 8.11 μmol/g at pH 1.5 and 5.5, respectively. This is 1.4 and 1.3 times more than on the surface of the initial compacted A-300 without the addition of pectin. It was noted that MB on the surface of A-300 and A-300/Pectin with 5% pectin in the composite exhibits similar adsorption activity. At all pH values, dye adsorption is greatest on the surface of the A-300/AM1/Pectin composite at a pectin content of 10%. A decrease in the amount of pectin in the composite to 5% is accompanied by a slight decrease in MB adsorption. From the analysis of the given data, it can be concluded that the adsorption activity of nanocomposite systems to MB, which contain hydrophobic silica, is largely determined by the features of the formation of the boundary layer of water that fills the interparticle space.

Table 3. Parameters of methylene blue adsorption on the investigated adsorbents at different pH

Adsorbent	contents pectin, %	pH	A_∞, μmol/g	ω_∞, nm^2	θ, %	-ΔG, kJ/mol	R
A-300/Pectin	5	1.5	5.92	2.9	41.2	25.07	0.9836
		5.5	6.54	2.4	49.2	24.71	0.9856
	10	1.5	7.4	1.8	67.8	23.94	0.9890
		5.5	8.11	2.3	53.3	25.69	0.9871
AM1/Pectin	5	1.5	2.72	8.8	13.6	21.04	0.9726
		5.5	4.92	2.8	43.2	23.75	0.9823
	10	1.5	4.38	3.8	31.4	24.99	0.9771
		5.5	5.71	2.4	50.3	23.32	0.9692
A-300/AM1/Pectin	5	1.5	8.35	2.1	56.5	26.57	0.9968
		5.5	11.8	1.8	65.2	29.38	0.9996
	10	1.5	9.53	2.2	54.1	27.73	0.9988
		5.5	12.65	1.6	73.0	27.8	0.9992
A-300	-	1.5	5.27	3.1	38.8	24.54	0.9775
		5.5	6.12	3.7	32.0	31.57	0.9981
AM1	-		0				
A-300/AM1	-	1.5	6.91	2.5	48.5	24.95	0.9969
		5.5	7.09	3.1	39.1	28.93	0.9951

Mathematical processing the adsorption isotherms of MB made it possible to obtain equations describing the adsorption process with high linear correlation coefficients (R). The values of the correlation coefficient when linearizing the adsorption isotherms show that its sorption is described with maximum probability by the Langmuir equation.

The calculated dye adsorption parameters for each case are presented in Table 3. The values of the change in Gibbs free energy (ΔG) for all the studied samples are slightly different. This allows us to expect that the degree of affinity of the dye to the surface of the adsorbents will also differ. The degree of surface coverage of MB samples was calculated according to adsorption data, taking into account the size of the dye molecule. The calculations show that for 1 molecule adsorbed from an aqueous solution, there are quite large values of the area occupied by the molecule in the adsorbed state ($\omega_\infty > 1.2$ нм^2). This may indicate the planar orientation of MB molecules during adsorption. This is confirmed by literature data [121] and the obtained degree of surface coverage (θ) of the adsorbents by the dye, calculated from the adsorption parameters at the flat position of the MB.

Features of the formation of aqueous layers in hydrated nanocomposite systems containing AM1 and pectin were investigated by the method of low-temperature ^{1}H NMR spectroscopy [25, 84, 86]. The ^{1}H NMR spectra of water in hydrated pectin (Fig. 18*a*, *b*) and Pectin/AM1/H_2O composites (*c*–*g*) obtained at different temperatures in the presence of air (*a*, *c*, *e*), deuterochloroform (*b, d, f*) and 5$CDCl_3$+1CF_3COOD mixture (*g*) are shown in Fig. 18. The main signal of water in the spectra is observed in the form of a broad signal with a chemical shift in the range of 4–6 ppm. As the temperature decreases, the signal intensity decreases due to partial freezing of the interfacial water. Chemical shift values shows that almost all water is strongly associated (SAW) [25, 84, 86], that is, its molecules form a spatial network of hydrogen bonds in which each water molecule is involved in at least two hydrogen bonds. In the environment of chloroform, and in some systems also in air (Fig. 18*c*), signals of weakly associated water (WAW), which does not participate in the formation of hydrogen bonds, appear in the spectra.

One should especially focus on the system containing pectin and a small amount of AM1 (Fig. 18*e*). A splitting of the water signal into two closely spaced signals with slightly different values of the chemical shift is observed in this system in the spectra, and its value is somewhat smaller than for the other studied systems. This could be indicated the presence of clusters with a partially destroyed network of hydrogen bonds at the interphase boundary.

Since the amount of water in the samples (*h*) is known, based on the measurement of NMR signal intensities at different temperatures, can be used to calculate the temperature dependences of the amount of non-freezing water (C_{uw}), and according to formulas (1) – (3) to determine the dependences of the change in Gibbs free energy (ΔG) from C_{uw} and distributions by radii of adsorbed water clusters $\Delta C(R)$ (Fig. 19*a*–*c*). According to the method described in [25, 84, 86], the thermodynamic parameters of interfacial water layers could be calculated (Table 4), in which $C_{uw}{}^S$ and $C_{uw}{}^W$ are the concentrations of strongly and weakly bound water, respectively, ΔG^S is the maximum change in Gibbs energy in layers of strongly bound water, which characterize the maximum decrease in free energy due to adsorption interactions (or clustering), γ_S is the interfacial energy, which refers to the overall decrease in free energy due to adsorption interactions (or clustering) applied to all interfacial water, and γ_S* interfacial energy per unit mass (expressed in g/g) of interfacial water.

On the dependences $\Delta G(C_{uw})$ (Fig. 19*b*), the horizontal line drawn at the level of ΔG = 0.5 kJ/mol determines the amount of strongly and weakly bound water. The data in Table 4 show that for hydrated pectin, the use of an organic weakly polar medium, in contrast to most heterogeneous systems studied earlier [25, 84, 86], leads to a significant increase in the value of the interfacial energy γ_S and γ_S*. Probably, under the influence of the organic environment, the restructuring of pectin polymer molecules is carried out, aimed at reducing the total amount of free energy, which is characterized by smaller sizes of water clusters located in the intermolecular (or

interparticle) space of pectin (Fig. 19*c*). Composite systems containing hydrophobic silica AM1 are characterized by a decrease in values γ_S* in a weakly polar environment, which is due to an increase in interphase water clusters (Fig. 19*c*). In the presence of a strong acid in the dispersion medium, the value of γ_S* increases (Table 4) due to solvation effects. At the same time, the size of the surface clusters of water decreases in the process of defrosting the system.

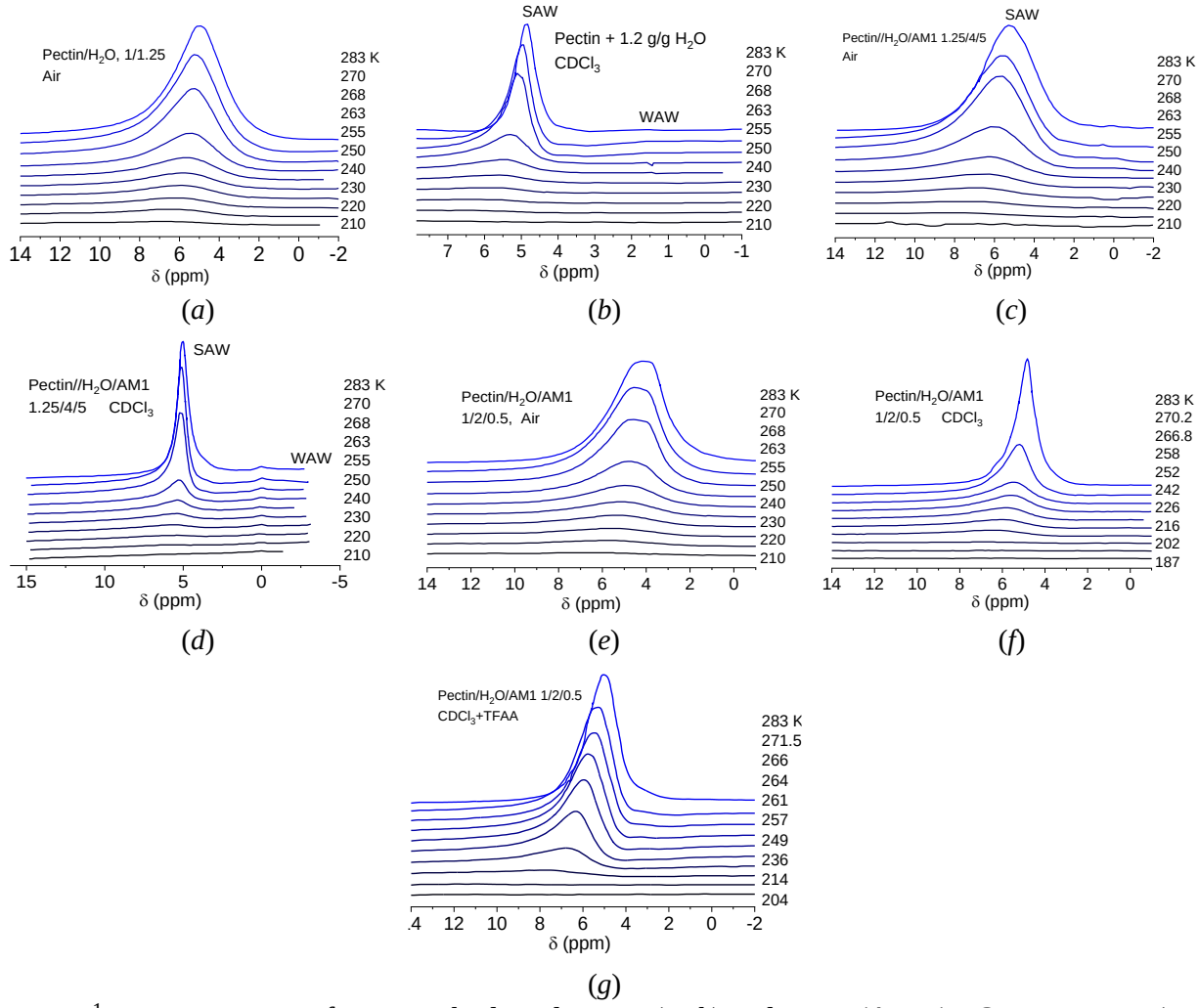

Fig. 18. ^{1}H NMR spectra of water in hydrated pectin (*a*, *b*) and pectin/AM1/H_2O composites (*c*–*f*) measured at different temperatures, in the presence of air (*a*, *c*, *e*), deuterochloroform (*b*, *d*, *f*) and mixtures $5CDCl_3$+$1CF_3COOD$ (*g*)

For the composite system containing a small amount of AM1 additive in the air environment are observed the maximum value of the interphase energy (Table 4). This is due to a significant amount of strongly bound water, which is concentrated in small clusters (Fig. 19*c*). That is, the amount and energy of water binding in heterogeneous systems based on pectin is primarily influenced not by the amount of hydrophobic substance forming the composite, but by the processes of interparticle interactions between disparate components. They probably also determine the degree of association of molecules in the water layer. These results also agree with the data obtained during the study of adsorption from the MB solution on the surface of various composite systems. Direct adsorption measurements did not reveal certain regularity between the hydrophobic properties of the matrix and the ratio of component concentrations.

The construction of composite systems containing pectins and silica materials can serve as a promising direction in the creation of nanomaterials with high adsorption characteristics in relation to molecules of medium and large molecular weight.

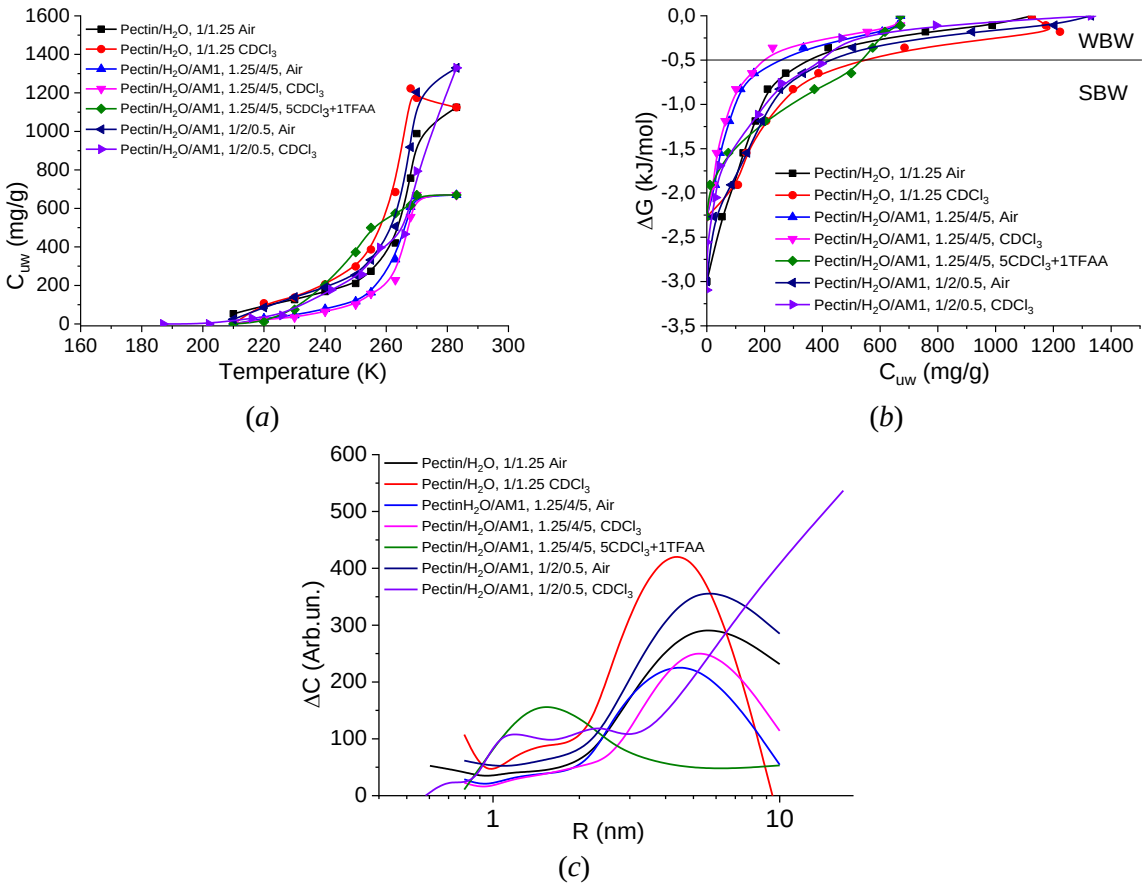

Fig. 19. Temperature dependences of the amount of non-freezing water (C_{uw}) (*a*), dependences of the changes in the Gibbs free energy (ΔG) on C_{uw} (*b*) and distributions of adsorbed water cluster radii $\Delta C(R)$ (*c*)

Table 4. Characteristics of interfacial water in hydrated pectin and its composites with hydrophobic silica AM1 in different environments

Sample	Medium	*h*, (mg/g)	C_{uw}^S, (mg/g)	C_{uw}^W, (mg/g)	ΔG^S, (kJ/mol)	γ_S/γ_S^* (J/g)
Pectin/H_2O	Air $CDCl_3$	1125	350 550	775 575	-3 -2.27	35.1/31.2 42.4/37.7
Pectin/H_2O/AM1 1.25/4/5	Air $CDCl_3$ $5CDCl_3$+1TFAA	670	250 200 550	420 470 120	-2.3 -2.3 -2.3	20.7/30.9 18.2/27.2 35.0/52.2
Pectin/H_2O/AM1 1/2/0.5	Air $CDCl_3$	1300	430 410	870 890	-3 -2.6	40.4/35.7 31.3/27.7

In particular, it shows the prospects of creating composites based on a mixture of hydrophobic and/or hydrophilic silicas (AM1 and/or A-300, respectively) with pectin. It has been shown that the maximum adsorption of MB occurs from the model solution at pH 5.5 on the surface of all the studied samples. The A-300/AM1/pectin composite system proved to be the best, regardless of the amount of pectin in the composite (5 or 10 %) at different pH values, compared to other adsorbents.

It is possible to control the structure of interfacial water and the energy of interaction between water and the surface by changing the concentration ratio of pectin and hydrophobic silica. In this way, new types of functionalized materials can be created for use in medical composites.

COMPOSITE SYSTEM BASED ON METHYL SILICA AND DISPERSED *AMANITA MUSCARIA* MUSHROOMS

In recent years, interest has increased in naturally occurring psychogenic substances, in particular those found in certain types of mushrooms. Thus, the bioactive components of the mushrooms *Amanita muscaria* are psilocybin, muscimol, muscarine and ibotenic acid, which have a long history of use in both traditional and non-traditional medicine [122–126]. Psilocybin is a psychoactive alkaloid that is naturally produced by about 200 species of mushrooms. Potential medical use of Psilocybin is possible for the treatment of mental disorders and as an effective sedative. Natural psychoactive substances can act as stimulants, hallucinogens or analgesics, depending on the dosage. Red and panther fly agarics have a long history of use as sedatives, and the main psychoactive compounds of these species are thought to be analogues of the neurotransmitter gamma-aminobutyric acid (GABA) and glutamic acids, especially muscimol and ibotenic acid, respectively [127, 128].

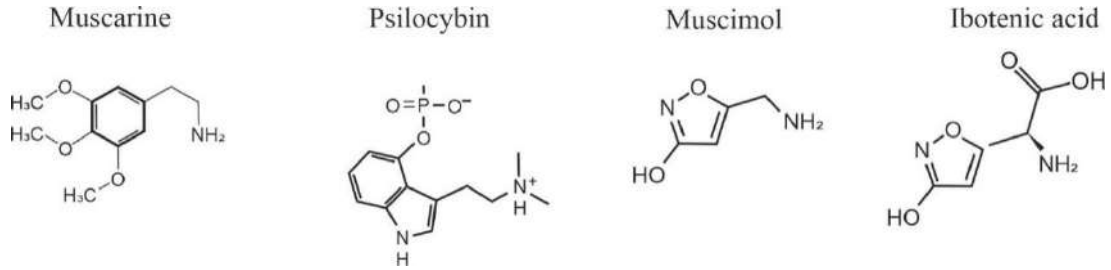

Fig. 20. Some bioactive compounds extracted from *Amanita muscaria*

The natural products muscimol and ibotenic acid are isoxazole alkaloids and have some structural similarities to gamma-aminobutyric acid, and both act on different parts of the GABA receptor. Muscimol is derived from ibotenic acid by decarboxylation [129]. Muscarine is a cholinergic agonist and was thought to contribute to the general psychoactivity of *Amanita muscaria*.

Currently, schemes are being developed for the use of natural psychogenic substances for medicinal purposes [130–132]. In this case, primary attention is paid to the dosage and methods of introduction into the body. Potentially promising products are composite systems created on the basis of highly dispersed silicas and crushed natural mushroom *Amanita muscaria* [133]. To ensure the process of prolonged release of bioactive components in the gastrointestinal tract during oral administration, methyl silica can be used as a mineral base, which is obtained from the corresponding hydrophilic silica by chemical grafting of dimethylsilyl groups [134, 135]. The use of hydrophobic methyl silica in composite systems serves several purposes: preventing moisture from entering the highly hydrophilic particles of dispersed mushrooms, which prevents the formation of mold and fungal infections; air microbubbles inside the composite particles and the hydrophobic surface of silica prevent the rapid penetration of water and aqueous solutions from biological media, and this significantly increases the desorption time of bioactive components. Compared to its hydroxylated analogue, methyl silica is more inert and weakly interacts with cellular structures, while maintaining high adsorption activity.

The goal of this work was to create a composite system in which the AM1/*Amanita* hydrophobic composite, on the one hand, maintains a high affinity for water, and on the other, ensures its clustering in the interparticle gaps of the composite and limited contact with the external environment.

Amanita muscaria mushrooms collected in the northern region of Ukraine were dried at 50°C in the ventilated room with additional air flow of 40 l/min. After drying to a residual moisture content of 2–3%, they were crushed in a screw homogenizer. To prepare the composite systems, the biomaterial powder was mixed in the required proportion with AM1 silica, then the powders were mixed in a ball mill for 30 min.

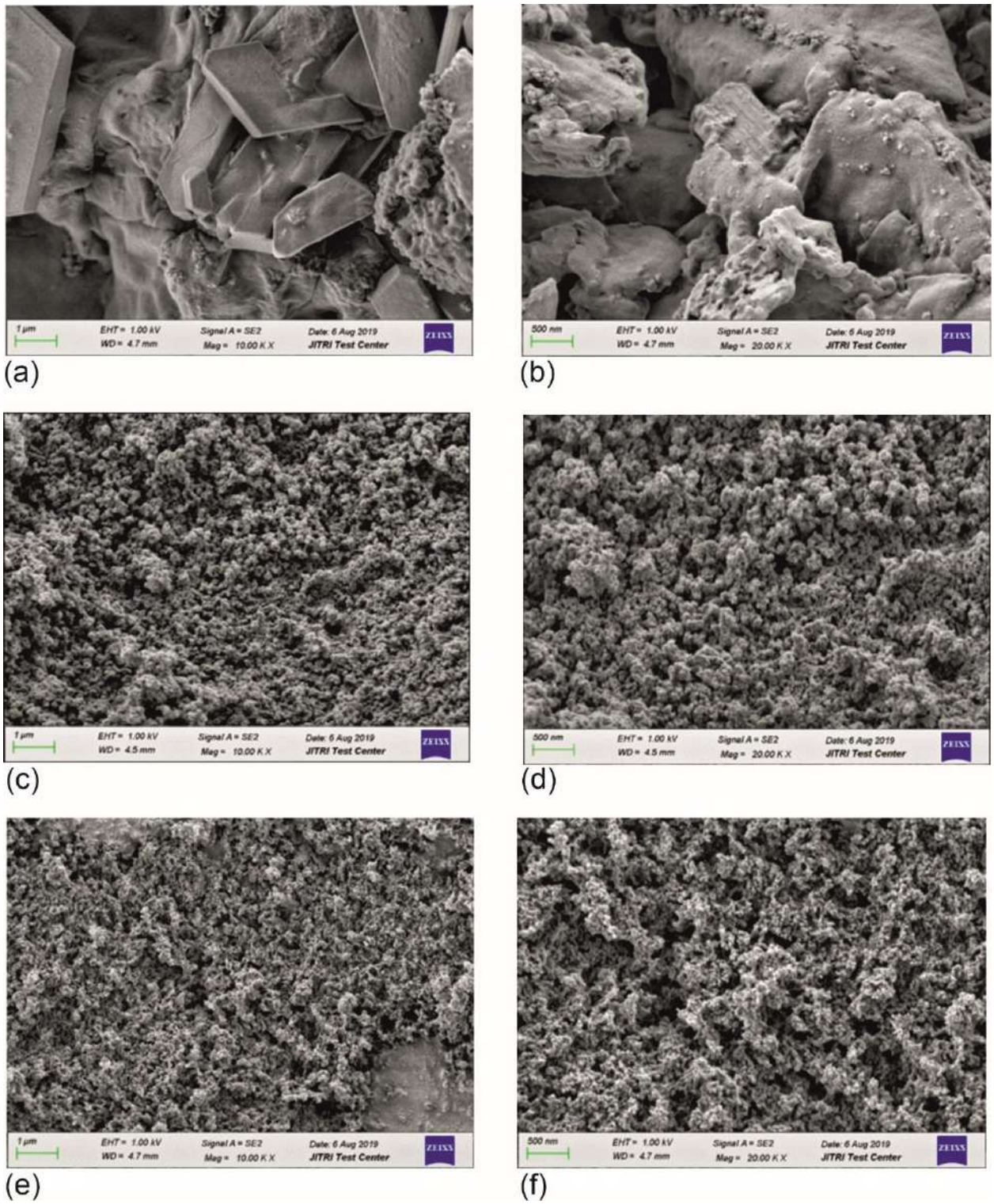

Fig. 21. Electron micrographs of the surface of the original *Amanita muscaria* biomaterial (*a*, *b*), the AM1/*Amanita* composite system (*c*, *d*) and AM1 methyl silica (*e*, *f*)

To obtain *Amanita muscaria* extract, 10 ml of water was added to 250 mg dried powdered mushroom material. The extraction was carried out under the ultrasonic at the temperature of 40°C for 1.5 hours. The obtained extract was filtered through a membrane filter made of polytetrafluoroethylene with a pore diameter of 0.45 µm and stored in a freezer at a temperature -20°C.

The content of ibotenic acid and muscimol in the extract was determined using an Agilent 1260 Infinity II automatic four-channel liquid chromatograph with a diode array detector and a chemical station, using a Poroshell 120 EC-C18 3.0x150 mm, 2.7 μm column. A mixture of aqueous solution (0.006 M H_3PO_4 and 0.0021 M $NaC_{12}H_{25}SO_4$) and methanol was used as the mobile phase. At the beginning of the elution, the fraction of methanol was 20 %, the flow rate through the column was 0.15 ml/min, gradually the fraction of methanol increased to 100 %, and the flow rate was up to 0.4 ml/min. The sample volume was 5 μl, the column temperature was 40 °C. Chromatograms were recorded at wavelengths of 206, 210, and 254 nm.

Identification and quantitative analysis were performed using standard solutions of ibotenic acid (purity 95 %, Sigma-Aldrich) and muscimol (purity 98 %, Sigma-Aldrich). The number of substances registered in the chromatograms was estimated by comparing the area of the corresponding signals with the area of the signals in the chromatograms of the standard substances. To confirm the presence of ibotenic acid and muscimol, 50 μl of standard solutions (0.5 mg/ml) were also added to the test extract.

Electron micrographs of the surface of the original Amanita muscaria biomaterial (*a*, *b*), the AM1/Amanita composite system (*c*, *d*) and AM1 methyl silica (*e*, *f*) are shown in Fig. 21. Crushed mushroom material is a system of irregularly shaped particles, the size of which can vary from fractions of a micron to several tens of microns. After processing in a ball mill with AM-1 methyl silica, the biomaterial is dispersed (Fig. 21*c*, *d*) and becomes indistinguishable from the original methyl silica sample (Fig. 21*e*, *f*). Micrographs clearly show silica agglomerates, which consist of strongly interacting primary silica particles.

The results of studying the aqueous extract of *Amanita muscaria* mushrooms using liquid chromatography are shown in Fig. 22. The peaks of ibotenic acid and muscimol are clearly identified in the chromatogram. Based on high performance liquid chromatography (HPLC) analysis, the extract contained <700 μg/g ibotenic acid and 73 μg/g muscimol.

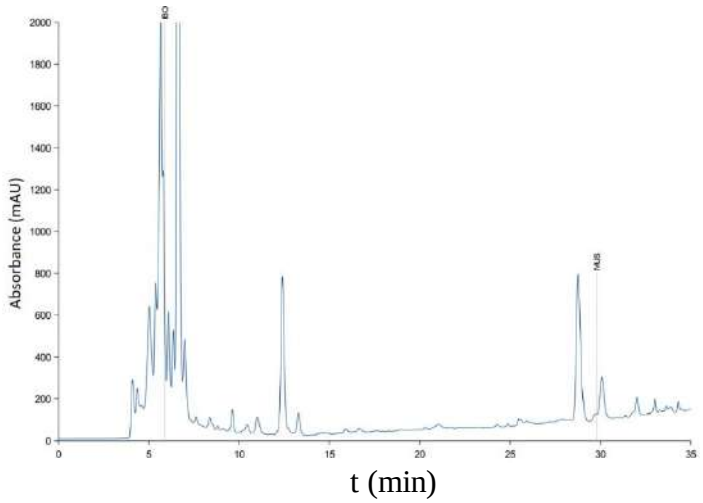

Fig. 22. HPLC chromatogram of the aqueous extract of *Amanita muscaria*

Fig. 23 shows the ^{1}H NMR spectra of water in hydrated AM1/*Amanita* (*a*–*h*), AM1 (*g*) and *Amanita muscaria* (*h*–*j*) composite systems taken at different temperatures, in air (*a*–*d*, *g*–*i*) and with the addition of deuterochloroform (*e*, *f*, *k*). In the air environment, the main signal in the spectra refers to strongly associated water (SAW), the chemical shift of which (δ_H) increases with decreasing temperature from δ_H = 5 to δ_H = 7 ppm. On the right side of the curve of the SAW signal at δ_H = 1 ppm a low-intensity signal of weakly associated water (WAW) is observed. When deuterochloroform is added to the hydrated powder (Fig. 23*e*, *f*), air being displaced from the interparticle gaps and the samples become more magnetically homogeneous, which leads to a narrowing of the NMR signals [25].

At the presence of a hydrophobic medium, the amount of weakly associated water increases noticeably and one recorded over the entire temperature range available for measurement. The spectra of water are presented for hydrated AM1 powder (Fig. 23*g*) and crushed *Amanita muscaria* powder (Fig. 23*h–j*). AM1 hydration was carried out by mechanical activation, according to the procedure described in [9, 10, 13]. In *Amanita muscaria* WAW has been observed in both air and organic environments. With a small amount of water (Fig. 23*i*, *j*), the WAW signal becomes dominant.

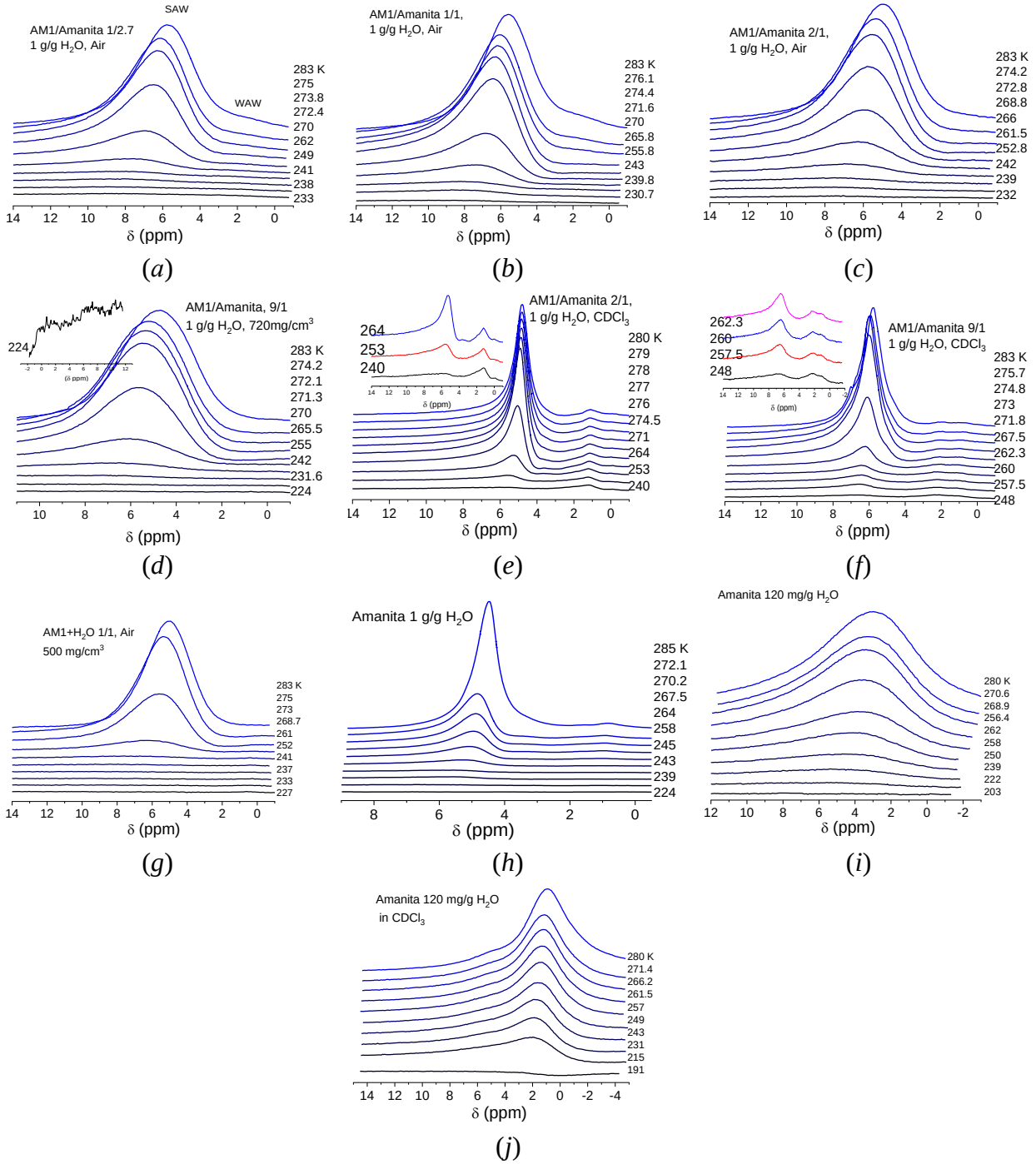

Fig. 23. ^{1}H NMR spectra of water taken at different temperatures in hydrated composite systems AM-1/*Amanita* (*a–h*), AM1 (*g*) and *Amanita muscaria* (*h–j*), in air (*a–d*, *g–i*) and with deuterochloroform addition (*e*, *f*, *j*)

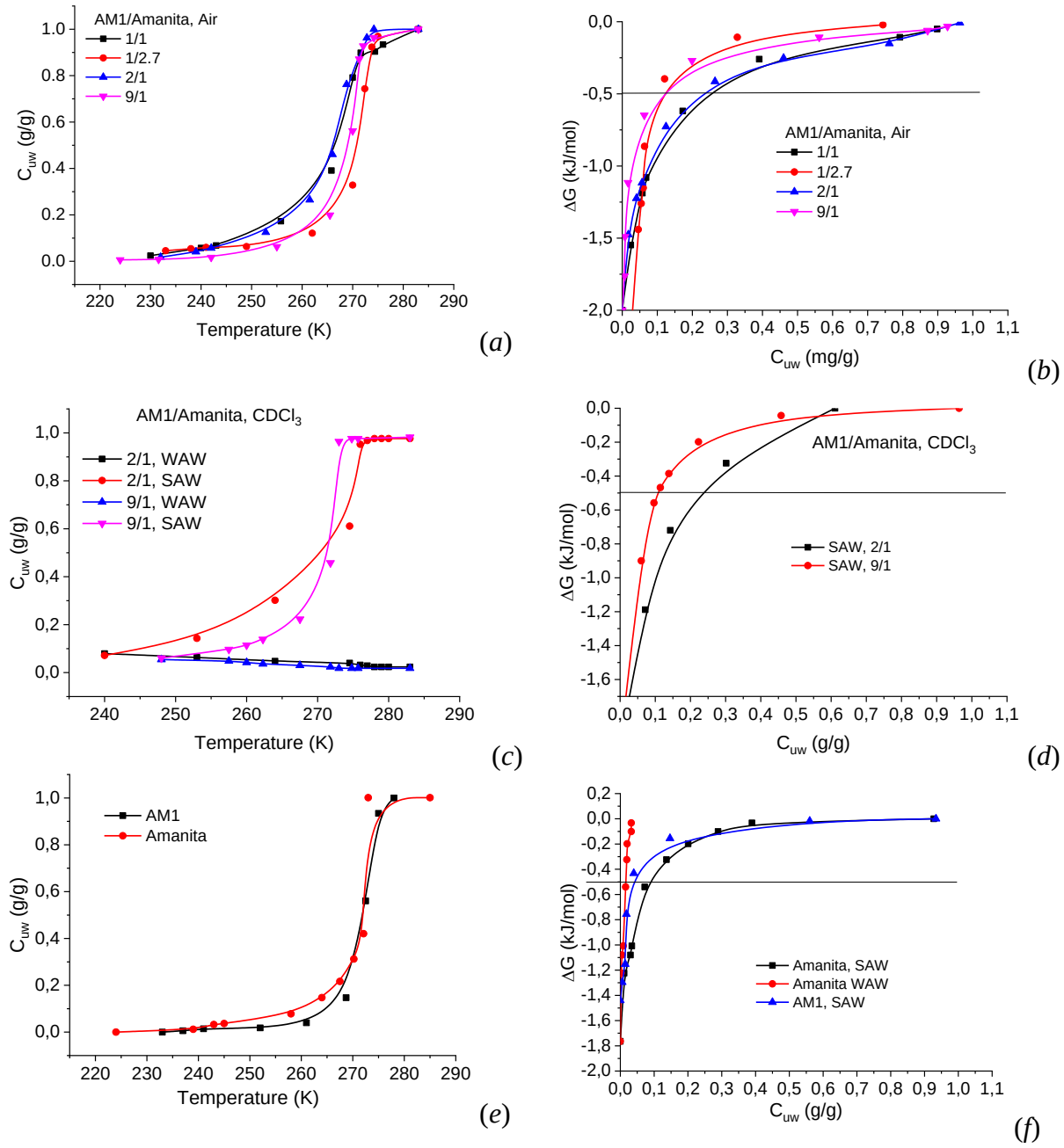

Fig. 24. Dependences of the concentration of unfrozen water on temperature (*a*, *c*, *d*) and, based on them, dependences of the change in Gibbs free energy on the concentration of unfrozen water (*b*, *d*, *e*) for composite AM1/*Amanita* systems and source materials at h = 1 g/g

Table 5. Characteristics of unfrozen water layers in *Amanita muscaria* mushrooms and in the AM1/*Amanita* composite system.

Sample		Medium	C_{uw}^S (mg/g)	C_{uw}^W (mg/g)	ΔG^S (kJ/mol)	Δs (J/g)
Amanita		Air	100	900	-1.7	8.1
AM1		Air	50	950	-1.5	5.8
AM1/*Amanita*	1/2.7	Air	112	888	-3	13,3
	1/1	Air	125	875	-2	20.5
	2/1	Air	120	880	-2	20
	9/1	Air	112	888	-2	12.2
	2/1	$CDCl_3$	240	760	-2	17.5
	9/1	$CDCl_3$	100	900	-2	10.9

From the data in Table follows that the value of interfacial energy is controlled by the amount of strongly bound water, which depends on the average radius of water clusters and the intensity of adsorption interactions. Since the value γ_S is integral, it reflects the entire set of interphase interactions that occur in a complex heterogeneous system.

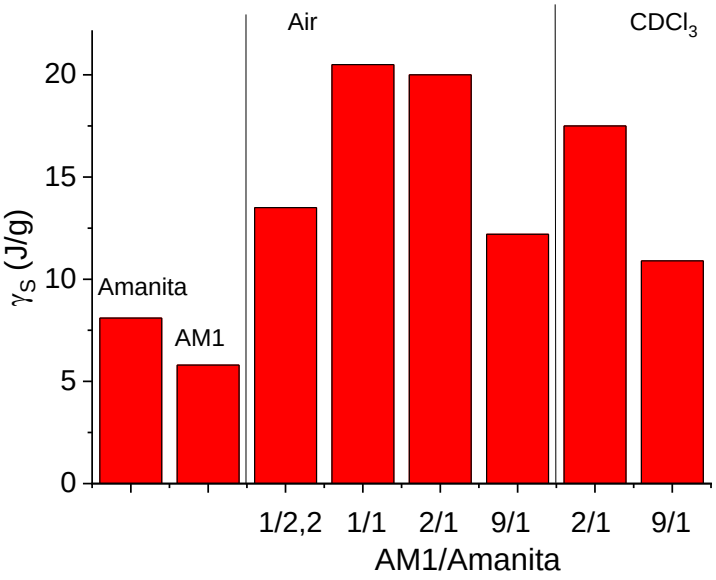

Fig. 25. Diagram of changes in interfacial energy depending on the composition of a heterogeneous system containing crushed *Amanita muscaria* and metyl silica AM1

The starting ingredients for the preparation of composite systems were a strongly hydrophilic powder of dried crushed mushrooms *Amanita muscaria* and hydrophobic powder AM1. While the mushroom biomaterial easily absorbs water and is balanced with it quickly and without much mechanical stress, then AM1 powder for humidification requires intensive mechanical processing, as a result of which the water is converted into a clustered state, and a significant part of the air is removed from the interparticle gaps of hydrophobic silica. As a result, at the same hydration, the interfacial energy of water in the interparticle gaps of AM1 is only slightly less than for water absorbed by the biomaterial of the mushrooms *Amanita muscaria*.

After preparing the AM1/*Amanita* composite system, the γ_S value increases, and the dependence of γ_S on the ratio of the concentrations of hydrophobic and hydrophilic components has a maximum at AM1/*Amanita* = 1/1. This value of the concentration ratio corresponds to the minimum value of the average radius of clusters of adsorbed water (R = 8 nm) (Fig. 25). Under conditions of a large excess of the hydrophobic component (AM1/*Amanita* = 9/1), the disappearance of small water clusters is observed. A probable reason may be the merging of water into clusters or domains of larger size; accordingly, the surface of the water/air interface decreases and the interfacial energy decreases.

The addition of chloroform is accompanied by a slight decrease in the γ_S value. Apparently, even when a significant part of the interparticle gaps is filled with water, chloroform is able to diffuse to the surface of hydrophobic particles, reducing the interaction of water clusters with the surface and creating conditions for their association into extended water structures.

It has been shown that hydrophobic silica AM1 can serve as a good nano-sized matrix for the preparation of composite systems with hydrophilic biogenic drugs. In the same time, it performs several functions at once: mechanically separates particles of biomaterial from each other, which prevents them from caking and becoming infected with fungal spores; transforms interfacial water into a clustered state (radius of water clusters 1–50 nm), which is characterized by excess free energy, and due to air microbubbles, does not allow rapid desorption of biologically active substances into the aqueous environment.

It has been established that in the AM1/*Amanita* composite systems, despite its hydrophobic properties, the energy of water binding is greater than in the original materials. The maximum value of interfacial energy of water was recorded at the same concentration of ingredients in the AM1/*Amanita* composite system. At a higher content of the hydrophobic component, due to the merging of nanosized water clusters, the process of formation of extended water structures begins, which is accompanied by a decrease in interfacial energy and an increase in the radii of adsorbed water clusters.

INTERFACIAL INTERACTIONS IN COMPOSITE SYSTEMS BASED ON SILICA AND INULIN

Inulin belongs to soluble polysaccharides of plant origin. Its peculiarity is ability to stimulate the activity of a certain type of intestinal microorganisms (mainly Bifidus group). Therefore, it is considered a prebiotic, i.e. a non-digestible food ingredient capable of improving health by stimulating the growth of activity of a certain type of bacteria [136–153]. Inulin is currently produced on an industrial scale from the roots of a number of plants such as Asteraceae: burdock, topinambur, dandelion root, chicory and many others [154–161]. Selective stimulation of intestinal microflora contributes to the increase of immunity of the organism, therefore inulin is considered to be an immunomodulatory substance. Unlike starch (a widespread reserve polysaccharide of plants), inulin is a D-fructose polymer containing up to 27–35 fructose residues in furanose form and one glucose residue [162–166] with the structural formula:

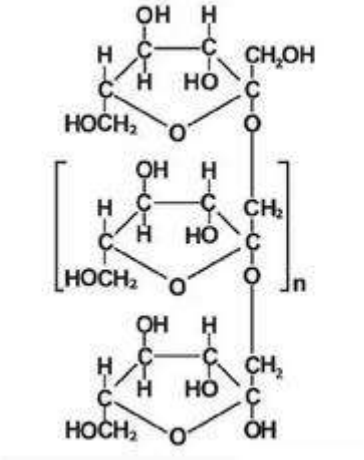

Inulin is available in the trade network mainly in two dosage forms of biologically active supplements – tablets and drops. Since prebiotics should not undergo hydrolysis by human digestive enzymes, as well as be absorbed in the upper parts of the digestive tract, a promising direction in the creation of new more effective dosage forms. The goal of this work was to create newer, more effective dosage forms by designing nanostructured composite systems based on pyrogenic silica with different hydrophobic-hydrophilic properties and powdered inulin. It is assumed that the composite system will consist with micron particles formed by silica, and inulin will predominantly be located in the inter-particle gaps. This will provide optimal conditions for the release of inulin in the colon, thereby enhancing the efficacy of the drug. Previously, composite systems based on silica and medicinal plants, mushrooms, also succinic acid were created and studied [140, 167–170], the results of which are summarized in monographs [8, 171].

The composite systems were prepared by grinding the compacted silica with inulin powder for 20 min. Then, 250 mg/g water was added to the compacted silica or composites and further grinded for 15–20 min. In all cases, a 1 g powder suspension was used. During such mechanical treatment, a part of air was displaced from the interparticle gaps of both hydrophilic and hydrophobic materials [99, 171].

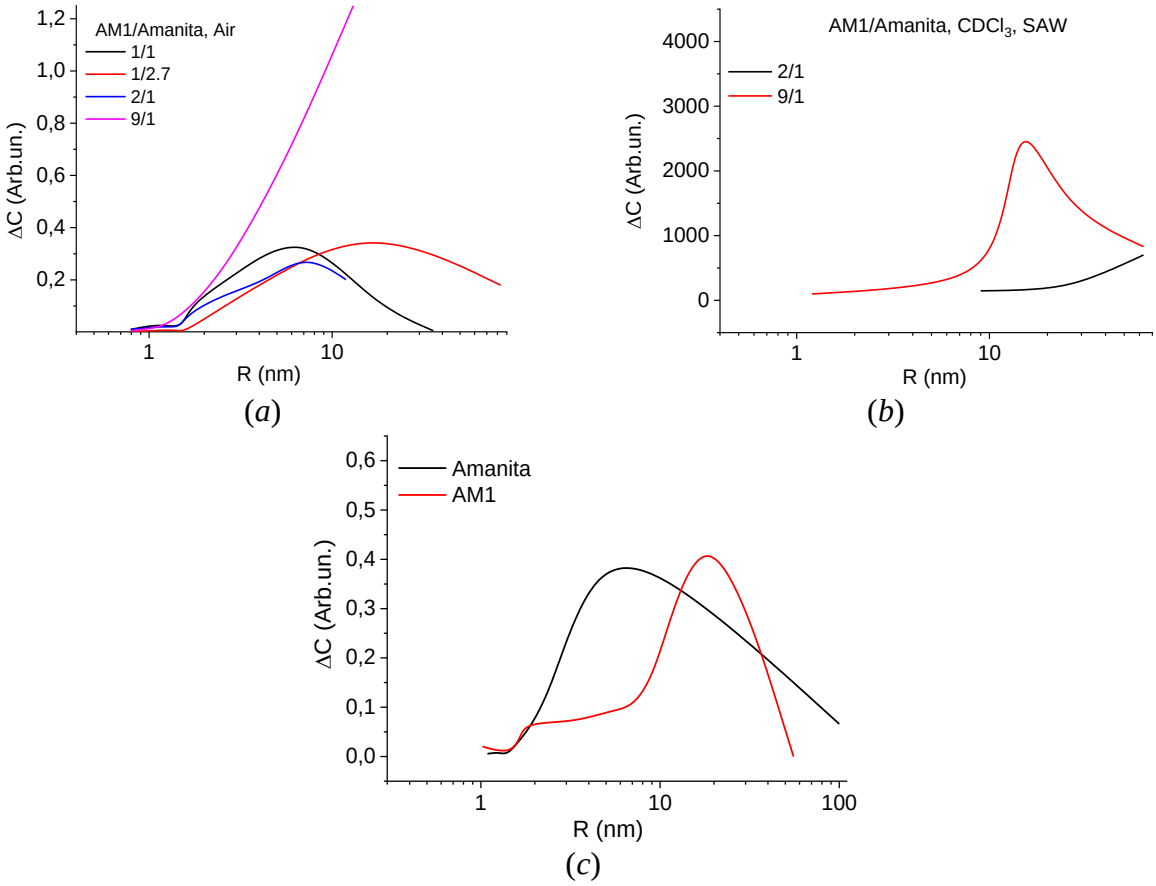

Fig. 26. Distributions along the radii of clusters of adsorbed water in AM1/*Amanita* composite systems with different ratios of component concentrations and initial ingredients at h = 1 g/g

Electron micrographs for particles of compacted silica A-300 (Fig. 27*a–c*), inulin (Fig. 27*d*, *e*), methyl silica AM-1 (Fig. 27*f–h*) and composite system (A-300+AM1)/inulin (Fig. 27*i–k*) are presented in Fig. 27. At low magnification, silica is in the form of agglomerates with particle sizes ranging from units μm to hundreds of μm. As the resolution of the microscope increases, a porous particle structure formed by closely spaced agglomerates and aggregates is observed. At the maximum magnification, primary silica particles with a size of 10–30 nm become distinguishable. Silica and methylsilica (comparing Fig. 27*a–c* and Fig. 27*f–h*) are characterised by a similar particle structure. Inulin is in the form of particles with no discernible crystalline structure (Fig. 27*d*, *e*). With increasing resolution, the fine structure characteristic of amorphous polymers becomes apparent. In the process of composite creation, polymeric inulin molecules are distributed over the surface of silica particles losing their individuality. As a result, the composite system in its appearance is close to the structure of the original silica particles (Fig. 26*i–k*).

Nitrogen adsorption isotherms and structural characteristics of the composite systems A-300/inulin are shown in (Fig. 28*a*) and (A-300+AM1)/inulin are shown in (Fig. 28*b*). The appearance of the isotherms is typical for mesoporous solids. Although pyrogenic silica refers to non-porous materials with a developed surface, the interparticle gaps form a secondary porous structure [172–175]. This structure is also preserved in composite systems based on inulin and hydrophilic (Fig. 28*a*) or a mixture of hydrophilic and hydrophobic silica (Fig. 28*b*). The average particle size forming the composite systems is 35–40 nm, the average pore radius is 15–20 nm, and the specific surface area by BET is 140–170 m^2/g. Since no large inulin crystals are observed on electron micrographs (Fig. 27), it can be assumed that during mechanical processing due to the high abrasive properties of silica there is a uniform distribution of inulin on the surface of silica particles.

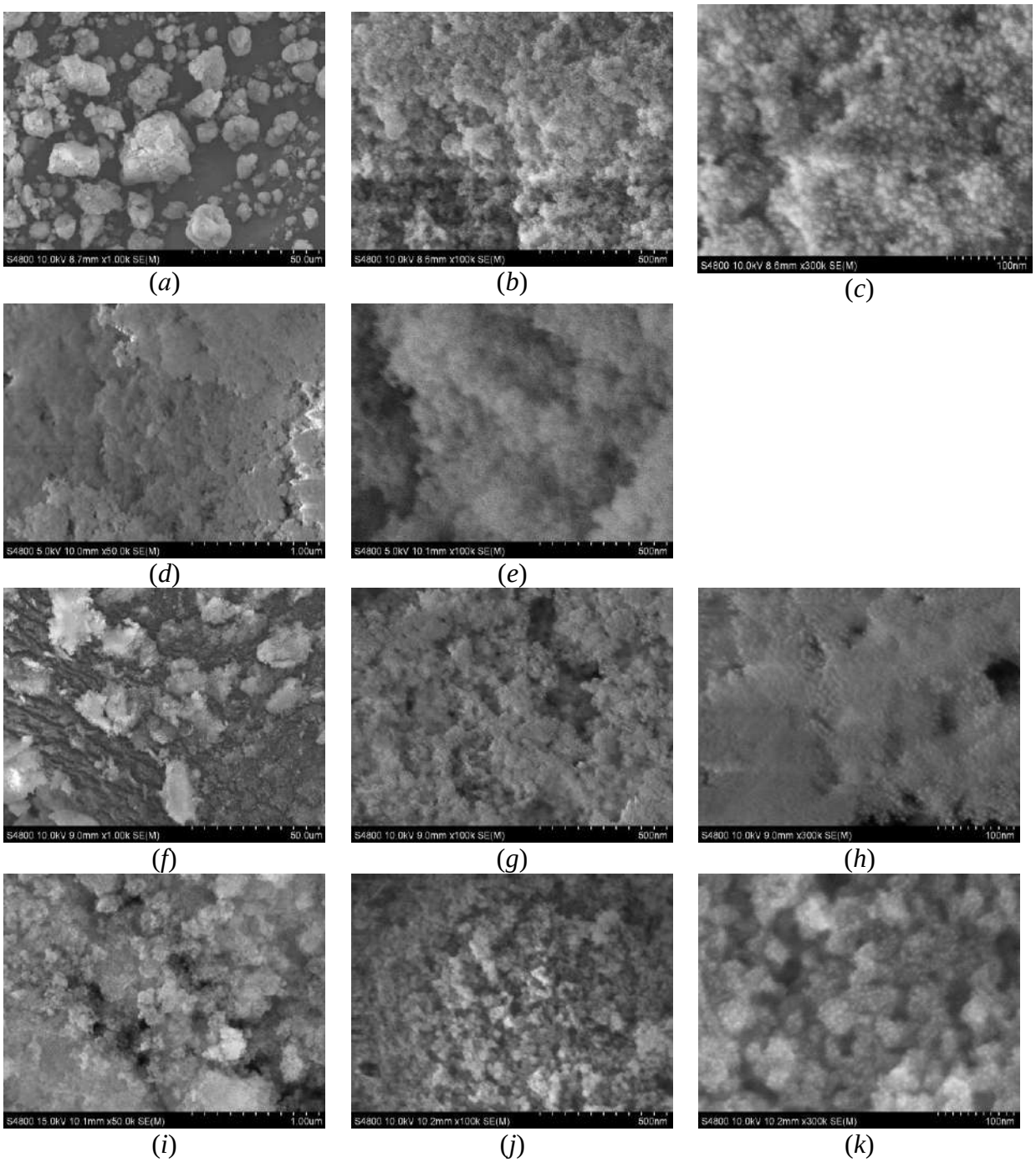

Fig. 27. Electron micrographs for particles of compacted silica A-300 (*a–c*), inulin (*d*, *e*), methyl silica AM1 (*f–h*) and composite system (A-300+AM1)/inulin (*i–k*)

The weight loss (TG), DTG and DTA curves for inulin (*a*), composites based on inulin and silica A-300 (*b*), its mixture with hydrophobic silica A-300+AM1 (*c*) or AM1 (*d*), individual A-300 (*e*) and AM1 (*f*) contained 50 % weight of the water are shown on Fig. 29. Measurements were carried out for dry materials without water added to them. Water evaporation is carried out at temperature $T < 150$°C. The residual water content in the samples is small. It does not exceed a few per cent. At higher temperatures, inulin polymer chains are destroyed, dehydrogenated, carbonised and oxidised to gaseous products. These processes can be observed on the DTG curve, which contains three weight loss maxima. In the case of composite systems, in addition to the processes associated with the dehydration of the sample (both inulin and silica) and the destruction

of inulin, processes associated with the dehydroxylation of silica A-300 and the destruction of dimethylsilyl groups AM1 occur. As a result, after heating the samples to 1000 °C, there remains a non-combustible residue, which is dehydroxylated and dehydrated silica.

Since in the process of joint mechanical treatment of the silica mixture with inulin its molecules are distributed in the interparticle gaps of silicas, a change in the phase state of inulin is possible, which can be recorded by the X-ray phase analysis method (Fig. 30). However, the presented X-ray patterns show that both the original inulin and its 1:3 composites with hydrophilic silica A-300, hydrophobic silica AM1 and a 1:1 mixture of A-300 + AM1 are X-ray amorphous and do not exhibit a pronounced crystalline structure.

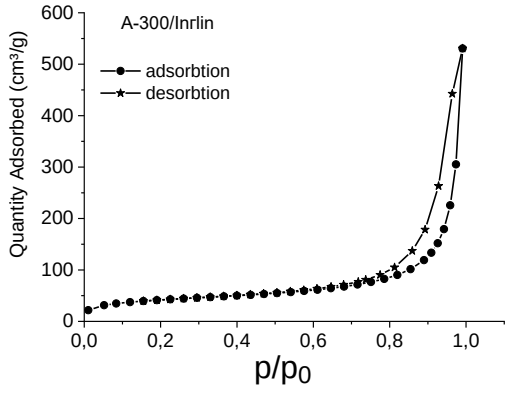

(*a*)

Single point surface area at P/P_0 = 0.295339957:140.4198 m²/g
BET Surface Area: 143.6 m²/g
t-Plot Micropore Area: 25.8 m²/g
t-Plot External Surface Area: 117.7 m²/g
Pore Volume
Single point adsorption total pore volume of pores
less than 211.1740 nm width at P/Po = 0.9908:0.82 cm³/g
Pore Size
Adsorption average pore width (4V/A by BET): 22.9 nm
Nanoparticle Size
Average Particle Size 41.7862 nm

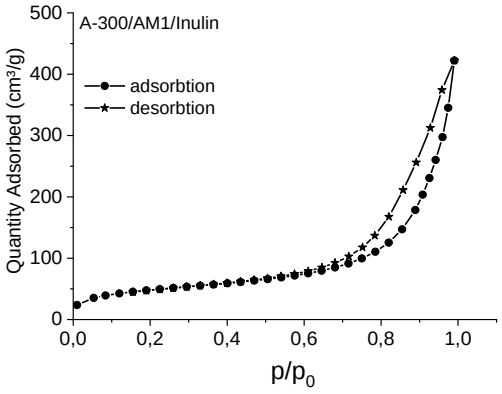

(*b*)

Surface Area
BET Surface Area: 168.6 m²/g
t-Plot Micropore Area: 16.5 m²/g
t-Plot External Surface Area: 152.0 m²/g
Pore Volume
Single point adsorption total pore volume of pores
less than 204.0193 nm width at P/P_0 = 0.9905:0.65 cm³/g
Pore Size
Adsorption average pore width (4V/A by BET): 15.5 nm
Nanoparticle Size
Average Particle Size 35.6 nm

Fig. 28. Low-temperature nitrogen adsorption isotherms and structural characteristics of composite systems A-300/inulin (a) and (A-300+AM1)/inulin (b)

Since inulin contains a sufficient amount of moisture adsorbed from the air, the IR Fourier spectra in the region of water and water-bound hydroxyl groups ν = 3700–3000 cm^{-1} were similar for all samples. On the other hand, the spectra of inulin/A-300 composite systems lack the characteristic peak ν = 3750 cm^{-1}, which corresponds to silanol groups not bound by hydrogen bonds. From this it can be concluded that during mechanical treatment, silanol groups of the silica surface bind to inulin molecules.

The ^{1}H NMR spectra of water in hydrophilic silica A-300 (Fig. 32 shows ^{1}H NMR spectra of water in hydrophilic silica A-300 (Fig. 32*a–c*), composite systems A-300/inulin (Fig. 32*d–f*), (A-300+AM1)/inulin (Fig. 32*g–i*), and inulin (Fig. 32*j*, *k*)) in air medium (*a*, *d*, *g*, *j*), deuterochloroform medium (Fig. 32*b*, *e*, *h*, *k*) and $5CDCl_3$+$1CF_3COOD$ medium (Fig. 32*c*, *f*, *i*, *l*). The measurements were performed at the same water content of the samples h = 250 mg/g. The

most intense signal in the spectra is due to strongly-associated water (SAW) [25, 84, 86, 92], whose molecules form a hydrogen bonding network in which each water molecule simultaneously participates in the formation of 2–3 hydrogen bonds. With decreasing temperature for all the studied systems, the intensity of the SAW signal decreases due to its partial freezing. At the same time, the freezing temperature is lower the more strongly the free energy of interfacial water is reduced by adsorption interactions (due to disruption of the geometry of the hydrogen bonding network or transformation of water into a system of nanoscale clusters).

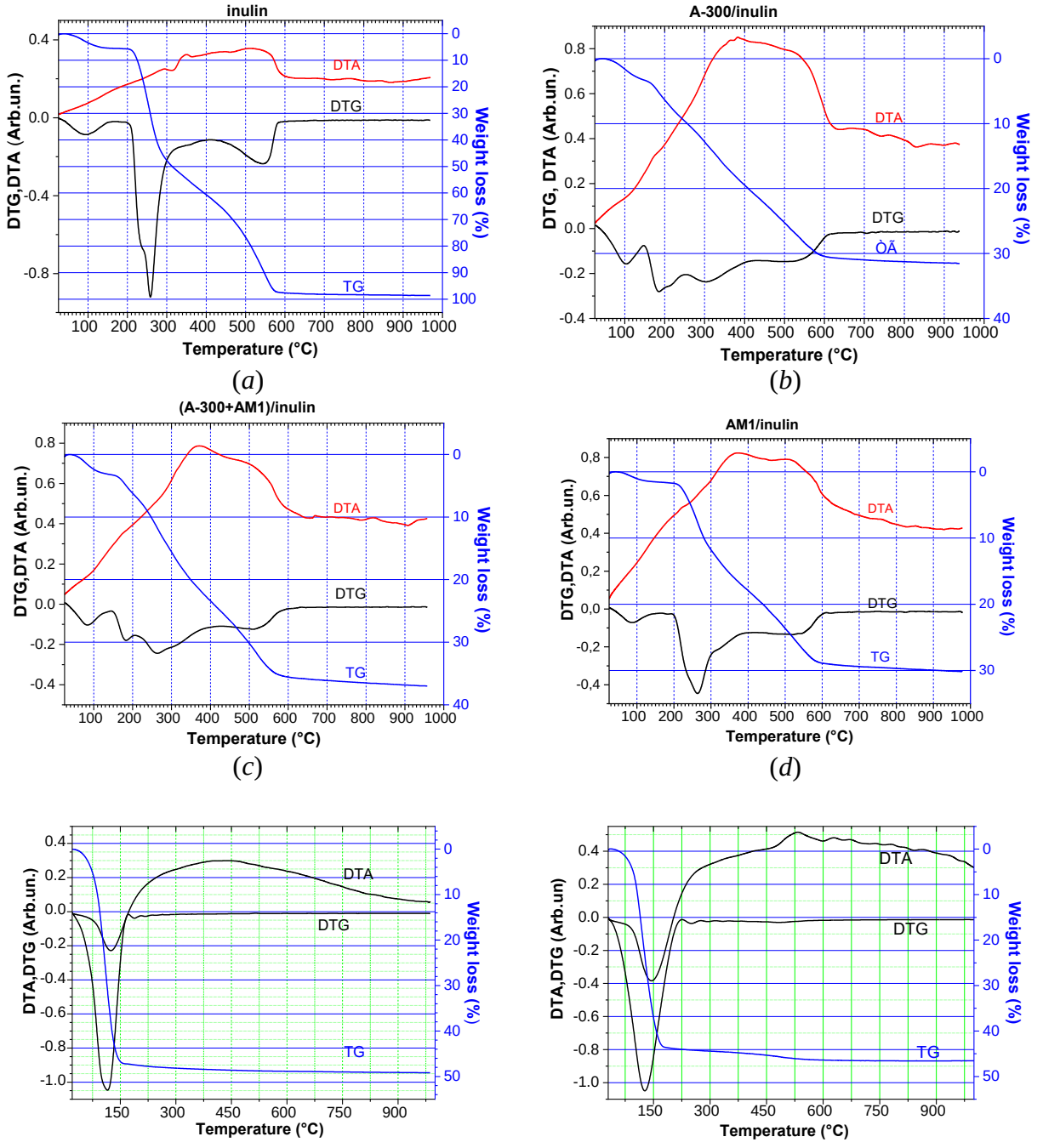

Fig. 29. Weight loss, DTG and DTA curves of inulin (*a*), A-300/inulin (*b*), (A-300+AM1)/inulin (*c*) and AM1/inulin (*d*), A-300 (*e*) and AM1 (f) when the samples were heated from room temperature to 1000°C

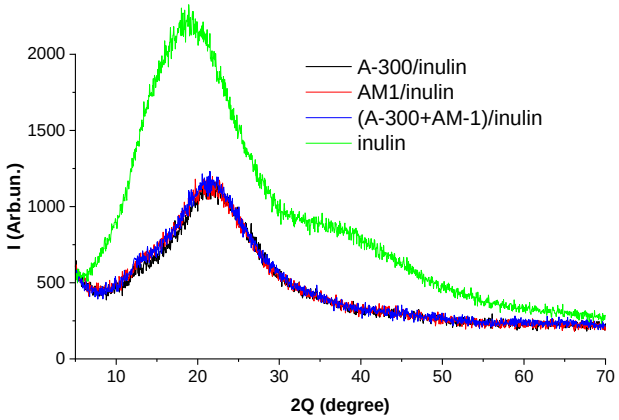

Fig. 30. Data of X-ray phase analysis of inulin and its composite systems 1:3 with hydrophilic silica A-300, hydrophobic – AM1 and a mixture of 1/1 A-300+AM1

Fig. 31 shows the results of the study of inulin and composite systems based on it, obtained by the method of IR Fourier spectroscopy (reflection):

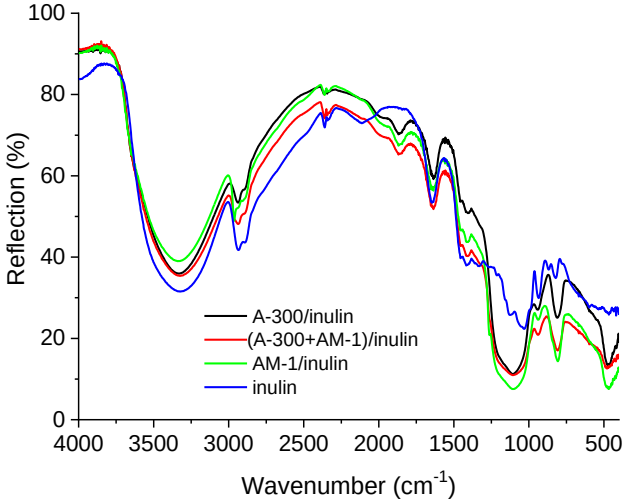

Fig. 31. IR spectra of inulin and its composite systems 1:3 with hydrophilic silica A-300, hydrophobic – AM1 and a mixture of 1/1 A-300+AM1

The spectral parameters of water adsorbed on silica (Fig. 32*a*–*c*) depend on the medium in which the measurements are carried out. Replacement of air with organic medium ($CDCl_3$) leads to a decrease in the width of the SAW signal, its shift to the region of lower values of chemical shift (Fig. 32*b*) and the appearance of a weakly intense signal of weakly-associated water (WAW) at δ_H = 0 ppm. Consequently, the weakly polar medium has a chaotropic (disordered) effect on the adsorbed water [75–77], leading to the disruption of the three-dimensional hydrogen bonding grid for the interfacial water. The addition of a small amount of trifluoroacetic acid (TFAA) to chloroform medium (Fig. 32*c*) is accompanied by a shift of the signal towards larger chemical shift values due to the 'acidic' protons of TFAA, which is characterized by the chemical shift value δ_H = 11 ppm. The freezing point of the water-acid solution is significantly increased due to the effect of solvation of acid molecules by water.

Despite the fact that inulin belongs to water-soluble polymers, the signal of its hydroxyl groups in the air medium (Fig. 32*d*, *g*, *j*), both in composites and inulin powder is not observed, which indicates its relatively low solubility in clustered water. Substitution of air medium with chloroform medium (Fig. 32*e*, *h*, *k*) leads to the signal appearance for inulin hydroxyl group δ_H = 3 ppm. Its intensity increases with increasing temperature due to the growth of solubility and the increase in the amount of non-freezing strongly-associated water.

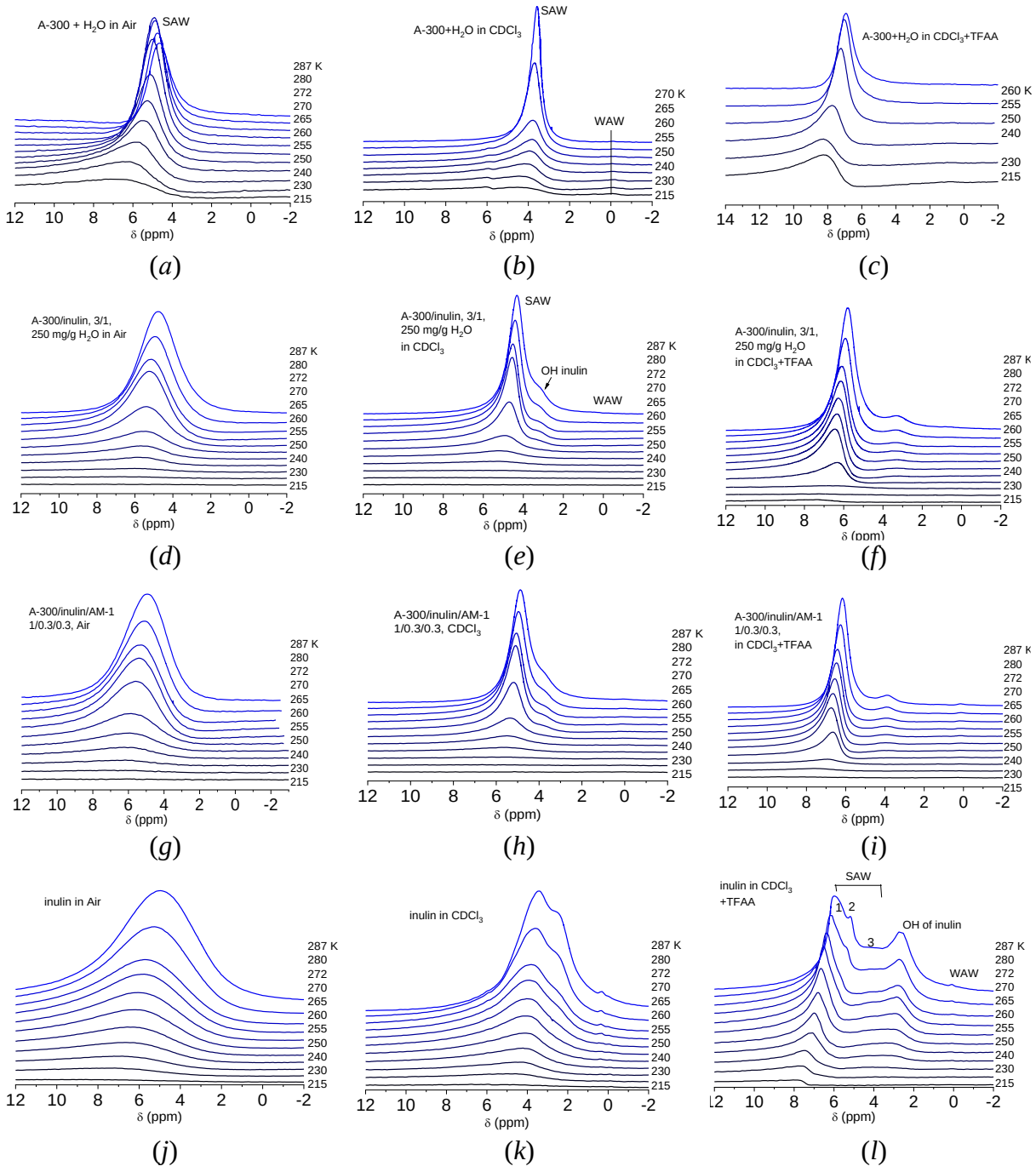

Fig. 32. ^{1}H NMR spectra of water in hydrophilic silica A-300 (*a*–*c*), composite systems A-300/inulin (*d*–*f*), A-300+AM1/inulin (*g*–*i*) and inulin (*j*, *k*) in air medium (*a*, *d*, *g*, *j*), deuterochloroform medium (*b*, *e*, *h*, *k*) and 5$CDCl_3$+1CF_3COOD medium (*c*, *f*, *i*, *l*)

The maximum signal intensity of hydroxyl groups is registered for inulin powder (Fig. 30*k*), when all water present in the sample is concentrated near with polymeric molecules, rather than distributed in the interparticle gaps of silica particles with inulin molecules immobilized on their surface. The spectra of hydrated inulin in a mixed organic medium containing TFAA have the most complex appearance (Fig. 30*l*). In addition to the WAW signal and inulin hydroxyl groups (δ_H = 3 ppm.), several signals of strongly-associated water differing in the magnitude of the chemical shift (signals 1–3) are recorded in the spectra. This is due to the

decreased solubility of acids in nanoscale water clusters [176, 177]. Then signal 3 (δ_H = 5 ppm.) should be attributed to water clusters that do not solubilise TFAA. Signal 2 – to clusters that dissolve a limited amount of water, and signal 1 – to the water-acid solution. The increase in chemical shift with decreasing temperature is due to the increase in acid concentration as the bulk of the water from the solution freezes.

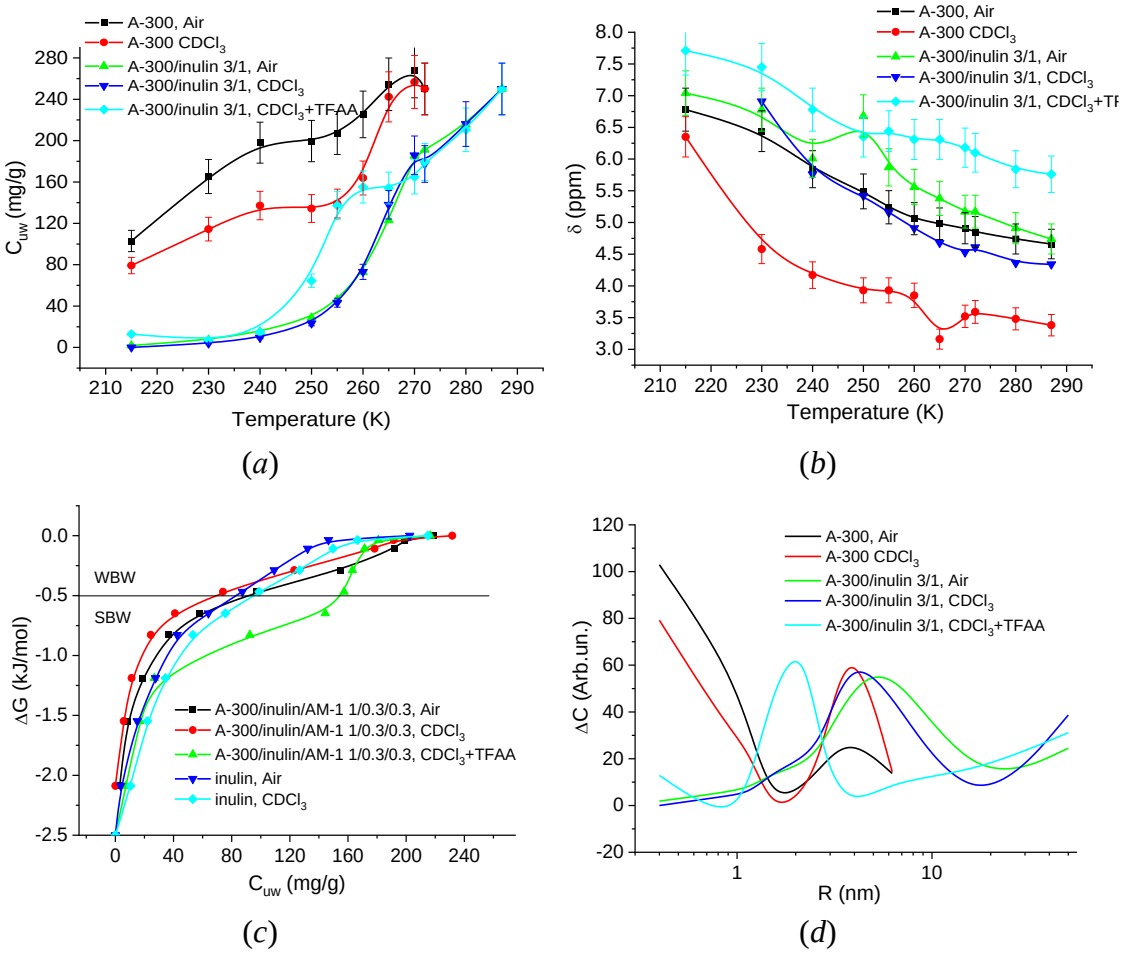

Fig. 33. Temperature dependences of non-freezing water concentration (a) and its chemical shift value (b); Gibbs free energy change from non-freezing water concentration (c) and radius distribution of adsorbed water clusters (d) for silica A-300 and its composite with inulin in air and organic media

Figs. 33, 34 show the temperature dependences of the concentration of non-freezing water (*a*) and the value of its chemical shift (*b*), the Gibbs free energy change from the concentration of non-freezing water (*c*) and the radius distribution of adsorbed water clusters (*d*) for silica A-300 and its composite with inulin (Fig. 33) and for inulin powder and its composite with a mixture of A-300 and AM-1 in air and organic media. At the same time, the dependences $\Delta G(C_{uw})$ and $\Delta C(R)$ were constructed on the basis of the dependences $\Delta C_{uw}(T)$ in accordance with formulas (1)–(3).

The chemical shifts of strongly adsorbed water (Fig. 33*b*, and 34*b*), vary in the range from 3 to 8 δ_H and depend on the ordering of the hydrogen bond network forming the adsorbed water clusters [84, 92]. A common pattern for all the studied systems is a decrease in the chemical shift of water when the air medium is replaced by chloroform medium (chaotropic effect). In some cases, the dependences $\delta_H(T)$ are not monotonic, i.e., in some areas, an increase in the value of chemical shift with increasing temperature is recorded (cosmotropic effect). This may be related to the ordering effect of the surface on water clusters of a certain size.

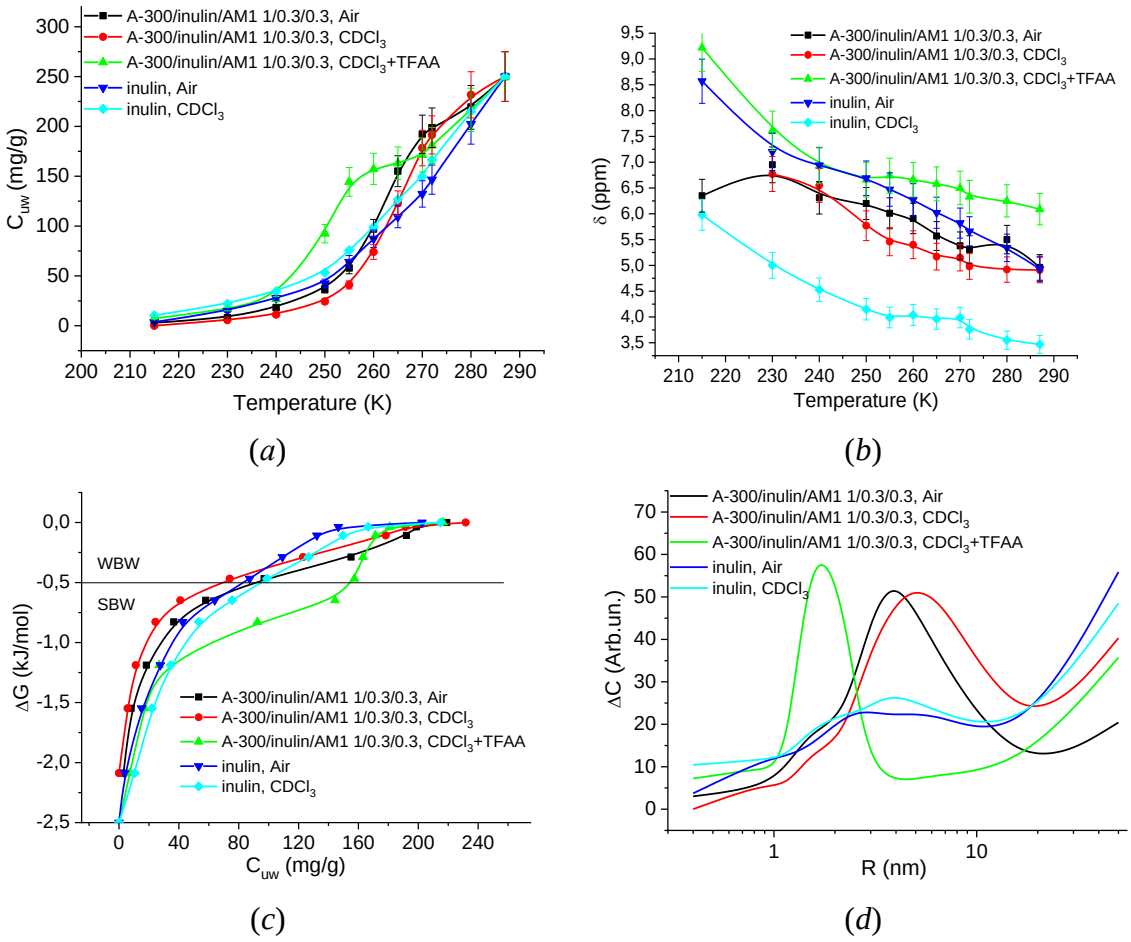

Fig. 34. Temperature dependences of non-freezing water concentration (*a*) and its chemical shift value (*b*); Gibbs free energy change from non-freezing water concentration (*c*) and radius distribution of adsorbed water clusters (*d*) for inulin powder and its composite with A-300 and AM1 mixture in air and organic media

Table 6. Characteristics of water layers adsorbed at nanosilica A-300, inulin powder and composite systems containing inulin

Sample	Medium	ΔG^S (kJ/mol)	$C_{uw}{}^S$ (mg/g)	$C_{uw}{}^W$ (mg/g)	γ_S (J/g)
A-300	Air	-3	225	25	13.9
	$CDCl_3$	-3	165	85	5.5
A-300/inulin 3/1	Air	-2.5	70	180	5.4
	$CDCl_3$	-2.1	70	180	5.4
	$CDCl_3$+TFAA	-2.1	150	100	7.8
(A-300+AM1)/inulin/ 1/0.3/0.3	Air	-2.5	90	160	6.1
	$CDCl_3$	-2.1	70	180	5.2
	$CDCl_3$+TFAA	-2.5	155	95	9.1
inulin	Air	-2.5	83	167	5.8
	$CDCl_3$	-2.5	90	160	7.1

Based on the $\Delta G(C_{uw})$ dependences (Figs. 33*c* and 34*c*), the thermodynamic parameters of interfacial water can be determined: the concentration of strongly and weakly bound water (($C_{uw}{}^S$ and $C_{uw}{}^W$, respectively), the maximum reduction of the Gibbs free energy in the strongly bound water layer (ΔG_S) and the interfacial energy, which determines the total free energy reduction that applies to the entire bound water layer (Table 6). Since the amount of water in all samples was the same, the effect of changing the composite composition and medium on water binding in the samples can be evaluated by the value of γ_S. In this case, the part of non-freezing water for which

the Gibbs free energy change exceeded 0.5 kJ/mol was considered to be strongly bound [84, 92]. The radius distributions of adsorbed water clusters were determined on the basis of the Gibbs-Thomson equation (3). According to Figs. 33*d* and 34*d*, water is in the form of clusters with radii ranging from a few tenths of nm to tens of nm. The smallest water clusters are formed in hydrated silica powder A-300. Chloroform medium stabilizes water clusters of larger radius, and additions of TFAA to it promote the formation of smaller radius clusters during freezing of suspensions. In the hydrated inulin powder, water is in the form of clusters with radius 2–20 nm. $CDCl_3$ medium has little effect on the cluster radius distribution of water adsorbed by inulin.

The maximum water binding (γ_S = 13.9 J/g) is observed for silica A-300, which is due to the formation of subnanometer-sized clusters of adsorbed water in the interparticle gaps (Fig. 33*d*). The chloroform medium stabilizes the water clusters with radius R = 4 nm. Inulin in the composite with A-300 lowers the interfacial energy of water to 5.5 J/g. However, the addition of hydrophobic silica AM1 to the composite in air increases the surface-water interaction (γ_S = 6.1 J/g). Comparing the data from Table 6 and Fig. 33*d* (34*d*) we can conclude that the main parameter responsible for the value of interfacial energy is the radius of adsorbed water clusters. Both the composition of the composite and the medium can significantly influence the radius of adsorbed water clusters.

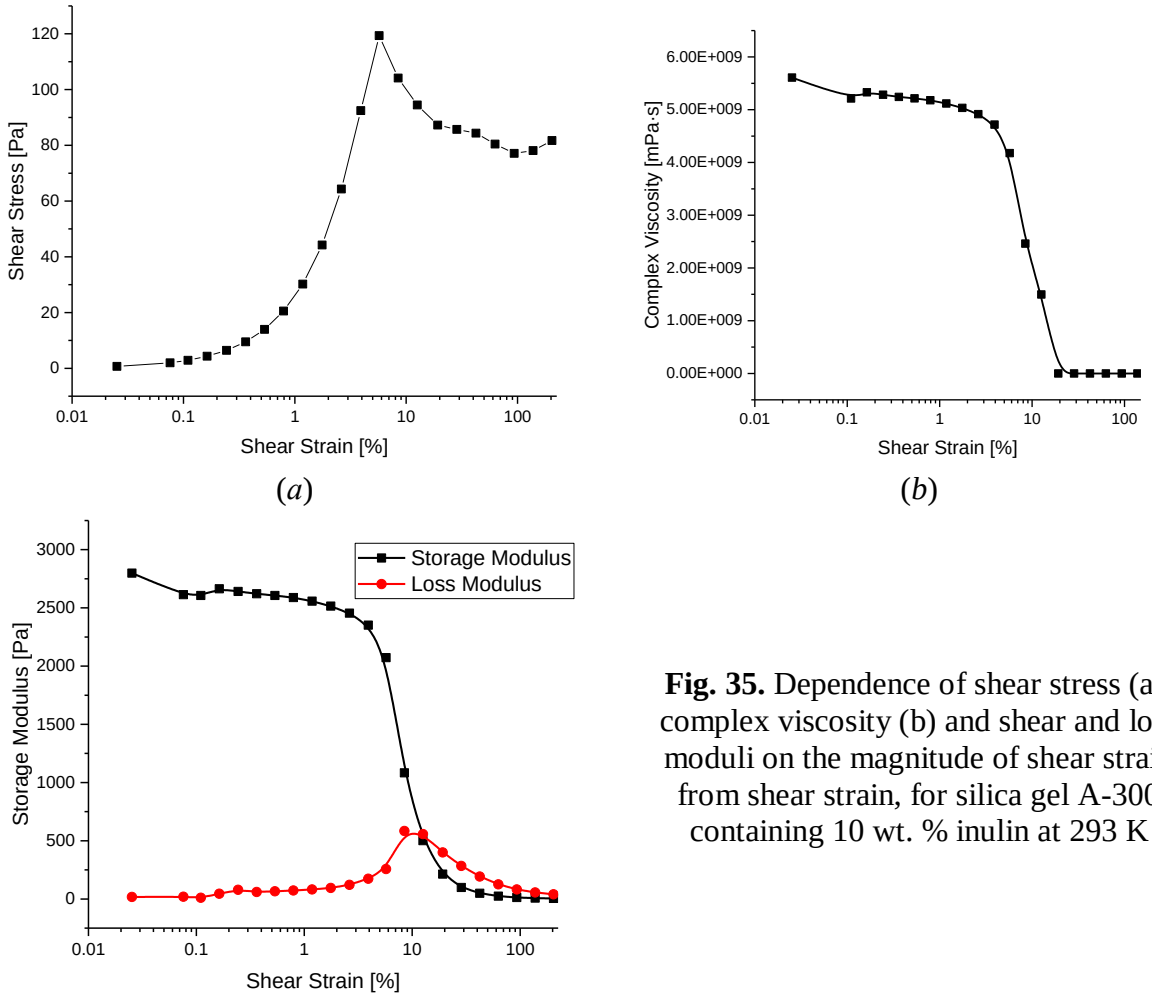

Fig. 35. Dependence of shear stress (a), complex viscosity (b) and shear and loss moduli on the magnitude of shear strain from shear strain, for silica gel A-300 containing 10 wt. % inulin at 293 K

The results of rheological studies of the composite system based on hydrophilic silica A-300 and inulin immobilised at its surface, taken in a mass ratio of 10/1 and containing 8 g/g H_2O are shown in Fig. 35. The dependence of shear stress on shear strain (Fig. 35*a*) has a complex form characteristic of non-Newtonian fluids. In the initial part of the dependence $\gamma(\tau)$ value the shear stress increases with increasing shear strain, and the more strongly, the greater the magnitude

of the strain. This pattern corresponds to a pseudoplastic gel in which irreversible displacement of some gel layers relative to others occurs with increasing strain. After reaching the maximum value τ starting its decrease, which is associated with the dissipation of mechanical energy of the rotor associated with the rearrangement of the gel structure (dilant gel). At the curve of dependence of complex viscosity (η) on shear strain (Fig. 35*b*), this process is observed as a gradual decrease in viscosity with increasing strain for pseudoplastic gel and its sharp decrease for dilant gel.

Under the influence of shear deformation, gels can transition from a solid-elastic state to a viscous liquid state [178–181]. The transition criterion is the equality of conservation and loss moduli. The corresponding dependences for the silica/inulin composite system are shown in Fig. 35*c*, which shows that the equality of these rheological parameters is observed at $\gamma = 10.5$ %.

Inulin forms composite systems with hydrophilic or a mixture of hydrophilic and hydrophobic silica during mechanical processing, maintaining a high specific surface area of the composite system. At the same time polymer molecules are uniformly distributed on the surface of mineral particles.

Both in initial materials and in composite systems, adsorbed water is in the form of nanoscale or subnanoscale clusters formed by strongly-associated water, molecules of which simultaneously participate in the formation of 2–3 hydrogen bonds. A weakly polar organic medium has a disordering (chaotropic) effect on water. As the temperature decreases, the ordering of adsorbed water molecules increases, although in some systems, temperature intervals are fixed at which the cosmotropic effect of the surface on adsorbed water takes place.

The addition of hydrophobic silica AM1 to the A-300/inulin composite system leads to an increase in the surface-water interaction. The magnitude of the interfacial energy correlates with a decrease in the radius of the adsorbed water clusters.

Aqueous gels created from silica and inulin exhibit the properties of non-Newtonian fluids, which depending on the magnitude of shear strain can exhibit both pseudoplastic and dilatant properties.

CONCLUSIONS

Technologies have been developed for the production of nanocomposite systems based on hydrophilic and hydrophobic silicas or their mixtures with biologically active plant-based compounds, such as betulin, ginseng, pectin, and inulin. The physicochemical properties and structure of the adsorption layer have been studied, and the concentration ratios of the components at which the active substances are in their most active, nanoscale state have been determined. Information has been obtained on the possibilities of regulating the release rate of biologically active components from composite systems.

Inulin forms composite systems with hydrophilic or a mixture of hydrophilic and hydrophobic silica during mechanical processing, maintaining a high specific surface area of the composite system. At the same time polymer molecules are uniformly distributed on the surface of mineral particles. Both in initial materials and in composite systems, adsorbed water is in the form of nanoscale or subnanoscale clusters formed by strongly-associated water, molecules of which simultaneously participate in the formation of 2–3 hydrogen bonds. A weakly polar organic medium has a disordering (chaotropic) effect on water. As the temperature decreases, the ordering of adsorbed water molecules increases, although in some systems, temperature intervals are fixed at which the cosmotropic effect of the surface on adsorbed water takes place. The addition of hydrophobic silica AM1 to the A-300/inulin composite system leads to an increase in the surface-water interaction. The magnitude of the interfacial energy correlates with a decrease in the radius of the adsorbed water clusters. Aqueous gels created from silica and inulin exhibit the properties of non-Newtonian fluids, which depending on the magnitude of shear strain can exhibit both pseudoplastic and dilatant properties.

The process of formation of composite systems based on nanosilica A-300 and biologically active substances (BAS): gallic acid (GA), glycyrrhizic acid (GLA) and its salts was studied using a set of physicochemical methods. It was shown that when BAS are immobilized on the silica surface by the method of joint grinding in a porcelain mortar, they pass into a nanosized X-ray amorphous state. Water adsorbed on the surface of such composite systems is also in a clustered state, and the radius of adsorbed water clusters is in the range of 0.4–50 nm. The chloroform environment has a complex effect on the size of water clusters. In general, there is a tendency for the radius of water clusters to increase when air is replaced by a chloroform environment. However, this does not always lead to a decrease in the interfacial energy. The possibility of the existence of metastable ice in the temperature range up to 287 K, stabilized by the surface of composite systems, was discovered. The amount of such ice can reach 20 % of the total water content in the sample. The possibility of using complex viscosity measurements for hydrated silica powders and silica containing immobilized biologically active substances is shown. These measurements allow recording changes in the phase state of complex mixtures during the formation of compact composite forms under the influence of periodic mechanical loading.

It is shown that silica chemically modified by grafting dimethylsilyl groups can be subjected to structural modification by mechanical activation with water, resulting in the formation of a compact material with a bulk density of 200–250 mg/cm^3, in which part of the interfacial water passes into a weakly associated state. The addition of chloroform entails the formation of a common water-chloroform system, in which almost all water becomes weakly associated. A method has been developed for the formation of a hydrated silica/betulin composite system, which makes it possible for a significant amount of weakly associated forms of water to exist in the surface layer, some of whose properties are close to those of supercritical water. During hard hydration (grinding with water in a porcelain mortar), water penetrates into the gaps between hydrophobic particles of methylsilica or methylsilica with immobilized betulin and forms clusters of weakly associated water, the radius of which can be 0.4–8 nm. This type of interfacial water exists in a wide temperature range, its amount increases with increasing temperature.

The construction of composite systems containing pectins and silica materials can serve as a promising direction in the creation of nanomaterials with high adsorption characteristics in relation to molecules of medium and large molecular weight.In particular, it shows the prospects of creating composites based on a mixture of hydrophobic and/or hydrophilic silicas (AM1 and/or A-300, respectively) with pectin. It has been shown that the maximum adsorption of MB occurs from the model solution at pH 5.5 on the surface of all the studied samples. The A-300/AM1/pectin composite system proved to be the best, regardless of the amount of pectin in the composite (5 or 10 %) at different pH values, compared to other adsorbents. It is possible to control the structure of interfacial water and the energy of interaction between water and the surface by changing the concentration ratio of pectin and hydrophobic silica. In this way, new types of functionalized materials can be created for use in medical composites.

It has been established that in the AM1/*Amanita* composite systems, despite its hydrophobic properties, the energy of water binding is greater than in the original materials. The maximum value of interfacial energy of water was recorded at the same concentration of ingredients in the AM1/*Amanita* composite system. At a higher content of the hydrophobic component, due to the merging of nanosized water clusters, the process of formation of extended water structures begins, which is accompanied by a decrease in interfacial energy and an increase in the radii of adsorbed water clusters.

REFERENCES

1. Ashton S., Song Y. H., Nolan J., Cadogan E., Murray J., Odedra R., Foster J., Hall P. A., Low S., Taylor P., Ellston R., Polanska U. M., Wilson J., Howes C., Smith A., Goodwin R. J. A., Swales J. G., Strittmatter N., Takáts Z., Nilsson A., Andren P., Trueman D., Walker

M., Reimer C. L., Troiano G., Parsons D., Witt D. De., Ashford M., Hrkach J., Zale S., Jewsbury Ph. J., Barr S. T. Aurora kinase inhibitor nanoparticles targets tumors with favorable therapeutic index *in vivo*. *Sci. Transl. Med*. 2016. **8**(325): 325ra17.

2. Bawa R., Audette G. F., Reese B. E. *Handbook of clinical nanomedicine: law, business, regulation, safety, and risk*. (Pan Stanford Publishing, 2016).
3. Nair M., Guduru R., Liang P., Hong J., Sagar V., Khizroev S. Externally controlled on-demand release of anti-HIV drug using magneto-electric nanoparticles as carriers. *Nat. Commun.* 2013. **4**(1): e1707.
4. Ward E. M., Sherman R. L., Henley S. J., Jemal A., Siegel D. A. Feuer E. J., Firth A. U, Kohler B. A., Scott S., Ma J., Anderson R.N., Benard V., Cronin K.A. Annual report to the nation on the status of cancer, featuring cancer in men and women age 20-49 years. *J. Natl. Cancer Inst.* 2019. **111**(12): 1279.
5. Yang J., Wang Z., Zong S., Chen H., Zhang R., Cui Y. Dual-mode tracking of tumor-cell-specific drug delivery using fluorescence and label-free SERS technique. *Biosens. Bioelectron.* 2014. **51**: 82.
6. Gray M. D., Lyon P. C., Mannaris C., Folkes L. K., Stratford M., Campo L. Focused ultrasound hyperthermia for targeted drug release from thermosensitive liposomes: results phase I trial. *Radiol.* 2019. **291**: 232.
7. Turov V. V., Krupska T. V., Guzenko N. V., Borysenko M. V., Nychiporuk Yu. M., Gun'ko V. M. Controlled confined space effects on clustered water bound to hydrophobic nanosilica with nonpolar and polar co-adsorbates. *Colloid. and Surf. A: Physicochem. and Engin. Aspects.* 2022. **644**: e 128919.
8. Turov V. V., Gerashchenko I. I., Krupskaya T. V., Suvorova L. *Nanochemistry in solving problems of exo- and endoecology*. (Stavropol: Zebra, 2017.) [in Russian]
9. Gun'ko V. M., Turov V. V., Pakhlov E. M., Krupska T. V., Borysenko M. V., Kartel M. T., Charmas Barbara Water Interactions with Hydrophobic versus Hydrophilic Nanosilica *Langmuir*. 2018. **34**: 12145.
10. Gun'ko V. M., Turov V. V., Pakhlov E. M., MatkovskyA. K., Krupska T. V., Kartel M. T., Charmas Barbara Blends of amorphous/crystalline nanoalumina and hydrophobic amorphous nanosilica. *J. Of Non-Crystalline Solids*. 2018. **500**: 351.
11. Muller V. M. Theory of reversible coagulation. *Colloid Journal*. 1996. 58(5): 634. [in Russian]
12. Efremov I.F. *Periodic colloidal structures.* (Leningrad: Chemistry, 1971). [in Russian]
13. Turov V. V., Krupska T. V. Influence of mechanical loads on the state of water in the hydrophobic environment of methyl silica particles. *Theor. Exp. Chem*. 2022. **58(**1); 48.
14. Turov V. V., Gun'ko V. M., Turova A. A. Morozova L. P., Voronin E. F. Interfacial behavior of concentrated HCl solution and water clustered at a surface of nanosilica in weakly polar solvents media. *Coll. Surf. A: Physicochem. Engin. Aspects.* 2011. **390**(1-3): 48
15. Gun'ko V. M., Turov V. V., Turov A. V. Hydrogen peroxide – water mixture bound to nanostructured silica. *Chem. Phys. Lett*. 2012. **531**: 132.
16. Gun'koV. M., Turov V. V., Pakhlov E. M., KrupskaT. V., Charmas B. Effect of water content on the characteristics of hydro-compacted nanosilica. *Applied Surf. Scien*. 2018. **459**: 171.
17. Gun'ko V. M. Morphological and textural features of various materials composed of porous or nonporous nanoparticles differently packed in secondary structures. *Applied Surf. Science.* 2021. **569**: 151117.
18. Gregg S. J., Sing K. S. W. *Adsorption, Surface Area and Porosity*. (London: Academic Press,1982).

19. Adamson A. W., Gast A. P. *Physical Chemistry of Surface. Sixth edition.* (New York: Wiley, 1997).
20. Rüger R., Franchini M., Trnka T., Yakovlev A., van Lenthe E., Philipsen P., van Vuren T., Klumpers B., Soini N. AMS 2024.102. SCM, Theoretical Chemistry, Vrije Universiteit, Amsterdam, The Netherlands. Available online: https://www.scm.com (accessed on 6 February 2024).
21. Stewart J. J. P. MOPAC 2022.1.1, Stewart Computational Chemistry. Available online: http://OpenMOPAC.net (accessed on 6 February 2024).
22. Gun'ko V. M., Turov V. V. *Nuclear Magnetic Resonance Studies of Interfacial Phenomena*. (CRC Press, Boca Raton. 2013).
23. Strange J. H., Rahman M., Smith E. G. Characterization of porous solids by NMR. *Phys. Rev. Lett.* 1993. **71**: 3589.
24. Mitchell J., Webber J. B. W., Strange J. H. Nuclear magnetic resonance cryoporometry. *Phys. Rep.* 2008. **461**: 1.
25. Kimmich R. *NMR Tomography, Diffusometry, Relaxometry*. (Springer: Heidelberg, 1997).
26. Ow Y. Y., Stupans I. Gallic acid and gallic acid derivatives: effects on drug metabolizing enzymes. *Curr. Drug Metab. journal*. 2003. **4**(3): 241 PMID 12769668.
27. Gu C., Howell K., Dunshea F. R., Suleria H. A. R. LC-ESI-QTOF/MS characterisation of phenolic acids and flavonoids in polyphenol-rich fruits and vegetables and their potential antioxidant activities. *Antioxidants Basel*. 2019. **8**(9): 405,
28. Balkrishna A., Pokhrel S., Tomer M., Verma S., Kumar A., Nain P., Gupta A., Varshney A. Anti-acetylcholin esterase activities of mono-herbal extracts andexhibited synergistic effects of the phytoconstituents: a biochemical and computational study. *Molecules*. 2019. **24**(22):4175.
29. Govea-Salas M., Rivas-Estilla A. M., Rodríguez-Herrera R., Lozano-Sepúlveda S. A., Aguilar-Gonzalez C. N., Zugasti-Cruz A., Salas-Villalobos T. B., Morlett-Ch´avez J. A. Gallic acid decreases hepatitis C virus expression through its antioxidant capacity. *Exp. Ther. Med.* 2016. **11(**2): 619.
30. Nouri A., Heibati F., Heidarian E. Gallic acid exerts anti-inflammatory, anti-oxidative stress, and nephroprotective effects against paraquat-induced renal injury in male rats. *Naunyn Schmiedebergs Arch. Pharmacol.* 2020. **394**: 1.
31. BenSaad L. A., Kim K. H., Quah C. C., Kim W. R., Shahimi M. Anti-inflammatory potential of ellagic acid, gallic acid and punicalagin A&B isolated from Punica granatum. *BMC Complement, Altern. Med.* 2017. **17(**1): 47.
32. Bai Jinrong, Zhang Yunsen, Tang Ce, Houa Ya, Ai Xiaopeng, Chen Xiaorui, Zhang Yi, Wang Xiaobo, Meng Xianli Gallic acid: Pharmacological activities and molecular mechanisms involved in inflammation-related diseases. *Biomedicine & Pharmacotherapy*. 2021. **133**: e110985.
33. Hashimoto O., Kuniishi H., Nakatake Y., Yamada M., Wada K., Sekiguchi M. Dexamethasone-loaded HO-activatable anti-inflammatory nanoparticles for on-demand therapy of inflammatory respiratory diseases. *Nanomedicine*. 2020. **14**: e102301.
34. Lima K. G., Krause G. C., Schuster A. D., Catarina A. V., Basso B. S., De Mesquita F. C., Pedrazza L., Marczak E. S., Martha B. A., Nunes F. B., Chiela E. C. F., Jaeger N., Thom´e M. P., Haute G. V., Dias H. B., Donadio M. V., De Oliveira J. R. Gallic acid reduces cell growth by induction of apoptosis and reduction of IL-8 in HepG2 cells. *Biomed. Pharmacother.* 2016. **84**: 1282.
35. Ho H. H., Chang C. S., Ho W. C., Liao S. Y., Lin W. L., Wang C. J. Gallic acid inhibits gastric cancer cells metastasis and invasive growth via increased expression of RhoB, downregulation of AKT/small GTPase signals and inhibition of NF-κB activity. *Toxicol. Appl. Pharmacol*. 2013. **266(**1): 76.

36. Schimites P. I., Segat H. J., Teixeira L. G., Martins L. R., Mangini L. T., Baccin P. S., Rosa H. Z., Milanesi L. H., Burger M. E., Soares A. V. Gallic acid prevents ketamine-induced oxidative damages in brain regions and liver of rats. *Neurosci. Lett.* 2020. **714**: e134560.
37. Vuolo M. M., Batista A. G., Biasoto A. C. T., Correa L. C., Júnior M. R. M., Liu R. H. Red-jambo peel extract shows antiproliferative activity against HepG2 human hepatoma cells. *Food Res, Int.* 2019. **124**: 93.
38. Shahrzad S., Aoyagi K., Winter A., Koyama A., Bitsch I. Pharmacokinetics of gallic acid and its relative bioavailability from tea in healthy humans. *J. Nutr.* 2001. **131(**4): 1207.
39. Zhong Y. X., Jin X. L., Gu S. Y., Peng Y., Zhang K. R., Ou-Yang B. C., Wang Y., Xiao W., Wang Z. Z., Aa J. Y., Wang G. J., Sun J. G. Integrated identification, qualification and quantification strategy for pharmacokinetic profile study of Guizhi Fuling capsule in healthy volunteers. *Sci. Rep.* 2016. **6**: e 31364.
40. Zhu H., Liu X., Zhu T. T., Wang X. L., Qin K. M., Pei K., Cai B. C. UHPLC-MS/MS method for the simultaneous quantitation of five anthraquinones and gallic acid in rat plasma after oral administration of prepared rhubarb decoction and its application to a pharmacokinetic study in normal and acute blood stasis rats. *J. Sep. Sci*. 2017. **40(**11): e 2382.
41. Tsang M. S., Jiao D., Chan B. C., Hon K. L., Leung P. C., Lau C. B., Wong E. C., Cheng L., Chan C. K., Lam C. W., Wong C. K. Anti-inflammatory activities of Pentaherbs Formula, Berberine, gallic acid and chlorogenic acid in atopic dermatitis-like skin inflammation. *Molecules*. 2016. **21(**4): 519.
42. Yoon C. H., Chung S. J., Lee S. W., Park Y. B., Lee S. K., Park M. C. Gallic acid, a natural polyphenolic acid, induces apoptosis and inhibits proinflammatory gene expressions in rheumatoid arthritis fibroblast-like synoviocytes. *Joint Bone Spine*. 2013. **80(**3): 274.
43. Correa L. B., P´adua T. A., Seito L. N., Costa T. E., Silva M. A., Cand´ea A. L., Rosas E. C., Henriques M. G. Anti-inflammatory effect of Methyl Gallate on experimental arthritis: inhibition of neutrophil recruitment, production of inflammatory mediators, and activation of macrophages. *J. Nat. Prod*. 2016. **79**(6): 1554.
44. Kononova P. A., Selyutina O. Y., Polyakov N. E. Glycyrrhizic acid as a multifunctional drug carrier - From physicochemical properties to biomedical applications: A modern insight on the ancient drug. *Membranes.* 2023. **13(**5): 505.
45. Selyutina Yu., Kononova P. A., Polyakov N. E. Effect of glycyrrhizic acid on phospholipid membranes in media with different pH. *Russ Chem Bull.* 2021. **70(**12): 2434.
46. Selyutina O. Y., Polyakov N. E. Glycyrrhizin-Assisted Transport of Praziquantel Anthelmintic Drug through the Lipid Membrane: An Experiment and MD Simulation. *Int. J. Pharm.* 2019. **559**: 271.
47. Kim A.V., Shelepova E.A., Selyutina O.Y., Meteleva E.S., Dushkin A.V., Medvedev N.N., Polyakov N.E., Lyakhov N.Z. Glycyrrhizic acid: A promising carrier material for anticancer therapy. *Mol Pharm.* 2019. 16(7): 3188
48. Abragam A. *Principles of nuclear magnetic resonance*. (Oxford: Oxford Science Publcations. 1989).
49. Gun'ko V. M., Turov V. V. Interfacial Phenomena in Nanostructured Systems with Various Materials. *ChemPhysChem*. 2024. **25**(6): e202300622.
50. *Thermodynamic properties of individual substances.* (edited by V.P. Glushko). (Moscow: Science, 1978). [in Russian].
51. Haddad Y. M. *Viscoelasticity of Engineering Materials.* (London: Chapman and Hall, 1995).

52. Gentile L., Silva B.F., Balog S., Mortensen K., Olsson U. Structural transitions induced by shear flow and temperature variation in a nonionic surfactant/water system. *J. of Coll. and Interf. Sci.* 2012. **372**: 32.
53. Giomi L., Liverpool T. B., Marchetti M. C. Sheared active fluids: Thickening, thinning, and vanishing viscosity. *Physical Review E.* 2010. **81**: e051908.
54. Hatwalne Y., Ramaswamy S., Rao M., Simha R. A. Rheology of Active-Particle Suspensions. *Phys. Rev. Lett.* 2004. **92**: e118101.
55. Kuo-Hsiung Lee, Morris-Natschke Susan Recent advances in the discovery and development of plant-derived natural products and their analogs as anti-HIV agents. *Pure and Appl. Chem*. 1999. **71**(6): 1045.
56. Patent US 5962527. Pezzuto J. M., Dac Gupta T. P., Schmidt M. L., Kuzmanoff K. M., Ling-Indeck L., Kim Darrick S. H. L. Methods and composition for treating cancers. 1999.
57. Drag M., Surowiak P., Drag-Zalesinska M., Dietel M., Lage H., Oleksyszyn J. Comparison of the Cytotoxic Effects of Birch Bark Extract. Betulin and Betulinic Acid Towards Human Gastric Carcinoma and Pancreatic Carcinoma Drug-sensitive and Drug-Resistant Cell Lines. *Molecules*. 2009. **14(**4): 1639.
58. Pokrovsky A. G., Plyasunova O. A., Ilyicheva T. N. Synthesis of derivatives of plant triterpenes and study of their antiviral and immunostimulating activity. *Chemistry for sustainable development.* 2001. **9**: 485.
59. Lavoie Serge, Pichette Andre, Garneau Francois-Xavier, Girard Michel, Gaudet Daniel Synthesis of betulin derivatives with solid supported reagents (Laseve, Univ. du Quebec a Chicoutimi, 555 boul. Univ., Chicoutimi, Quebec, Canada, G7H 2B1). *Synth. Commun*. 2001. **31**(10): 1565.
60. Khlebnikova T. B., Pai Z. P., Kuznetsov B. N., Matzat Yu. V., Kuznetsova S. A., Berdnikova P. V., Skvortsova G. P. Catalytic oxidation of betulin and betulin diacetate using environmentally friendly oxidizing agents. *J. of the Siber. Fed. Univ. Chem*. 2008. (3): 277. [in Russian]
61. Kuznetsova S. A., Vasil'eva N. Yu., Kalacheva G. S., Titova N. M., Redkina E. S., Skvortsova G. P. Obtaining Betulin Diacetate from Outer Birch Bark and Studying its Antioxidant Activity. *J. of the Siber. Fed. Univ. Chem*. 2008. **2**: 151.
62. Levdansky V.A. Condensation products of betulinic acid with some aliphatic amines and amino acids. *J. of the Siber. Fed. Univ. Chem*. 2008. **1**: 88.
63. Kogay T.I. An improved two-stage method for obtaining betulinic acid from botulin. *J. of the Siberian Federal University. Chemistry*. 2008. **1**: 97.
64. Kogay T.I., Kuznetsov B.N. Reduction of betulonic acid to betulinic acid under conditions of interfacial catalysis. *Chemistry of plant raw materials*. 2008. **2**. 95.
65. Liby K.T., Yore M.M., Sporn M.B. Triterpenoids and rexinoids as multifunctional agents for the prevention and treatment of cancer. *Nat. Rev. Cancer*. 2007. **7(**5): 357.
66. Hsu T.-I., Chen Y.-J., Hung C.-Y., Wang Y.-C., Lin S.-J., Su W.-C., Lai M.-D., Kim S.-Y., QiangW., Keduo Q., Goto M., Zhao Y., Kashiwada Y., Lee K.-H., Chang W.-Ch., Hung J.-J. A novel derivative of betulinic acid, SYK023, suppresses lung cancer growth and malignancy. *Oncotarget*. 2015. **6**(15): 13671.
67. Alakurtti S., Mäkelä T., Koskimies S., Yli-Kauhaluoma J. Pharmacological properties of the ubiquitous natural product betulin. *Eur. J. Pharm. Sci.* 2006. **29**(1): 1.
68. Lin W. Y., Lin F. H., Sadhasivam S., Savitha S. Antioxidant effects of betulin on porcine chondrocyte behavior in gelatin/C6S/C4S/HA modified tricopolymer scaffold. *Mater. Sci. Eng. C.* 2010. **30(**4): 597.
69. Chintharlapalli S., Papineni S., Ramaiah S. K., Safe S. Betulinic acid inhibits prostate cancer growth through inhibition of specificity protein transcription factors. *Cancer Res*. 2007. **67**(6): 2816.

70. Yogeeswari P., Sriram D. Betulinic Acid and Its Derivatives: A Review on their Biological Properties. *Curr. Med. Chem*. 2005. **12**(6): 657.
71. Fulda S. Betulinic acid for cancer treatment and prevention. *Int. J. Mol. Sci.* 2008. **9**(6) 1096.
72. Gao Yang, Ma Qing, Ma Yan-Bin, Ding Liang, Xu Xiao-Long, Wei De-Fei, Wei Lei, Zhang Jing-Wei Betulinic acid induces apoptosis and ultrastructural changesin MDA-MB-231breast cancer cells. *Ultra Pathol*. 2018. **42**(1): 49.
73. Jäger S., Laszczyk M. N., Scheffler A. A preliminary pharmacokinetic study of betulin, the main pentacyclic triterpene from extract of outer bark of birch (Betulae albacortex). *Molecules*. 2008. **13**(12): 3224
74. Hordyjewska A., Ostapiuk A., Horecka A. Betulin and betulinic acid in cancer research. *J. Pre Clin Clin Res.* 2018. **12**(2): 72
75. Wiggins P. M., MacClement B. A. E. Two States of Water Found in Hydrophobic Clefts: Their Possible Contribution to Mechanisms of Cation Pumps and Other Enzymes. *Internat. Rev. Cytol.* 1987. **108**: 249.
76. Dore J. Structural Studies of Water in Cinfined Geometry bu Neutron Difraction. *Chem. Phys.* 2000. **258**: 327.
77. Chaplin M. F. A Proposal for Structuring of Water. *Biophys. Chem*. 1999. **83**: 211.
78. Wiggins P. M. Role of Water in Some Biological Proceses. *Microbiol. Rev.* 1990. **54**: 432.
79. Wiggins P. M. High- and Low-Density Water in Gel. *Progr. Polim. Sci.* 1995. **20**: 1121.
80. Wiggins P. M. High- and Low-Density Intracellular Water. *Coll. Mol. Biol*. 2001. **47**: 735.
81. Galkin A. A., Lunin V. V. Water in sub- and supercritical states − a universal medium for the implementation of chemical reactions. *Uspekhi Chemistry*. 2005. 74(1): 24.
82. Marsall W., Jones E. Liquid–vapor critical temperatures of aqueous electrolyte solutions. *J. Inorg. Nucl. Chem*.1974. **36**(10): 2313.
83. Turov V. V., Leboda R. Application of ^{1}H NMR Spectroscopy Method for Determination of Characteristics of Thin Layers of Water Adsorbed on the Surface of Dispersed and Porous Adsorbents. *Adv. Colloid Interface Sci*. 1999. **79**: 173.
84. Gunko V. M., Turov V. V., Gorbik P. P. *Water at the interface*. (Kyiv: Naukova Dumka, 2009).
85. Gun'ko V. M., Turov V. V. Structure of Hydrogen Bonds and ^{1}H NMR Spectra of Water at the Interface of Oxides. *Langmuir*. 1999. **15**: 6405.
86. Gun'ko V. M., Turov V. V., Bogatyrev V. M., Zarko V. I., Leboda R., Goncharuk E. V., Novza A. A., Turov A. V., Chuiko A. A. Unusual Properties of Water at Hydrophilic/Hydrophobic Interfaces. *Adv. Colloid Interf. Sci*. 2005. **118**: 125 .
87. Turov V. V., Leboda R. ^{1}H NMR Spectroscopy of adsorbed molecules and free surface energy of carbon adsorbents. *Physical and Chemistry of Carbons*. 2000. **27**: 67.
88. Turov V. V., Gun'ko V. M. Bogatyrev V. M., Zarko V. I., Gorbik S. P., Pakhlov E. M., Leboda R., Shulga O. V., Chuiko A. A. Structured Water in Partially Dehydrated Yeast Cells and at Partially Hydrophobized Fumed Silica Surface. *J. Colloid Interface Sci*. 2005. **283**: 329.
89. Tassaing T., Danten Y., Besnard M. Supercritical water: Local or molecular dynamics. *Pure Appl. Chem*. 2004. **76**(1): 133.
90. Patent UA 138023. Krupska T. V., Turov V. V., Gunko V. M., Kartel M. T. The method of transferring in water the middle of the sum of hydrophilic and hydrophobic silicas in the path of victoria of high mechanical strength. 2019. [in Ukrainian]
91. Patent UA 138129. Krupska T. V., Turov V. V., Kartel M. T. The method of transferring hydrophobic silica in the middle waterway through the path of high mechanical strength. 2019.

92. Turov V. V., Gunko V. M. *Clustered water and ways of its use.* (Kyiv: Naukova Dumka. 2011. – 316 p.
93. Emsley J. W., Feenej J., Sutcliffe L. H. *High Resolution Nuclear Magnetic Resonance Spectroscopy.* (Oxford: Pergamon Press. 1965).
94. Bell A. T., Pines A. (Eds) *NMR techniques in catalysis*. (New York: Marcel Dekker. 1994).
95. Brunner E., Pfeifer H. NMR spectroscopic techniques for determining acidity and basicity. *Molecular sieves*. 2008. **6**: 1. (In: Karge H. G., Weitkamp J. (Eds) Acidity and Basicity. Springer)
96. *Medical chemistry and clinical application of silicon dioxide.* (Edited by O.O. Chuiko). (Kyiv: Naukova Dumka, 2003). [in Ukrainian]
97. Dening T. J., Rao S., Thomas N., Prestidge C. A. Novel nanostructured solid materials for modulating oral drug delivery from solid-state lipid-based drug delivery systems. *AAPS J.* 2016. **18**(1): 23.
98. Turov V. V., Gun'ko V. M., Pakhlov E. M., Krupska T. V., Tsapko M. D., Charmas B., Kartel M. T. Influence of hydrophobic nanosilica and hydrophobic medium on water bound in hydrophilic components of complex systems. *Colloids Surf. A. Physicochem. Eng. Asp.* 2018. **552**(5): 39.
99. Karpovich N. S., Donchenko L. V., Nelina V. V., Kompantsev V. A., Melnik G. S. *Pectin. Production and application.* (Kyiv: Urozhai, 1989). [in Russian].
100. Minzanova S. T., Mironov V. F., Arkhipova D. M., Khabibullina A. V., Mironova L. G., Zakirova Y. M., Milyukov V. A. Biological activity and pharmacological application of pectic polysaccharides: a review. *Polymers.* 2018. **10**(12): 1407.
101. Popova N. V., Lytvynenko V. I., Kutsanyan A. S. *Medicinal plants of the world flora*. (Kharkiv: Disa plus. 2016). [in Russian].
102. Lara-Espinoza C., Carvajal-Millán E., Balandrán-Quintana R., López-Franco Y., Rascón-Chu A. Pectin and pectin-based composite materials: beyond food texture. *Molecules.* 2018. **23(**4): 942.
103. Ovodov Yu. S., Ovodova R. G., Popov S. V., Golovchenko V. V. *The latest knowledge on pectin polysaccharides*. (Syktyvkar: Publishing House of Komi Scientific Center, Ural Branch of the Russian Academy of Sciences. 2010). [in Russian].
104. Leclere L., Fransolet M., Cote F., Cambier P., Arnould T., Van Cutsem P., Michiels C. Heat-modied citrus pectin induces apoptosislike cell death and autophagy in HepG2 and A549 cancer cells. *PLoS One*. 2015. **10**(3): e0115831.
105. Zainal Arin S. H., Yeen W. W., Zainol Abidin I. Z., Abdul Wahab R. M., Arin Z. Z., Sena S. Cytotoxicity effect of degraded and undegraded kappa and iota carrageenan in human intestine and liver cell lines. *BMC Complement Altern Med*. 2014. **14**: e 508.
106. Razina T. G., Zueva E. P., Amosova E. N., Krylova S. G., Khotimchenko M. Y., Lopatina K. A., Efimova L. A., Safonova E. A., Rybalkina O. Yu. Effects of pectins of various molecular mass on growth of Ehrlich adenocarcinoma and Lewis lung carcinoma, cyclophosphane efficiency in mice. *Pacific Medical Journal.* 2010. **2**(32): 32. [in Russian].
107. Watanabe K., Reddy B. S., Weisburger J. H., Kritchevsky D. Effect of dietary alfalfa, pectin and wheat bran on azoxymethane- or methylnitrosourea-induced colon carcinogenesis in F344 rats. *J. Natl Cancer Inst*. 1979. **63**(1): 141.
108. Unger K., Rupprecht H., Valentin B., Kircher W. The use of porous and modified silicas as drug delivery and stabilizing agents. *Drug Dev. Ind. Pharm*. 1983. **9**(1-2): 69.
109. Daniels R., Kerstiens B., Tischinger-Wagner H., Rupprecht H. The stability of drug adsorbates on silica. *Drug Dev. Ind. Pharm*. 1986. **12**(11-13): 2127
110. Slinyakova I. B., Denisova T. I. *Organosilicon adsorbents: production, properties, application.* (Kyiv: Naukova Dumka. 1988). [in Russian].
111. *The surface properties of silicas.* (edited by A.P. Legrand). (New York: Wiley. 1998).

112. FAO/WHO Codex Alimentarius Commission. *List of Additives Evaluated for their Safety-in-Use in Food*. CAC/Fal 1-1973.
113. Gun'ko V. M., Turov V. V., Krupska T. V., Ruban A. N., Kazanets A. I., Leboda R., Skubiszewska-Zieba J. Interfacial behavior of silicone oils interacting with nanosilica and silica gels. *J. Colloid and Interface Science*. 2013. **394(**1): 467.
114. Krupskaya T. V., Turov V. V., Barvinchenko V. N., Filatova K. O., Suvorova L. A., Iraci G., Kartel M. T. Influence of the "wetting-drying" compaction on the adsorption characteristics of nanosilica A-300. *Adsorpt. Sci. Technol*. 2017. **36**(1-2): 88
115. Patent UA 105151. Krupskaya T. V., Turov V. V., Barvinchenko V. M., Filatova K. O., Suvorova L. A., Kartel M. T. The method of compaction of nanosilica. 2016. [in Ukrainian].
116. *State Pharmacopoeia of Ukraine* (Kharkiv: RIREG. 2001).
117. Gerashchenko I.I. Physicochemical aspects of therapeutic effect of enterosorbents (theoretical research). *Him. Fiz. Tehnol. Poverhni*. 2018. **9**(4): 373.
118. Escher W.J., Davis T.A., Klein E. *Sorbents and their clinical application*. (Kyiv: Nauk. dumka, 1989). [in Russian].
119. Lukychev B. G., Tsyura V. Y., Panina I. Yu., Avyzova T. S. *Enterosorption.* (Leningrad: Center of sorption technologies. 1991). [in Russian].
120. *Adsorption from solution at the solid/liquid interface.* Edited by G.D. Parfitt, C.H. Rochester. (London; New York: Academic Press. 1983).
121. Fuzzati N., Gabetta B., Jayakar K., Pace R., Ramaschi G., Villa F. Determination of Ginsenosides in Panax ginseng Roots by Liquid Chromatography with Evaporative Light-Scattering Detection. *J AOAC Int.* 2000. **83**(4): 820.
122. Arunotayanun W. *Natural product (Fungal and herbal) novel psychoactive substances.* In: Dargan P., Wood D., editors. *Novel psychoactive substances: Classification, pharmacology and toxicology.* (Cambridge, MA: Academic Press. 2013).
123. Kuypers K. Pc, Ng L., Erritzoe D., Knudsen G. M, Nichols Ch. D, Nichols D. E, Pani L., Soula Anaïs, Nutt D. Microdosing psychedelics: More questions than answers? An overview and suggestions for future research. *J Psychopharmacol*. 2019. **33**(9): 1039.
124. Toby Lea, Nicole Amada, Henrik Jungaberle, Henrike Schecke, Michael Klein Microdosing psychedelics: Motivations, subjective effects, and harm reduction. *Int J Drug Policy*. 2020. **75**: e102600.
125. Grob C. S., Danforth A. L., Chopra G. S., Hagerty M., McKay Ch. R., Halberstadt A. L., Greer G. R. Pilot study of psilocybin treatment for anxiety in patients with advanced-stage cancer. *Arch Gen Psychiatry*. 2011. **68**(1): 71.
126. Davis A. K., Barrett F. S., May D. G., Cosimano M. P., Sepeda N. D., Johnson M. W., Finan P. H., Griffiths R. R. Effects of psilocybin-assisted therapy on major depressive disorder: A randomized clinical trial. *JAMA Psychiatry*. 2021. **78**(5): 481.
127. Petersen J. G., Bergmann R., Krogsgaard-Larsen P., Balle T., Frølund B. Probing the orthosteric binding site of GABAA receptors with heterocyclic GABA carboxylic acid bioisosteres. *Neurochemical Research.* 2014. **39**: 1005.
128. Graham A. R. Johnston GABA(A) Receptor Channel Pharmacology. *Curr Pharm Des.* 2005. 11(15): 1867.
129. McCarry B. E., Savard Marc A facile synthesis of muscimol. *Tetrahedron Lett.* 1981. **22**(51): 5153.
130. Foster A. C. Glutamate- and GABA-based CNS therapeutics. *Curr Opin Pharmacol*. 2006. **6**(1): 7.
131. Dougherty D. A. Cys-loop neuroreceptors: structure to the rescue? *Chem Rev.* 2008. **108**: 1642.
132. Johnston G. A. R., Curtis D. R., de Groat W. C., Duggan A. W. Central actions of ibotenic acid and muscimol. *Biochem Pharmacol.* 1968. **17(**12): 2488.

133. Krupskaya T., Paulius J., Bieliauskienė R., Yelahina N., Charmas B., Turov V. Water structure in fungi Amanita musscaria and their composite system 1:9 with hydrocompacted nanosilica A-300. *Annales UMCS Sectio AA (Chemia).* 2017. **72**(2): 26.
134. Barthel H., Rösch L., Weis J. *Fumed silica – production, properties, and applications. in book Organosilicon Chemistry. 2. From Molecules to Materials* / Eds N. Auner J. Weis. (Weinheim: VCH. 1995).
135. Laskowski J., Kitchener J. A. Hydrophilic–hydrophobic transition on silica. *J. Colloid Interface Sci.* 1969. **29**(4): 670.
136. Xinhuan Wan, Hao Guo, Yiyu Liang, Changzheng Zhou, Zihao Liu, Kunwei Li, Fengju Niu, Xin Zhai, Lizhu Wang The physiological functions and pharmaceutical applications of inulin: A review. *Carbohydrate Polymers.* 2020. **246**. e116589.
137. Knyazkova I.I. Potential of inulin in therapeutic practice. *Health of Ukraine*. 2021. **9**: 44. [in Russian]
138. Barszcz M., Taciak M., Tuśnio A., Święch E., Skomiał J. Dose-dependent effects of two inulin types differing in chain length on the small intestinal morphology, contractility and proinflammatory cytokine gene expression in piglets. *Arch Anim Nutr*. 2019. 1.
139. Serbaeva E. R., Yakupova A. B., Magasumova Yu. R., Farkhutdinova K. A., Akhmetova G. R., Kuluev B. R. Inulin: natural sources, features of metabolism in plants and practical application. *Biomics.* 2020. **12(**1): 57.
140. Shoaib M., Shehzad A., Omar M., Rakha A., Raza H., Sharif H. R., Shakeel A., Ansari A., Niazi S. Inulin: properties, health benefits and food applications. *Carbohydr Polym*. 2016. **147**: 444.
141. Gao T., Jiao Y., Liu Y., Li T., Wang Z., Wang D. Protective effects of konjac and inulin extracts on type 1 and type 2 diabetes. *J Diabetes Res*. 2019. e3872182.
142. Watson A.W., Houghton D., Avery P.J., Stewart C., Vaughan E.E., Meyer P.D., de Bos Kuil M. J. J., Weijs P. J. M., Brandt K. Changes in stool frequency following chicory inulin consumption, and effects on stool consistency, quality of life and composition of gut microbiota. *Food Hydrocoll*. 2019. **96**: 688–698.
143. Guaragni A., Boiago M.M., Bottari N.B., Morsch V.M., Lopes T.F., Schafer da Silva A. Feed supplementation with inulin on broiler performance and meat quality challenged with Clostridium perfringens: Infection and prebiotic impacts. *Microb Pathog*. 2019. **139**. e103889.
144. Nitin Gupta, Ashok Kumar Jangid, Deep Pooja, Hitesh Kulhari Inulin: A novel and stretchy polysaccharide tool for biomedical and nutritional applications. *Int. J. of Biol. Macromol.* 2019. **132**: 852.
145. Tadesse F. Teferra Possible actions of inulin as prebiotic polysaccharide: A review. *Food Frontiers.* 2021. **2**: 407.
146. Mahmoud M. Tawfick, Hualing Xie, Chao Zhao, Ping Shao, Mohamed A. Farag Inulin fructans in diet: Role in gut homeostasis, immunity, health outcomes and potential therapeutics. *Int. J. of Biol. Macromol.* 2022. **208**. 948.
147. Mousumi Tudu, Amalesh Samanta Natural polysaccharides: Chemical properties and application in pharmaceutical formulations. *Europ. Pol. J.* 2023. **184**: e111801.
148. Kathy R. Niness Inulin and Oligofructose: What Are They? *The J. Nutrition.* 1999. **129** (7**)**: 1402S.
149. Wasim Akram, Vikas Pandey, Rajeev Sharma, Ramakant Joshi, Neeraj Mishra, Navneet Garud, Tanweer Haider, Inulin: Unveiling its potential as a multifaceted biopolymer in prebiotics, drug delivery, and therapeutics. Internat. *J. of Biological Macromol*. 2024. **259**(1): e129131.

150. Franklin Afinjuomo, Sadikalmahdi Abdella, Souha H Youssef, Yunmei Song, Sanjay Garg Inulin and Its Application in Drug Delivery. *Pharmaceuticals (Basel)*. 2021. **14**(9): 855.
151. Tiwari R., Sethi P., Rudrangi S. R. S., Padarthi P. K., Kumar V., Rudrangi S., Vaghela K. J. Inulin: a multifaceted ingredient in pharmaceutical sciences. *Biomater Sci Polym Ed*. 2024. **29**: 1.
152. Akram W., Pandey V., Sharma R., Joshi R., Mishra N., Garud N., Haider T., Inulin: Unveiling its potential as a multifaceted biopolymer in prebiotics, drug delivery, and therapeutics. *Int J Biol Macromol.* 2024. **259**(1): e129131.
153. Ghali E. N. H. K., Pranav, Chauhan S. C., Yallapu M. M. Inulin-based formulations as an emerging therapeutic strategy for cancer: A comprehensive review. *Int J Biol Macromol*. 2024. **259**(1) e 129216.
154. Serbaeva E. R., Yakupova A. B., Magasumova Yu. R., Farkhutdinova K. A., Akhmetova G. R., Kuluev B. R. Inulin: natural sources, features of metabolism in plants and practical application. *Biomics.* 2020. **12**(1): 57.
155. Wancong Li, Jun Zhang, Chunwei Yu, Qing Li, Fang Dong, Gang Wang, Guodong Gu, Zhanyong Guo Extraction, degree of polymerization determination and prebiotic effect evaluation of inulin from Jerusalem artichoke. *Carbohydrate Polymers.* 2015. **121**: 315.
156. Fei Luan, Yafei Ji, Lixia Peng, Qi Liu, Haijuan Cao, Yan Yang, Xirui He, Nan Zeng Extraction, purification, structural characteristics and biological properties of the polysaccharides from Codonopsis pilosula: A review. *Carbohydrate Polymers*. 2021. **261**: e117863.
157. Shaojie Zhang, Ziteng Song, Lijuan Shi, Linan Zhou, Jie Zhang, Jianlin Cui, Yuhao Li, Da-Qing Jin, Yasushi Ohizumi, Jing Xu, Yuanqiang Guo A dandelion polysaccharide and its selenium nanoparticles: Structure features and evaluation of anti-tumor activity in zebrafish models. *Carbohydrate Polymers*. 2021. **270**. e118365.
158. Kosasih W., Pudjiraharti Sri, Ratnaningrum Diah, Priatni Sri Preparation of Inulin from Dahlia Tubers. *Procedia Chemistry*. 2015. **16**: 190.
159. Escobar F., Sánchez V., Vera E., Ciobotă V., Vargas Jentzsch P., Jaramillo L. Extraction of Inulin from Andean Plants: An Approach to Non-Traditional Crops of Ecuador. *Molecules.* 2020. **25**(21): 5067.
160. Boeckner L. S., Schnepf M. I., Tungland B. C. Inulin: a review of nutritional and health implications. *Advances in Food and Nutrition Research*. 2001. **43**: 1.
161. Le Bastard Q., Chapelet G., Javaudin F., Lepelletier D., Batard E., Montassier E. The effects of inulin on gut microbial composition: a systematic review of evidence from human studies. *Eur J Clin Microbiol Infect Dis.* 2019. **39**: 403.
162. Mensink M. A., Frijlink H. W., van der Voort Maarschalk K., Hinrichs W. L. Inulin, a flexible oligosaccharide. II: Review of its pharmaceutical applications. *Carbohydr Polym*. 2015. **134**: 418.
163. Mensink M. A., Frijlink H. W., van der Voort Maarschalk K., Hinrichs W. L. J. Inulin, a flexible oligosaccharide I: Review of its physicochemical characteristics. *Carbohydrate Polymers.* 2015. **130**: 405.
164. Cooper P. D., Harinda Rajapaksha K., Barclay T. G., Ginic-Markovic M., Gerson A. R., Petrovsky N. Inulin crystal initiation via a glucose-fructose cross-link of adjacent polymer chains: Atomic force microscopy and static molecular modelling. *Carbohydrate Polymers.* 2015. **117**: 964.
165. André I., Mazeau K., Tvaroska I., Putaux J.-L., Winter W. T., Taravel F. R., Chanzy H. Molecular and Crystal Structures of Inulin from Electron Diffraction Data. *Macromolecules.* 1996. **29**(13): 4626.

166. Cooper P. D., Barclay T. G., Ginic-Markovic M., Petrovsky N. The polysaccharide inulin is characterized by an extensive series of periodic isoforms with varying biological actions. *Glycobiology*. 2013. **23**(10): 1164.
167. Gun'ko V. M., Lupascu T., Krupska T. V., Golovan A. P., Pakhlov E. M., Turov V. V. Influence of tannin on aqueous layers at a surface of hydrophilic and hydrophobic nanosilicas. *Colloids and Surfaces A*. 2017. **531**(9): 17.
168. Turov V. V., Krupska T. V., Golovan A. P., Andrijko A. P., Tcapko M. D., Ostrovska G. V., Kalmykova G. V., Kartel M. T. Influence of silica on hydratability of the grinded flowers of a hibiscus sabdariffa in neutral and acidic mediums. *Nanosystems, Nanomaterials and Nanotechnologies.* 2016. **14**(4): 643.
169. Krupska T. V., Turova A. A., Gun'ko V. M., Turov V. V. Influence of highly dispersed materials on physiological activity of yeast cells. *Biopolymers and Cell*. 2009. **25**(4): 290.
170. Krupska T. V., Terebinska M. I., Klymenko N. Yu., Vitiuk N. V., Wei Qiliang, Zheng Jinju, Yang Weiyou Turov V. V. Construction of composites for medical purpose based on pyrogenic silica with immobilized succinic acid and their properties. *Int J Nanomater Nanotechnol Nanomed*. 2024. **10**(1): 023.
171. Turov V. V., Gun'ko V. M., Krupska T. V. *Hydrophobic agents in nanocomposites for medical purposes*. (Kiev: Intersevis. 2023).
172. Ulrich G. D. Theory of particle formation and growth in oxide synthesis flame. *Combust. Sci. Technol.* 1971. **4**: 47.
173. Stark W. J. Pratsinis S. E. Aerosol flame reactors for manufacture of nanoparticles. *Powder Technol.* 2002. **126**: 103.
174. Tassaing T., Danten Y., Besnard M. Supercritical water: Local or molecular dynamics. *Pure Appl. Chem*. 2004. **76**(1): 133.
175. Iler R. K. *The Chemistry of Silica: Solubility, Polymerization, Colloid and Surface Properties and Biochemistry*. (New York: John Wiley and Sons Ltd. 1979).
176. Turov V. V., Gun'ko V. M., Turova A. A., Morozova L. P., Voronin E. F. Interfacial behavior of concentrated HCl solution and water clustered at a surface of nanosilica in weakly polar solvents media. *Colloids Surf. A: Physicochem. Eng. Aspects*. 2011. **390(**1): 48.
177. Gun'ko V. M., Morozova L. P., Turova A. A., Turov A. V., Gaishun V. E., Bogatyrev V. M., Turov V. V. Hydrated phosphorus oxyacids alone and adsorbed on nanosilica. *J. Colloid and Interface Science*. 2012. **368**: 263.
178. Product Design and Engineering: Formulation of Gels and Pastes, FirstEdition. Editedby Ulrich Brockel, Willi Meier, and Gerhard Wagner. ©2013 Wiley-VCH Verlag GmbH & Co. KGaA. Published 201 3by Wiley-VCH Verlag GmbH &Co. KGaA.
179. Koos E., Willenbacher N. Capillary forces in suspension rheology. *Science*, 2011. **331**(6019): 897.
180. Willenbacher N., Vesaratchanon J. S., Thorwarth O., Bartsch E. An alternative route to highly concentrated, freely flowing colloidal dispersions. *Soft Matter*. 2011. **7**: 5777.
181. Rebinder P. A. *Surface phenomena in dispersed systems: Colloidal chemistry*. (M.: Nauka. 1979) [in Russian].

UDK: 544.7+547.3+543.2 *DOI: 10.15407/Surface.2025.17.413*

МЕДИЧНІ НАНОКОМПОЗИТИ НА ОСНОВІ ГІДРОФІЛЬНИХ ТА ГІДРОФОБНИХ КРЕМНЕЗЕМІВ ТА ЇХ ВЛАСТИВОСТІ

Т. В. Крупська, М. В. Борисенко, Н. Ю. Клименко, Л. В. Зроль, О. А. Новікова, В. В. Туров

Інститут хімії поверхні імені О. О. Чуйка НАН України, вул. Олега Мудрака, 17, Київ, 03164, Україна, е-пошта: krupska@ukr.net

Розроблено технології для виробництва нанокомпозитних систем на основі гідрофільних та гідрофобних кремнеземів або їх сумішей з біологічно активними сполуками рослинного походження, такими як бетулін, пектин та інулін. Були досліджені фізико-хімічні властивості та структура адсорбційного шару, а також визначені співвідношення концентрацій компонентів, за яких активні речовини знаходяться в своєму найбільш активному, нанорозмірному стані. Отримано інформацію про можливості регулювання швидкості вивільнення біологічно активних компонентів з композитних систем. Інулін та інші біоактивні речовини (БАР) утворюють композитні системи з гідрофільним або сумішшю гідрофільного та гідрофобного кремнезему під час механічної обробки, зберігаючи високу питому поверхню композитної системи. Водночас БАР рівномірно розподілені на поверхні мінеральних частинок. Як у вихідних матеріалах, так і в композитних системах адсорбована вода знаходиться у вигляді нано- або субнанорозмірних кластерів, утворених сильноасоційованою водою, молекули якої одночасно беруть участь в утворенні 2–3 водневих зв'язків. Слабкополярне органічне середовище має розупорядкувальний (хаотропний) вплив на воду. Зі зниженням температури впорядкування адсорбованих молекул води збільшується, хоча в деяких системах фіксовані температурні інтервали, за яких відбувається космотропний вплив поверхні на адсорбовану воду. Додавання гідрофобного кремнезему АМ1 до композитної системи А-300/БАР приводить до збільшення взаємодії між поверхнею та водою. Величина міжфазної енергії корелює зі зменшенням радіуса адсорбованих кластерів води. Водні гелі, створені з діоксиду кремнію та БАР, демонструють властивості неньютонівських рідин, які, залежно від величини деформації зсуву, можуть проявляти як псевдопластичні, так і дилатаційні властивості.

Ключові слова: *гідрофільний та гідрофобний кремнеземи, пектин, інулін, бетулін, бурштинова кислота, композитні системи, сильно- та слабоасоційована вода.*